

การจับอนุภาคแม่เหล็กแบบการแพร่โดยกลุ่มตัวจับทรงกระบอกแบบสุ่ม



นายกนก หวลกำเนิด

สถาบันวิทยบริการ

วิทยานิพนธ์นี้เป็นส่วนหนึ่งของการศึกษาตามหลักสูตรปริญญาวิทยาศาสตรมหาบัณฑิต

สาขาวิชาฟิสิกส์ ภาควิชาฟิสิกส์


คณะวิทยาศาสตร์ จุฬาลงกรณ์มหาวิทยาลัย

ปีการศึกษา 2547

ISBN 974-53-1783-7

ลิขสิทธิ์ของจุฬาลงกรณ์มหาวิทยาลัย

DIFFUSIVE CAPTURE OF MAGNETIC PARTICLES BY AN ASSEMBLAGE
OF RANDOM CYLINDRICAL COLLECTORS



Mr. Kanok Hournkumnuard

สถาบันวิทยบริการ
จุฬาลงกรณ์มหาวิทยาลัย

A Thesis Submitted in Partial Fulfillment of the Requirements
for the Degree of Master of Science in Physics

Department of Physics
Faculty of Science
Chulalongkorn University
Academic Year 2004
ISBN 974-53-1783-7

Thesis Title DIFFUSIVE CAPTURE OF MAGNETIC PARTICLES BY AN
ASSEMBLAGE OF RANDOM CYLINDRICAL COLLECTORS
By Mr. Kanok Hournkumnuard
Field of study Physics
Thesis Advisor Associate Professor Mayuree Natenapit, Ph.D.

Accepted by the Faculty of Science, Chulalongkorn University in Partial
Fulfillment of the Requirements for the Master's Degree

..... Dean of the Faculty of Science
(Professor Piamsak Menasveta, Ph.D.)

THESIS COMMITTEE

..... Chairman
(Assistant Professor Pisistha Ratanavararak, Ph.D.)

..... Thesis Advisor
(Associate Professor Mayuree Natenapit, Ph.D.)

..... Member
(Sojiphong Chatraphorn, Ph.D.)

..... Member
(Patcha Chatraphorn, Ph.D.)

กนก หวลกำเนิด: การจับอนุภาคแม่เหล็กแบบการแพร่โดยกลุ่มตัวจับทรงกระบอกแบบ
 สุ่ม. (DIFFUSIVE CAPTURE OF MAGNETIC PARTICLES BY AN ASSEMBLAGE
 OF RANDOM CYLINDRICAL COLLECTORS) อ. ที่ปรึกษา: รศ. ดร. มยุรี เนตรนภิส,
 142 หน้า. ISBN 974-53-1783-7.

งานวิจัยนี้เป็นการพัฒนาแบบจำลองทางทฤษฎีเพื่อใช้อธิบายการจับอนุภาคแม่เหล็ก
 อย่างอ่อนที่มีขนาดเล็กกว่าระดับไมครอนมากๆ ในสนามแม่เหล็กเกรเดียนท์สูง โดยเริ่มศึกษาการ
 จับอนุภาคในหนึ่งมิติด้วยตัวจับแม่เหล็กเฟอร์โรทรงกระบอกเดี่ยว จากนั้นขยายไปสู่การจับอนุภาค
 ในสองมิติ ทำยสุดได้ศึกษาปัญหาการจับอนุภาคแม่เหล็กในสองมิติกรณีตัวจับอนุภาคเป็นกลุ่ม
 ทรงกระบอกแม่เหล็กแกนขนานที่กระจายตัวแบบสุ่มในของไหลสถิต ในงานวิจัยนี้ได้ใช้วิธีตัว
 กลางยังผลในการสร้างแบบจำลองการจับอนุภาคซึ่งเป็นการปรับปรุงงานของเดวิสและเกอร์เบอร์
 ที่ได้สมมติให้มีเพียงตัวจับอนุภาคเดี่ยว ในแบบจำลองนี้ได้พิจารณาเฉพาะในเซลล์ตัวแทนหนึ่ง
 เซลล์ ส่วนเซลล์อื่นๆ รอบๆ ถูกแทนที่ด้วยตัวกลางเนื้อเดียวกันที่มีค่าความซาบซึมได้ทางแม่เหล็กยัง
 ผล เราหาผลเฉลยของสมการความต่อเนื่องที่อธิบายการเปลี่ยนแปลงค่าความเข้มข้นของอนุภาค
 ณ ตำแหน่งต่างๆ เมื่อเวลาผ่านไป ผลเฉลยที่สภาวะคงตัวถูกคำนวณโดยวิธีการเชิงวิเคราะห์ ส่วน
 ผลเฉลยที่ขึ้นกับเวลาอยู่ในรูปแบบค่าเชิงตัวเลข ในงานวิจัยนี้เราได้พัฒนาโปรแกรมคอมพิวเตอร์
 เพื่อใช้ในการจำลองการจับอนุภาคแม่เหล็ก

จากผลการจำลองการจับอนุภาคแม่เหล็ก เส้นแสดงระดับความเข้มข้นของอนุภาคที่ถูก
 สร้างขึ้นในสถานการณ์ทางฟิสิกส์หลายแบบได้ถูกนำมาวิเคราะห์และผลที่ได้แสดงให้เห็นบริเวณ
 อิมตัว บริเวณสะสม และบริเวณเจือจางรอบตัวจับอนุภาค สำหรับกรณีการจับอนุภาคโดยกลุ่มตัว
 จับแม่เหล็ก เราพบว่าลักษณะการกระจายค่าความเข้มข้นรอบตัวจับทรงกระบอกแม่เหล็กเปลี่ยน
 ไปอย่างไม่มีนัยสำคัญเมื่อแปรค่าสัดส่วนการบรรจุทรงกระบอกแม่เหล็กในของไหลในช่วงค่าเบา
 บาง แต่ปริมาตรของอนุภาคที่ถูกจับอยู่ในบริเวณอิมตัวบนผิวตัวจับประมาณเพิ่มขึ้นในลักษณะที่
 แปรผันตรงกับค่าสัดส่วนการบรรจุตัวจับในของไหลและเพิ่มขึ้นอย่างรวดเร็วเมื่อสนามแม่เหล็กคง
 ตัวที่ป้อนให้กับระบบมีค่าเพิ่มขึ้น

ภาควิชา.....ฟิสิกส์.....ลายมือชื่อนิสิต.....

สาขาวิชา.....ฟิสิกส์.....ลายมือชื่ออาจารย์ที่ปรึกษา.....

ปีการศึกษา 2547

4472201123 : MAJOR PHYSICS

KEY WORD: DIFFUSIVE CAPTURE / HGMS / EFFECTIVE MEDIUM MODEL/ CAPTURE SIMULATION

KANOK HOURNKUMNUARD : DIFFUSIVE CAPTURE OF MAGNETIC PARTICLES
BY AN ASSEMBLAGE OF RANDOM CYLINDRICAL COLLECTORS.

THESIS ADVISOR : ASSOC. PROF. MAYUREE NATENAPIT, Ph.D., 142 pp.

ISBN 974-53-1783-7.

Theoretical models describing the capture of ultra-fine weakly magnetic particles in high gradient magnetic field are developed. We begin with the capture of ultra-fine particles in one dimension by a single ferromagnetic cylindrical collector. Later, we extend to the two dimensional case. Finally, we investigate the capture of ultra-fine particles by an assemblage of parallel magnetic cylinders randomly distributed in static fluid in two dimensions. An effective medium treatment is used to improve the theoretical model describing the capture of ultra-fine particle of Davies and Gerber which assumed a single collector in fluid. In our model, only one representative cell is considered while the surrounding cells are replaced by a homogeneous medium with an effective permeability. The continuity equation describing dynamics of particle volume concentration is solved and the steady-state solution is determined analytically while the time-dependent solutions are obtained numerically. In this research, we develop a computer program to simulate the capture of ultra-fine particles in various physical situations.

From our results, the concentration contours generated in various physical situations are analyzed which indicate saturation, accumulation and depletion regions around the collector. In the case of the capture of ultra-fine particles by an assemblage of random magnetic collectors, the distribution of concentration around collectors changes insignificantly with varying packing fraction of the collectors in the dilute limit. The amount of particles captured in saturation regions on the collector surface increases, approximately, linearly proportional to the collector packing fraction in the fluid and increases rapidly with the strength of the uniform external magnetic field.

Department.....Physics..... Student's signature.....

Field of study.....Physics..... Advisor's signature.....

Academic year 2004

Acknowledgements

This thesis is finished with the great kindly and helpful suggestions and supports from my thesis advisor, Associate Professor Dr. Mayuree Natenapit .

Consequently, I wish to express my sincere gratitude to her. The completeness of this thesis is achieved with valuable comments and suggestions from all thesis committee, Assistance Professor Dr. Pisistha Ratanavararak, Dr. Sojiphong Chatraphorn, and Dr. Patcha Chatraphorn and my sincere gratitude is also expressed for every committee.

My great gratitude is also expressed to every staffs of the Department of Physics at Chulalongkorn University and Silpakorn University for their encouragements.

Lastly, I would like to give a special thank to my parents for my birth, their loves and encouragements.



สถาบันวิทยบริการ
จุฬาลงกรณ์มหาวิทยาลัย

Contents

	page
Abstract in Thai.....	iv
Abstract in English.....	v
Acknowledgements.....	vi
Contents.....	vii
List of Figures.....	xi
List of Notations.....	xiv
Chapter	
I INTRODUCTION.....	1
1.1 Introduction to High Gradient Magnetic Separation.....	1
1.2 Thesis Background.....	1
1.3 Thesis Objectives.....	3
1.4 Thesis Outline.....	3
II General Theory of Ultra-Fine Particle Capture in	
High Gradient Magnetic Separation.....	4
2.1 The Physical Principle and the Mechanism of	
High Gradient Magnetic Separation.....	4
2.2 HGMS Theory Describing the Capture of Ultra-fine Magnetic Particles.....	7
2.2.1 The Continuity Equation.....	7
2.3 Capture of Ultra-fine Particles by a Single Cylindrical Collector.....	9
2.3.1 The Magnetic Field and the Magnetic Traction Force.....	10
2.3.2 One Dimensional Capture of Ultra-fine Weakly	
Magnetic Particles.....	12
2.3.3 Two Dimensional Capture of Ultra-fine Weakly	
Magnetic Particles.....	14

Chapter	page
III Capture of Ultra-fine Magnetic Particles by an Assemblage of Random Cylindrical Collectors	16
3.1 Character of the Problem.....	16
3.2 The Effective Medium Model.....	17
3.3 Continuity Equation Describing the Capture of Ultra-Fine Weakly Magnetic Particles by an Assemblage of Random Cylindrical Paramagnetic Collectors.....	20
IV Simulations of HGMS Capture of Ultra-Fine Particles	23
4.1 One Dimensional Simulation of the Capture of Ultra-Fine Particles by a Single-Ferromagnetic Cylindrical Collector.....	23
4.1.1 The Steady-State Solution.....	24
4.1.2 Time-Dependent Solution.....	25
4.1.2.1 Errors of the Computation.....	28
4.1.2.2 Stability of the Computation.....	29
4.1.2.3 Initial Condition of the Computation.....	31
4.1.2.4 Saturation Condition.....	31
4.1.2.5 Boundary Conditions of the Computation.....	32
4.1.2.5.1 Outer Boundary Condition.....	32
4.1.2.5.2 Boundary Condition at the Impervious Surface.....	32
4.1.2.6 Parameters of Simulations.....	33
4.1.2.7 Procedures of the Simulation.....	34
4.2 Two Dimensional Simulations of the Capture of Ultra-Fine Particles.....	35
4.2.1 The Two Dimensional Computational Domain.....	36
4.2.2 The Computation of Approximated Time-Dependent Solutions.....	37

Chapter	page
4.2.3 Errors of the Computation.....	40
4.2.4 The Stability of the Simulation.....	41
4.2.5 Initial Condition of the Simulation.....	42
4.2.6 Saturation Condition.....	42
4.2.7 Boundary Conditions.....	43
4.2.7.1 Outer Boundary Condition.....	43
4.2.7.2 Boundary Condition at the Surface of the Collector or at the Surface of the Saturation Region.....	45
4.2.8 Parameters of Simulations.....	46
4.2.9 Procedure of the Simulation.....	46
V Results of Simulations and Discussions	47
5.1 One Dimensional Simulations of the Capture of Ultra-Fine Particles by a Single-Ferromagnetic Cylindrical Collector.....	47
5.1.1 Paramagnetic Mode of the Capture.....	47
5.1.2 Diamagnetic Mode of the Capture.....	51
5.2 Two Dimensional Simulations of the Capture of Ultra-Fine Particles by a Single-Ferromagnetic Cylindrical Collector.....	56
5.2.1 Paramagnetic Mode of the Capture.....	56
5.2.2 Diamagnetic Mode of the Capture.....	66
5.3 Two Dimensional Simulations of the Capture of Ultra-Fine Particles by an Assemblage of Random Paramagnetic Cylindrical Collectors.....	72
5.3.1 The Effect of Variation of Packing Fraction to Features of Concentration Distributions in the Representative Cell.....	72
5.3.2 The Effect of Variation of Packing Fraction to the Amounts of Particles Captured in Saturation Regions.....	83

Chapter	page
5.3.3 The Effect of Variation of Uniform External Magnetic Field to the Amounts of Particles Captured in Saturation Regions.....	85
VI CONCLUSIONS.....	87
REFERENCES.....	89
APPENDICES.....	91
APPENDIX A Magnetic Field Around a Ferromagnetic Cylindrical Collector.....	92
APPENDIX B Magnetic Field for an Assemblage of Random Cylindrical Paramagnetic Collectors.....	97
APPENDIX C Approximating Derivatives of Functions by Finite-Difference Relations.....	102
APPENDIX D Errors and Stability of the Computation for Simulations of the Capture of Ultra-Fine Particles in One Dimension.....	106
APPENDIX E Errors and Stability of the Computation for Simulations of the Capture of Ultra-Fine Particles in two Dimensions	111
APPENDIX F Approximating the Continuity Equation at the Point on the Impervious Surface.....	118
APPENDIX G Steady-State Solutions of HGMS Continuity quation.....	123
BIOGRAPHY.....	127

List of Figures

Figure	page
2.1 The mechanism of high gradient magnetic separation.....	6
2.2 A single cylindrical collector in formerly uniform magnetic field.....	10
3.1 A representative cylindrical cell.....	18
4.1 The grid in finite-difference method.....	26
4.2 Three main procedures of the simulation.....	34
4.3 A two dimensional circular grid.....	36
4.4 The outer boundary of the representative cell as an impervious surface.....	44
4.5 Surface of the collector or the saturation region as an impervious surface.....	45
5.1 Time evolution of concentration distribution at $\theta = 0$ radian in paramagnetic mode, $G_0^{ferro} = -16.62$, $K_w = 0.80$	48
5.2 Time evolution of concentration distribution at $\theta = \pi/2$ radian in paramagnetic mode, $G_0^{ferro} = -16.62$, $K_w = 0.80$	50
5.3 Time evolution of concentration distribution at $\theta = \pi/2$ radian in diamagnetic mode, $G_0^{ferro} = +17.18$, $K_w = 0.80$	52
5.4 Time evolution of concentration distribution at $\theta = 0$ radian in diamagnetic mode, $G_0^{ferro} = +17.18$, $K_w = 0.80$	53
5.5 Variation of τ_{sat} with H_0 in paramagnetic mode of one dimensional capture of $Mn_2P_2O_7$ particle.....	54
5.6 Variation of τ_{sat} with H_0 in paramagnetic mode of one dimensional capture of $Mn_2P_2O_7$ particles plotted in semi-logarithmic scale.....	55
5.7 A family of concentration contours around the ferromagnetic collector in paramagnetic mode, $G_0^{ferro} = -16.62$, $K_w = 0.80$	57
5.8 Concentration distribution at $\theta = 0, \pi$ radian at various normalized times in paramagnetic mode, $G_0^{ferro} = -16.62$, $K_w = 0.80$	59
5.9 Concentration distribution at $\theta = \pi/2, 3\pi/2$ radian at various normalized times in paramagnetic mode, $G_0^{ferro} = -16.62$, $K_w = 0.80$	60

Figure	page
5.10 Comparison between steady-state concentration distribution at $\theta = 0$ and $\pi/2$ radian in paramagnetic mode, $G_0^{ferro} = -16.62, K_W = 0.80$	61
5.11 Steady-state concentration contours around the ferromagnetic collector in paramagnetic mode, $G_0^{ferro} = -16.62, K_W = 0.80$	63
5.12 Variation of P_{sat} with τ in the paramagnetic mode, $G_0^{ferro} = -16.62, K_W = 0.80$	65
5.13 Variation of steady-state P_{sat} with H_0 in paramagnetic mode, $G_0^{ferro} = -16.62, K_W = 0.80$	66
5.14 A family of concentration contours around ferromagnetic collector in diamagnetic mode, $G_0^{ferro} = +17.18, K_W = 0.80, \tau = 0.10$	67
5.15 Time evolution of concentration distribution at $\theta = \pi/2, 3\pi/2$ radian in diamagnetic mode, $G_0^{ferro} = +17.18, K_W = 0.80$	68
5.16 Time evolution of concentration distribution at $\theta = 0, \pi$ radian in diamagnetic mode, $G_0^{ferro} = +17.18, K_W = 0.80$	69
5.17 Steady-state concentration contours around the ferromagnetic collector in diamagnetic mode, $G_0^{ferro} = +17.18, K_W = 0.80$	70
5.18 Variation of steady-state P_{sat} with H_0 in diamagnetic mode, $G_0^{ferro} = +17.18, K_W = 0.80$	71
5.19 A family of concentration contours around the paramagnetic collector in the representative cell, $F = 5\%, G_0^{random} = -16.95, \tau=0.10$	73
5.20 Time evolution of concentration distribution at $\theta = 0$ radian in the representative cell, $F = 5\%, G_0^{random} = -16.95$	75
5.21 Time evolution of concentration distribution at $\theta = \pi/2$ radian in the representative cell, $F = 5\%, G_0^{random} = -16.95$	76
5.22 A family of concentration contours around the paramagnetic collector in the representative cell, $F = 8\%, G_0^{random} = -17.16, \tau=0.10$	77
5.23 Time evolution of concentration distribution at $\theta = 0$ radian in the representative cell, $F = 8\%, G_0^{random} = -17.16$	78

Figure	page
5.24 Time evolution of concentration distribution at $\theta = \pi / 2$ radian in the representative cell, $F = 8\%$, $G_0^{random} = -17.16$	79
5.25 A family of concentration contours around the paramagnetic collector in the representative cell, $F = 10\%$, $G_0^{random} = -17.30$, $\tau=0.10$	80
5.26 Time evolution of concentration distribution at $\theta = 0$ radian in the representative cell, $F = 10\%$, $G_0^{random} = -17.30$	81
5.27 Time evolution of concentration distribution at $\theta = \pi / 2$ radian in the representative cell, $F = 10\%$, $G_0^{random} = -17.30$	82
5.28 Comparison of variations of P_{sat} with τ between $F = 5\%$, 8% , 10%	84
5.29 Comparison of variations of P_{sat} with τ between $H_0 = 2.0 \times 10^6$ A/m, 3.0×10^6 A/m	86
A.1 A magnetic collector and surrounding medium in a uniform magnetic field.....	92
B.1 A representative cylindrical composite cell.....	97
F.1 Impervious surface at the outer boundary of the representative cell.....	119
F.2 Impervious surface at the surface of the collector or the surface of saturation regions.....	121

List of Notations

u_m	magnetic energy density
\overline{H}	magnetic field
\overline{B}	magnetic induction
μ_0	magnetic permeability of free space
μ_c	magnetic permeability of the collector
μ_f	magnetic permeability of the fluid
μ_p	magnetic permeability of the ultra-fine particle
V	volume
U	increment of magnetic potential energy
χ_f	magnetic susceptibility of the fluid
χ_p	magnetic susceptibility of the ultra-fine particle
χ	effective magnetic susceptibility of the system composed of the fluid and ultra-fine particles
\overrightarrow{F}_m	magnetic force
c	particle volume concentration
\overline{J}	particle volume flux
D	diffusion coefficient
\vec{v}	drift velocity of the system of ultra-fine particles
u	mobility of ultra-fine particles in the fluid
k_B	Boltzmann's constant
T	absolute temperature in Kelvin
a	radius of cylindrical magnetic collector
b_p	radius of ultra-fine particle
M	magnetization of the ferromagnetic collector
\overrightarrow{H}_0	uniform external magnetic field
K_w	ratio $M / 2H_0$
r_a	normalized radial distance
τ	normalized time

F	packing fraction of cylindrical collectors in the fluid
b	radius of the representative cell
c_s	steady-state value of particle volume concentration
C_0	initial value of particle volume concentration
C_{sat}	saturation concentration
$(r_a)_i$	discrete normalized radial distance
τ^n	discrete normalized time
\mathbb{C}	numerical value of particle volume concentration
ε	order of approximating differential equation with difference equation
δc	error of computed numerical particle volume concentration
I	index of the position of an impervious point
τ_{sat}	the value of normalized time that saturation concentration begins to take place on the surface of the collector
P_{sat}	percent of the volume of ultra-fine particles captured in saturation regions from total volume of ultra-fine particles in the computational domain
Φ_M	magnetic scalar potential
$\Delta r_a, \Delta \theta, \Delta \tau$	grid steps

CHAPTER I

INTRODUCTION

1.1 Introduction to High Gradient Magnetic Separation

High Gradient Magnetic Separation (HGMS) is a powerful method for the removal of ultra-fine (diameter $\ll 1\mu\text{m}$) weakly magnetic particles from suspensions. The term “high gradient” comes from the character of this method that high gradient of magnetic field and magnetic energy density are produced in the separation process to maximize the magnetic force that acts on the magnetic particles to be captured. High Gradient Magnetic Separation of ultra-fine particles is applied in many fields of works, for example, chemical, blood separation in biochemical laboratory and pharmaceutical industries. Consequently, high gradient magnetic separation may become an important part of future technology and it is, therefore, desirable to understand its mechanism.

1.2 Thesis Background

The capture of weakly magnetic particles by high gradient magnetic separation had been studied by many researchers [1, 2]. Initially, the studies are performed for the capture of micron-size particles. In those studies, the capture of magnetic particles is studied by applying Newton's laws of motion to an individual particle. The motion of an individual particle is analyzed to know whether it will be captured by interception. The trajectories of the particles are determined so that features of the capture and capture radius are obtained to predict capture efficiency.

For ultra-fine weakly magnetic particles which are much smaller than the micron size, Brownian motion dominates the kinematics of such particles and this affects the capture process. Diffusion must be taken into account and diffusive capture is considered. In 1983, R. Gerber, M. Takayasu and F.J. Fridlaender formulated the HGMS theory describing the capture mechanism of ultra-fine particles [3, 4]. The theory of

R. Gerber and coworkers incorporate diffusion in describing the capture mechanism of ultra-fine particles. Capture of ultra-fine particles in one dimension by a single ferromagnetic cylindrical collector is simulated in various situations. Results of these simulations show the features of the build-up of ultra-fine particles on and around the collector and the qualitative agreement between the theoretical and experimental results is achieved. With these results, the mechanism of the capture of ultra-fine particles can be investigated. After the work of R. Gerber and coworkers, other researchers had studied HGMS capture of ultra-fine particles in various cases [5, 6, 7]. In 1990, L. P. Davies and R. Gerber developed a two dimensional theoretical model for the capture of ultra-fine particles on a single ferromagnetic cylindrical collector [8]. This model is a generalization of the theoretical model formulated in 1983. They considered two dimensional diffusive capture including magnetic force and fluid velocity drag force. The inter-particle forces are disregarded since the objective of the work is to obtain a simplified two dimensional model that highlight the main features of the retention of ultra-fine particles by a single ferromagnetic cylindrical collector at various times. The capture of ultra-fine particles was simulated in various cases. Results of simulations show the feature of the build-up of ultra-fine particles in various regions around the collector at various times. Consequently, the behavior of the build-up of ultra-fine particles on the collector were predicted. All former theoretical models considered the capture of ultra-fine particles by a single collector. However, in practical applications of HGMS, a certain magnetic separator does not contain only one collector but consists of many collectors. To study the capture of ultra-fine particles by these collectors, a generalized theoretical model must be formulated.

In this thesis, the former works of R. Gerber and coworkers are studied in more details, both one dimensional and two dimensional problems are investigated. Further more, we extend the single collector theoretical model for the capture of ultra-fine magnetic particles to the case of an assemblage of parallel cylindrical collectors randomly distributed in the static fluid. The only geometrical character of the system that we know is the ratio of total volume of collectors to the total volume of the system which is defined as the packing fraction (F) of the collectors in the system.

We study diffusive capture in various situations by, starting from the continuity equation, deriving equations describing concentration distribution of ultra-fine particles dispersed in a static fluid at various times. The steady-state solutions of these equations can be determined analytically whereas the time-dependent solutions are determined numerically. The given solutions can be examined to investigate the features of the capture in various physical situations. The SI units are used throughout this thesis.

1.3 Thesis Objectives

In conclusion, objectives of this thesis are:

- 1) Develop a theoretical model describing the capture of ultra-fine particles by an assemblage of randomly distributed cylindrical collectors.
- 2) Develop computer programs for performing simulations of the capture of ultra-fine particles in various physical situations.
- 3) Study HGMS capture of ultra-fine particles in both one and two dimensional problems in various physical situations.

1.4 Thesis Outline

A brief outline of this thesis is as follows: Chapter I provides introduction to high gradient magnetic separation, background and objectives of this research. Chapter II starts with physical principle and mechanism of high gradient magnetic separation then the formulation of the generalized theory describing the capture of ultra-fine particles is presented. In Chapter III, the problem of the capture of ultra-fine particles by an assemblage of randomly distributed cylindrical collectors in static fluid is described. The character of the problem and the model used in studying the problem are introduced. In Chapter IV, simulations of the capture of ultra-fine particles in various cases are studied. The main content of Chapter IV is the numerical method and simulation methodology. The results of the simulations and discussions are presented in Chapter V. Finally, Chapter VI provides the conclusions of this research.

CHAPTER II

General Theory of Ultra-Fine Particle Capture in High Gradient Magnetic Separation

The physical principle and the mechanism of high gradient magnetic separation are described in the first section. Subsequently in the second section, the formulation of the general theory describing the capture of ultra-fine particles in high gradient magnetic field is presented. Finally in the third section, some theoretical considerations on the capture of ultra-fine particles by a single cylindrical collector are introduced.

2.1 The Physical Principle and the Mechanism of High Gradient Magnetic Separation

From electromagnetic theory, the magnetic energy density in a medium is expressed in general as

$$u_m = \frac{1}{2} \vec{H} \cdot \vec{B}, \quad (2.1)$$

where \vec{H} and \vec{B} are magnetic field and magnetic induction in the medium, respectively.

Consider an assembly of ultra-fine magnetic particles dispersed in a fluid. In this thesis, we treat both fluid and ultra-fine particles as linear isotropic homogeneous magnetic media. Imagine a volume V_p demarcated inside the fluid. The magnetic energy of the fluid enclosed in this volume is $(\frac{1}{2} \vec{H} \cdot \vec{B}) V_p = \frac{1}{2} \mu_f V_p H^2$ where μ_f is the magnetic permeability of the fluid. Let us now remove the fluid from the volume V_p and replace it by an ultra-fine particle. The magnetic energy associated with the particle itself is $\frac{1}{2} \mu_p V_p H^2$ where μ_p is the magnetic permeability of the particle.

The energy increment U of the system (fluid + particle) is given as the difference

between these two energies, i.e.

$$U = \frac{1}{2}(\mu_p - \mu_f)V_p H^2. \quad (2.2)$$

Taking positive gradient ($\vec{\nabla}U$) of this energy increment, we get the magnetic force acting on the ultra-fine particle as

$$\vec{F}_m = \frac{1}{2}\mu_0\chi V_p \vec{\nabla}(H^2), \quad (2.3)$$

where $\chi = \chi_p - \chi_f$ is the difference between magnetic susceptibilities of the particle and the fluid, respectively, $\mu_0 = 4\pi \times 10^{-7} \text{ T} \cdot \text{m} / \text{A}$ is the permeability of free space.

The mechanism of high gradient magnetic separation is based on the utilization of this magnetic traction force which extracts the ultra-fine magnetic particles from the fluid. From equation (2.3), we can see that the magnetic traction force is proportional to the difference $\chi_p - \chi_f$. This difference is usually very small for weakly magnetic particles, and also the magnetic field magnitude H can not be increased above a certain upper limit for technical reasons. Thus an efficient extraction, which results from a large value of \vec{F}_m , requires that the value of $\vec{\nabla}(H^2)$ must be high.

The mechanism of operation of high gradient magnetic separation is shown in Figure 2.1

สถาบันวิทยบริการ
จุฬาลงกรณ์มหาวิทยาลัย

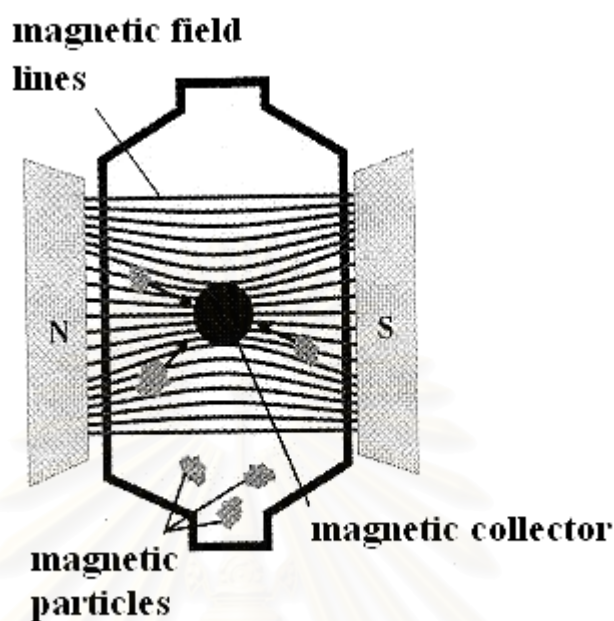


Figure 2.1: The mechanism of high gradient magnetic separation [9].

In Figure 2.1, a magnetic collector made from ferromagnetic or paramagnetic materials of cylindrical (or spherical) shape and a fluid with suspended magnetic particles are contained in a non-magnetic canister. A uniform external magnetic field \vec{H}_0 is applied perpendicular to the axis of the collector. The existence of the collector disturbs the uniformity of the applied magnetic field. Consequently, there exist regions of high gradient magnetic field outside the collector. Any magnetic particles in or entering these regions are subjected to the large magnetic traction force. To capture these particles at the collector, it is necessary that the magnetic traction force is directed towards the collector and is large enough to prevail over the action of other forces and processes so that particles are brought to and retained at the collector.

The other forces and processes involved can be the viscous drag force of the fluid, the gravity force, thermal diffusion, and inter-particles effects, etc. Not all of these forces and processes are significant in a certain situation. In some situations, we can reasonably approximate that some forces or processes are largely significant than others.

2.2 HGMS Theory Describing the Capture of Ultra-fine Magnetic Particles

The HGMS theory describing the capture of ultra-fine magnetic particles was formulated in 1983 by R.Gerber, M. Takayasu and F.J. Friedlander [3, 4]. The theory describes dynamics of ultra-fine magnetic particles dispersed in a fluid and subjected to high gradient magnetic separation process. In the theory, a statistical approach was used since, due to Brownian motion and diffusion, the actual trajectory and velocity of an ultra-fine particle are of little significance for the description of the capture process and it is difficult to decide whether a given particle will be captured.

2.2.1 The Continuity Equation

The HGMS theory formulated by Gerber and coworkers in 1983 describes dynamics of the capture of ultra-fine particles in terms of particle volume concentration and particle drift velocity denoted by c and \vec{v} , respectively. The particle volume concentration at a given point in the fluid is defined as the fraction of ultra-fine particles volume contained in an infinitesimal volume element of fluid at that point and is expressed as

$$c \equiv \lim_{\Delta V_f \rightarrow 0} \frac{\Delta V_p}{\Delta V_f}, \quad (2.4)$$

where subscripts p and f refer to the ultra-fine particle and the fluid, respectively.

The value of particle volume concentration is a function of positions in fluid and time and it satisfies the continuity equation

$$\frac{\partial c}{\partial t} + \vec{\nabla} \cdot \vec{J} = 0, \quad (2.5)$$

where \vec{J} is the total particle volume flux through an infinitesimal volume element of fluid locate at the considered point. The particle volume flux is defined as the net volume of

ultra-fine particles that flow through an area perpendicular to the flow per unit area per unit time.

For ultra-fine particles, \vec{J} at a given point in fluid is considered to consists of two contributions as

$$\vec{J} = \vec{J}_D + \vec{J}_F, \quad (2.6)$$

where \vec{J}_D denotes the diffusion flux due to diffusion and \vec{J}_F denotes the particle volume flux due to the actions of external forces on the system of particles.

Diffusion flux can be determined by Fick's law as [10]

$$\vec{J}_D = -D\vec{\nabla}c, \quad (2.7)$$

where D is the diffusion coefficient of ultra-fine particles in the fluid.

The particle volume flux due to the actions of external forces which impose a drift velocity \vec{v} on the system of ultra-fine particles is expressed as [11]

$$\vec{J}_F = c\vec{v}. \quad (2.8)$$

The drift velocity of ultra-fine particles at a given point in the fluid is determined by the relation [12]

$$\vec{v} = u\vec{F}, \quad (2.9)$$

where u is the mobility of ultra-fine particles in the fluid and \vec{F} is the total external force acted upon those particles. \vec{F} is the vectorial sum of magnetic traction force, fluid viscous drag force, electric force, gravitational force, and other forces those acted on the system of ultra-fine particles.

When expressions of \vec{J}_D and \vec{J}_F in equations (2.7) and (2.8), respectively, are substituted in equation (2.5) we obtain the continuity equation for the

system of ultra-fine particles as

$$\frac{\partial c}{\partial t} = \bar{\nabla} \cdot (D \bar{\nabla} c) - \bar{\nabla} \cdot (c \bar{v}). \quad (2.10)$$

The diffusion coefficient of ultra-fine particles in the fluid is determined, throughout this research, by Einstein's relation [12],

$$D = uk_B T, \quad (2.11)$$

where k_B and T are the Boltzmann's constant and the absolute temperature, respectively, and the value of D is assumed to be independent of the positions in fluid.

With this assumption, the continuity equation (2.10) is rewritten as

$$\frac{\partial c}{\partial t} = D \bar{\nabla}^2 c - \bar{\nabla} \cdot (c \bar{v}). \quad (2.12)$$

Equation(2.12) is the continuity equation describing dynamics of the system of ultra-fine particles in high gradient magnetic separation for the general case.

In this research, the capture of ultra-fine particles in high gradient magnetic separation is studied theoretically in various situations. In each situation, equation(2.12) is solved to obtain the time evolution of the concentration distribution in various regions around the collector when some initial and boundary conditions are assigned.

2.3 Capture of Ultra-fine Particles by a Single Cylindrical Collector

In this section, some theoretical studies about the capture of ultra-fine magnetic particles by a single cylindrical magnetic collector are introduced. These studies are bases of this research and are presented to show the development of the theoretical studying of the HGMS capture of ultra-fine particles.

2.3.1 The Magnetic Field and the Magnetic Traction Force

Consider a long circular cylindrical magnetic collector of radius a placed in a static fluid as shown in Figure 2.2. The magnetic permeability and susceptibility of the fluid are μ_f and χ_f , respectively.

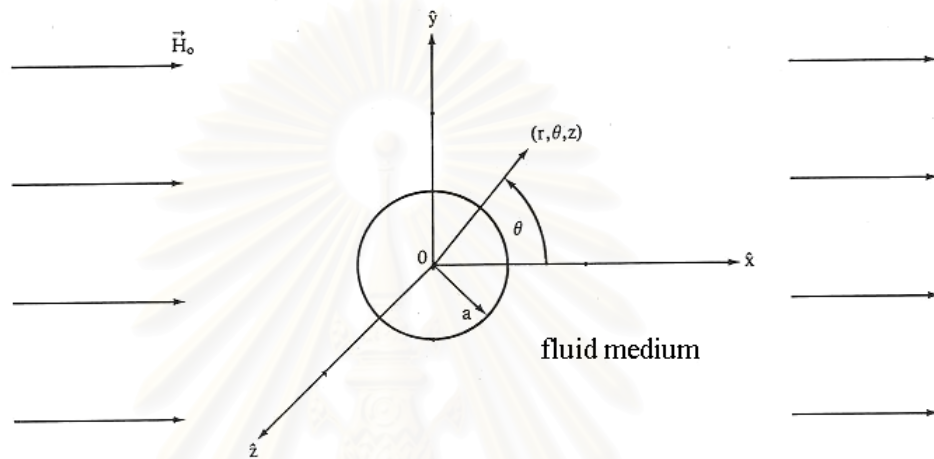


Figure 2.2: A single cylindrical collector in formerly uniform magnetic field.

In Figure 2.2, the z -axis of the cylindrical coordinate system is chosen to coincide with the axis of the collector. A uniform magnetic field \vec{H}_0 is applied perpendicular to the axis of the collector and is set to point in the positive X direction. The collector is considered very long compared with its diameter hence the problem of determining the magnetic field \vec{H} in and around the collector can be treated only in two dimensions. If the collector is the ferromagnetic one with the magnetization M then the magnetic field outside the collector can be determined in polar coordinates as (see Appendix A)

$$\vec{H}^{ferro}(r_a, \theta) = H_0 \left[\left(1 + \frac{K_w}{r_a^2} \right) \cos \theta \hat{r} - \left(1 - \frac{K_w}{r_a^2} \right) \sin \theta \hat{\theta} \right], \quad (2.13)$$

where

$$K_w = \frac{M}{2H_0}. \quad (2.14)$$

The variable

$$r_a \equiv \frac{r}{a} \quad (2.15)$$

is called the normalized radial distance and is defined as the radial distance from the axis of the collector to the considering point normalized by the radius of the collector.

In the other case where the collector is the paramagnetic one with the magnetic permeability μ_c , the magnetic field outside the collector is determined as

$$\vec{H}^{para}(r_a, \theta) = H_0 \left[\left(1 + \frac{K_C}{r_a^2} \right) \cos \theta \hat{r} - \left(1 - \frac{K_C}{r_a^2} \right) \sin \theta \hat{\theta} \right], \quad (2.16)$$

where

$$K_C \equiv \frac{\nu - 1}{\nu + 1}, \quad (2.17)$$

and

$$\nu \equiv \frac{\mu_c}{\mu_f}. \quad (2.18)$$

For the ferromagnetic cylindrical collector, the term $\vec{\nabla}(H^2)$ in equation (2.3) can be determined as

$$\vec{\nabla}(H^2)^{ferro} = -\frac{2MH_0}{a} \left[\left(\frac{\cos(2\theta)}{r_a^3} + \frac{K_W}{r_a^5} \right) \hat{r} + \left(\frac{\sin(2\theta)}{r_a^3} \right) \hat{\theta} \right]. \quad (2.19)$$

The magnetic traction force acting on the system of spherical ultra-fine particles, each of radius b_p , then can be obtained as

$$\vec{F}_m^{ferro} = -\frac{4\pi\mu_0(\chi_p - \chi_f)MH_0b_p^3}{3a} \left[\left(\frac{\cos(2\theta)}{r_a^3} + \frac{K_W}{r_a^5} \right) \hat{r} + \left(\frac{\sin(2\theta)}{r_a^3} \right) \hat{\theta} \right]. \quad (2.20)$$

For the case of paramagnetic collector, the term $\vec{\nabla}(H^2)$ is

determined as

$$\bar{\nabla} (H^2)^{para} = -\frac{4K_C H_0^2}{a} \left[\left(\frac{\cos(2\theta)}{r_a^3} + \frac{K_C}{r_a^5} \right) \hat{r} + \left(\frac{\sin(2\theta)}{r_a^3} \right) \hat{\theta} \right], \quad (2.21)$$

and the magnetic traction force acting on the system of spherical ultra-fine particles, each of radius b_p , then is obtained as

$$\vec{F}_m^{para} = -\frac{8\pi\mu_0 (\chi_p - \chi_f) K_C H_0^2 b_p^3}{3a} \left[\left(\frac{\cos(2\theta)}{r_a^3} + \frac{K_C}{r_a^5} \right) \hat{r} + \left(\frac{\sin(2\theta)}{r_a^3} \right) \hat{\theta} \right]. \quad (2.22)$$

From equations (2.20) and (2.22), we can see that if other parameters such as the difference $\chi_p - \chi_f$ and the radius of ultra-fine particle b_p are held fixed then the large applied external uniform magnetic field \vec{H}_0 and the very small radius a of the collector can give rise to a large magnetic traction force per unit volume of ultra-fine particle. This large magnetic traction force causes the separation to be efficient.

2.3.2 One Dimensional Capture of Ultra-fine Weakly Magnetic Particles

The capture of ultra-fine magnetic particles in one dimension was studied theoretically by Gerber and coworkers in 1983 [3, 4]. In their study, the single cylindrical collector is modeled to be a ferromagnetic one and the capture is considered only in the radial direction.

The continuity equation (2.12) in the one dimensional problem can be written as

$$\frac{\partial c}{\partial t} = D \frac{\partial^2 c}{\partial r^2} - \frac{\partial}{\partial r} (c v_r). \quad (2.23)$$

In their study, a new dimensionless variable called normalized time, denoted by τ , is defined as

$$\tau \equiv \frac{Dt}{a^2}. \quad (2.24)$$

With the definitions of this normalized time and the normalized radial distance r_a defined in equation (2.15), we can obtain the continuity equation rewritten in terms of these dimensionless variables as

$$\frac{\partial c}{\partial \tau} = \frac{\partial^2 c}{\partial r_a^2} - \frac{\partial}{\partial r_a}(G_r c), \quad (2.25)$$

where it is defined that

$$G_r \equiv \frac{av_r}{D}. \quad (2.26)$$

The equation (2.25) describes dynamics of the system of ultra-fine particles in high gradient magnetic separation in one dimension. In their work, it is assumed that only the dominant magnetic traction force are considered, consequently the expression of G_r can be determined by using equations (2.9), (2.11) and (2.20) as

$$G_r(r_a, \theta) = G_0^{ferro} \left[\frac{\cos(2\theta)}{r_a^3} + \frac{K_W}{r_a^5} \right], \quad (2.27)$$

where it is defined that

$$G_0^{ferro} \equiv -\frac{4\pi\mu_0(\chi_p - \chi_f)MH_0b_p^3}{3k_B T}. \quad (2.28)$$

From this definition of G_0^{ferro} , when $\chi_p > \chi_f$ the capture is called to be the paramagnetic mode. For the opposite case where $\chi_p < \chi_f$, the capture is called to be the diamagnetic mode.

The one dimensional capture of ultra-fine weakly magnetic particles by a single ferromagnetic collector was studied theoretically by solving equation (2.25) for various cases when some initial and boundary conditions are given. This theoretical study is performed in Chapter IV.

2.3.3 Two Dimensional Capture of Ultra-fine Weakly Magnetic Particles

The one dimensional theoretical model for the capture of ultra-fine weakly magnetic particles developed in 1983 by Gerber and coworkers [3, 4] was generalized to the two dimensional case in 1990 by Gerber and L. P. Davies [8]. The objective of the later work was to construct a simplified two dimensional theoretical model which will highlight the main features of the time dependent HGMS capture of ultra-fine weakly magnetic particles by a single ferromagnetic cylindrical collector.

The continuity equation (2.12) for this generalized problem is

$$\frac{\partial c}{\partial t} = D \left[\frac{1}{r} \frac{\partial}{\partial r} \left(r \frac{\partial c}{\partial r} \right) \right] + \frac{D}{r^2} \frac{\partial^2 c}{\partial \theta^2} - \left[\frac{1}{r} \frac{\partial}{\partial r} (rcv_r) + \frac{1}{r} \frac{\partial}{\partial \theta} (cv_\theta) \right]. \quad (2.29)$$

Equation (2.29) can be rewritten in terms of the normalized radial distance r_a and the normalized time τ defined in equations (2.15) and (2.24), respectively as

$$\frac{\partial c}{\partial \tau} = \left\{ \frac{\partial^2 c}{\partial r_a^2} + \frac{1}{r_a} \frac{\partial c}{\partial r_a} + \frac{1}{r_a^2} \frac{\partial^2 c}{\partial \theta^2} \right\} - \left\{ \frac{G_r c}{r_a} + \frac{\partial}{\partial r_a} (G_r c) + \frac{1}{r_a} \frac{\partial}{\partial \theta} (G_\theta c) \right\}, \quad (2.30)$$

where it is defined that

$$G_\theta \equiv \frac{av_\theta}{D}, \quad (2.31)$$

and G_r is already defined in equation (2.26).

By using equations (2.9), (2.11) and (2.20), it is determined, for the case of the ferromagnetic collector, that

$$G_r(r_a, \theta) = G_0^{ferro} \left[\frac{\cos(2\theta)}{r_a^3} + \frac{K_w}{r_a^5} \right], \quad (2.32)$$

and

$$G_\theta(r_a, \theta) = \frac{G_0^{ferro} \sin(2\theta)}{r_a^3}, \quad (2.33)$$

where G_0^{ferro} for this ferromagnetic case is already defined in equation (2.28).

From equations(2.32) and (2.33), we can see that when the single cylindrical collector is a paramagnetic one, the forms of these equations are remain the same but the variable K_w is replaced by K_c . The expression of factor G_0 for the paramagnetic case can be obtained, by using equations (2.9), (2.11) and (2.22), as

$$G_0^{para} = - \frac{8\pi\mu_0 (\chi_p - \chi_f) K_c H_0^2 b_p^3}{3k_B T}, \quad (2.34)$$

where K_c is already defined in equation (2.17);

The capture of ultra-fine weakly magnetic particles in two dimensions by a single cylindrical collector is studied in this research in the case of ferromagnetic cylindrical collector.

CHAPTER III

Capture of Ultra-fine Magnetic Particles by an Assemblage of Random Cylindrical Collectors

In this chapter, the consideration on HGMS capture of ultra-fine magnetic particles is extended from the case of single cylindrical collector which has been described in the previous chapter to the case of randomly distributed cylindrical collectors. The main work of this research is to study, theoretically, the capture of ultra-fine weakly magnetic particles by an assemblage of random cylindrical paramagnetic collectors in high gradient magnetic field. The first section of this chapter provides the character of the problem to be studied. Subsequently in the second section, the model used for the study of the problem is introduced. The connection between the old problem in the previous chapter and the extended one in this chapter is also shown in the second section. Finally in the third section, the continuity equation describing dynamics of the system of ultra-fine particles for the new problem is presented.

3.1 Character of the Problem

We consider a system consists of two parts. The first part is a static fluid with an assembly of monotype ultra-fine weakly magnetic particles as a suspension. Both fluid and particle are considered to be linear isotropic homogeneous magnetic media. The other part is an assemblage of paramagnetic cylindrical collectors randomly distributed in the fluid. These collectors are considered to have characteristic distributions of cylindrical radii and are very long compared with their diameters. In this research, axes of these collectors are considered all parallel. The system of fluid and collectors are contained in a non-magnetic canister. A uniform magnetic field \vec{H}_0 is applied perpendicular to axes of these collectors. We study dynamics of the capture of

ultra-fine particles by these collectors. The only characteristic of the system we know is the packing fraction, denoted by F , of the cylindrical collectors in the system which is defined as the ratio of total volume of cylindrical collectors to the total volume of the system.

3.2 The Effective Medium Model

Basically, the capture of ultra-fine particles by an assemblage of random cylindrical collectors is different from the case of single cylindrical collector. When the number of the collector used in the capture process is more than one, the existence of other collectors produces some effects on the capture operation of an individual collector. These effects must be estimated and taken into account when the capture of ultra-fine particles by an assemblage of random cylindrical collectors is studied.

Since all collectors in the system are randomly distributed, when an arbitrary collector is considered, all residual collectors locate randomly with respect to it. This situation is the same for any collectors in the system. Since the assemblage of collectors have characteristic distributions of cylindrical radii, the distribution of collectors' radii surrounding an arbitrary collector is random. From this, we can reasonably approximate that the capture operation of an arbitrary collector is affected by the existence of other collectors equally.

From the theoretical consideration on the capture of ultra-fine particles by a single paramagnetic collector in chapter II, we can see, from equations (2.30), (2.32), (2.33) and (2.34), that these equations do not depend on the size (radius) of the collector explicitly since they are expressed in term of normalized radial distance r_a and there is no factor which depend on the radius of the collector explicitly. This means that when capture operations of ultra-fine particles by two cylindrical collectors of difference radii are considered separately, the distributions of particle volume concentration at the same normalized radial distance from the axes of these collectors have the same feature.

The magnetic field around the assemblage of cylindrical paramagnetic collectors randomly distributed in a fluid had been determined in 1988 by Natenapit [13]. In that calculation, the effective medium model originally conceived by Hashin [14] is adopted. In the effective medium model, the system of magnetic cylinders (permeability μ_c) and surrounding fluid (permeability μ_f) is considered to be composed of cylindrical composite cells, each containing exactly one of the cylinders. In this model, only a representative cell is considered, while the neighbor cells are replaced by a homogeneous medium with effective permeability μ^* to be determined. Figure 3.1 shows a representative cell in the effective medium model which is used to determine the magnetic field in the cell.

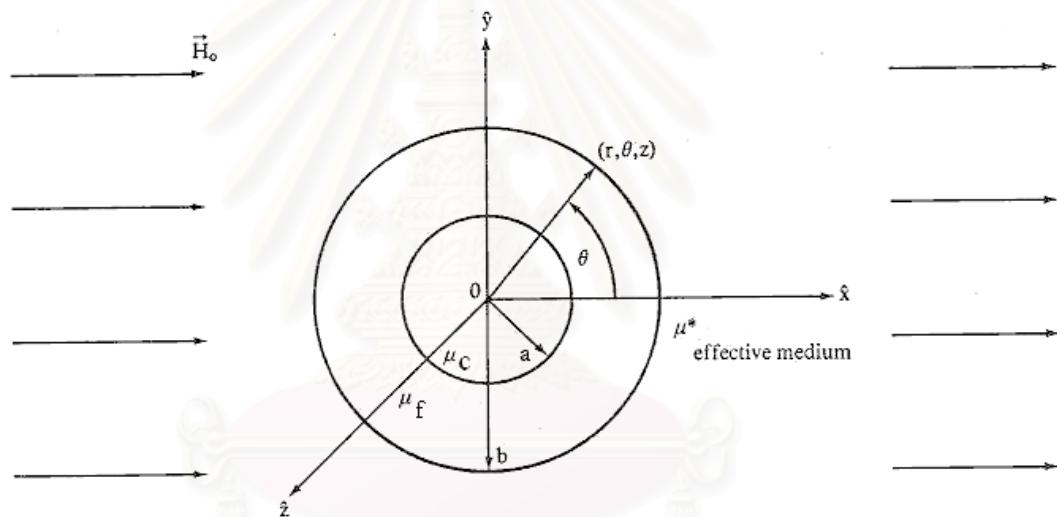


Figure 3.1: A representative cylindrical cell [13].

In Figure 3.1, a is radius of the collector where b is the radius of the representative cell. Since the ratio of the collector to cell volume is set equal to the packing fraction of collectors in the fluid then we obtain

$$F = \frac{a^2}{b^2}. \quad (3.1)$$

The Z -axis of cylindrical coordinate system is set along the cylinder axis.

To determine the magnetic field in the cell, the boundary value problem of coaxial magnetic cylinders subject to the boundary condition of uniform magnetic field at far away from the cell is solved. Since according to the effective medium model, any composite cell can be chosen to be the representative cell and the residual cells are considered to be a homogeneous effective medium, then a self consistency must be satisfied that the magnetic induction (\vec{B}) averaged over the representative cell (cylindrical collector plus fluid) must equal to the volume average of the magnetic induction over the effective medium.

According to Natenapit [13], the magnetic field in the fluid surrounding the collector in a representative cell is determined as (see Appendix B)

$$\vec{H}_f = AH_0 \left[\left(1 + \frac{K_C}{r_a^2} \right) \cos \theta \hat{r} - \left(1 - \frac{K_C}{r_a^2} \right) \sin \theta \hat{\theta} \right], \quad 1 < r_a < \frac{b}{a}, \quad (3.2)$$

where

$$A \equiv \frac{1}{1 - FK_C}, \quad (3.3)$$

and K_C has been already defined in equation (2.17) of chapter II.

The magnetic field in the effective medium outside the representative cell is determined as

$$\vec{H}_{Eff} = \vec{H}_0, \quad \frac{b}{a} < r_a < \infty. \quad (3.4)$$

The magnetic permeability of effective medium, μ^* , can be expressed in term of ratio ν^* which is defined as

$$\nu^* \equiv \frac{\mu^*}{\mu_f}, \quad (3.5)$$

where the value of ν^* is determined as

$$\nu^* = \frac{\nu(1+F) + (1-F)}{\nu(1-F) + (1+F)}. \quad (3.6)$$

We can see from equation (3.4) that, according to the effective medium model, the gradient $\bar{\nabla}(H_{eff}^2)$ outside the representative cell equal to zero hence the capture of ultra-fine particles can be studied by consider only in the representative cell.

From equations (3.2) and (3.3), we can see that the effects of the existence of other collectors on the magnetic field around an arbitrary collector are contained in the factor A . In the limit of packing fraction approach to zero, the factor A approach to unity and the problem is reduced to the case of single paramagnetic cylindrical collector as shown in equation (2.16) of chapter II.

At this point, we can see that, by using the effective medium model, the problem of HGMS capture of ultra-fine magnetic particles by an assemblage of random cylindrical paramagnetic collectors can be transformed to the problem of ultra-fine particles capture by a single cylindrical paramagnetic collector in the representative cell. As a result of this, the consideration that has been done for the case of single cylindrical collector in chapter II can be adjusted and adopted here.

3.3 Continuity Equation Describing the Capture of Ultra-Fine Weakly Magnetic Particles by an Assemblage of Random Cylindrical Paramagnetic Collectors

In the previous section, the problem of ultra-fine particle capture by an assemblage of random cylindrical collectors is transformed to the case of single cylindrical collector in a representative cell. Consequently, the continuity equation (2.30) in chapter II can be applied to the present problem and dynamics of the system of ultra-fine particles in the fluid in a representative cell can be described with this equation

$$\frac{\partial c}{\partial \tau} = \left\{ \frac{\partial^2 c}{\partial r_a^2} + \frac{1}{r_a} \frac{\partial c}{\partial r_a} + \frac{1}{r_a^2} \frac{\partial^2 c}{\partial \theta^2} \right\} - \left\{ \frac{G_r c}{r_a} + \frac{\partial}{\partial r_a} (G_r c) + \frac{1}{r_a} \frac{\partial}{\partial \theta} (G_\theta c) \right\}. \quad (3.7)$$

Expressions of terms G_r and G_θ for this case is the same as those have been defined in equations (2.26) and (2.31)

By using equations (2.9) and (2.11) in chapter II, we can express G_r and G_θ in other forms as

$$G_r = \frac{aF_r}{k_B T}, \quad (3.8)$$

and

$$G_\theta = \frac{aF_\theta}{k_B T}, \quad (3.9)$$

where F_r and F_θ denote the radial and angular components of total external force acting on the system of ultra-fine magnetic particles, respectively.

In this research, we consider the situation that the magnetic traction force dominates the capture operation and other forces or processes produce very small influence on the capture operation. Consequently, we assumed that the total external force on the system of ultra-fine particles is due to magnetic traction force only.

From equation (3.2) term $\vec{\nabla}(H_f^2)$ is determined as

$$\vec{\nabla}(H_f^2) = -\frac{4A^2H_0^2K_C}{a} \left[\left(\frac{\cos(2\theta)}{r_a^3} + \frac{K_C}{r_a^5} \right) \hat{r} + \left(\frac{\sin(2\theta)}{r_a^3} \right) \hat{\theta} \right]. \quad (3.10)$$

Then the expression of magnetic traction force acting on the system of ultra-fine weakly magnetic particles in the representative cell can be obtained as

$$\vec{F}_m(r_a, \theta) = -\frac{8\pi\mu_0(\chi_p - \chi_f)A^2H_0^2K_C b_p^3}{3a} \left[\left(\frac{\cos(2\theta)}{r_a^3} + \frac{K_C}{r_a^5} \right) \hat{r} + \left(\frac{\sin(2\theta)}{r_a^3} \right) \hat{\theta} \right]. \quad (3.11)$$

From this equation we can determine expressions of G_r and G_θ in equations (3.8) and (3.9) as

$$G_r(r_a, \theta) = G_0^{random} \left(\frac{\cos(2\theta)}{r_a^3} + \frac{K_C}{r_a^5} \right), \quad (3.12)$$

and

$$G_\theta(r_a, \theta) = G_0^{random} \left(\frac{\sin(2\theta)}{r_a^3} \right), \quad (3.13)$$

where the factor G_0^{random} for this case is defined by the expression

$$G_0^{random} \equiv -\frac{8\pi\mu_0(\chi_p - \chi_f)A^2H_0^2K_C b_p^3}{3k_B T}. \quad (3.14)$$

When the expressions of G_r and G_θ in equations (3.12) and (3.13) are substituted in equation (3.7), we obtain the continuity equation describing the capture of ultra-fine weakly magnetic particles in the representative cell. This continuity equation can be solved, with some assigned initial and boundary conditions, to study dynamics of the system of ultra-fine particles subjected to high gradient magnetic separation. In this research time-dependent solutions of the continuity equation (3.7) is determined by using numerical method and the capture process in the representative cell is simulated in various situations.

สถาบันวิทยบริการ
จุฬาลงกรณ์มหาวิทยาลัย

CHAPTER IV

Simulations of HGMS Capture of Ultra-Fine Particles

To study the capture of ultra-fine magnetic particles in high gradient magnetic separations, the continuity equation describing dynamics of the system of ultra-fine particles is solved when some initial and boundary conditions are assigned.

In some situations, the continuity equation can be solved analytically but in many situations, solving the continuity equation analytically is very difficult and some numerical methods are used. By solving the continuity equation numerically, the HGMS capture of ultra-fine particles can be simulated in various situations. In this chapter, we simulate HGMS capture of ultra-fine particles in one dimension and two dimensions in various cases. The content in this chapter consists of the simulation methodology, errors and stability of the computation, initial and boundary conditions, parameters of simulations, and the procedures of simulations.

4.1 One Dimensional Simulation of the Capture of Ultra-Fine Particles by a Single-Ferromagnetic Cylindrical Collector

In section 2.3.2 of Chapter II, the continuity equation describing the capture of ultra-fine particles in one dimension obtained as

$$\frac{\partial c}{\partial \tau} = \frac{\partial^2 c}{\partial r_a^2} - \frac{\partial(G_r c)}{\partial r_a}. \quad (4.1)$$

This equation can be solved to obtain the distribution of particle volume concentration in some radial directions at various normalized times. The steady-state solution of equation (4.1) can be solved analytically but the time-dependent solutions will be solved numerically.

4.1.1 The Steady-State Solution

At steady state, the value of particle volume concentration at any points in fluid is independent of the normalized time, consequently, we get $\partial c / \partial \tau = 0$. Let $c_s(r_a)$ denotes the value of steady-state particle volume concentration. We can solve for $c_s(r_a)$ from the equation

$$\frac{d}{dr_a} \left(\frac{dc_s}{dr_a} - G_r c_s \right) = 0, \quad (4.2)$$

where partial derivatives becomes total derivatives at steady state.

Recalling the original continuity equation (2.5) of chapter II, at steady state we have

$$\bar{\nabla} \cdot \bar{\mathbf{J}} = 0. \quad (4.3)$$

Since $\bar{\mathbf{J}} = \bar{\mathbf{J}}_D + \bar{\mathbf{J}}_F$, equation (4.3) means that, at steady state, the particle volume flux due to diffusion and the particle volume flux due to the action of total external force on the system of ultra-fine particles balances each other dynamically at every points. Consequently, from equation (4.2) we obtain

$$\frac{dc_s}{dr_a} - G_r c_s = 0. \quad (4.4)$$

We assign the initial conditions for equation (4.4) that, at initial, the value of particle volume concentration at every points equal to a constant C_0 . We assign the boundary condition for equation (4.4) that the value of particle volume concentration at $r_a \rightarrow \infty$, where the influence of the magnetic force can be neglected, is fixed equal to the initial value C_0 . Finally we obtain

$$c_s(r_a) = C_0 \exp \left[\int_{\infty}^{r_a} G_r(x) dx \right]. \quad (4.5)$$

From this equation, we can see that the value of c_s changes with r_a exponentially. In practical, the value of c_s can not greater than a limited value called the saturation concentration denoted by C_{sat} . Consequently, the value of c_s in equation (4.5) must be restricted in a range $0 \leq c_s \leq C_{sat}$.

It is shown in equation (4.5) that the value of c_s depend on the spatial function G_r . If the magnetic collector is a ferromagnetic cylindrical one of radius a and all influences of other forces and processes are much smaller than the influence of the magnetic force then we obtain the expression of G_r as

$$G_r(r_a, \theta) = G_0^{ferro} \left[\frac{\cos(2\theta)}{r_a^3} + \frac{K_W}{r_a^5} \right], \quad (4.6)$$

where the factor G_0^{ferro} has been defined in equation (2.28) of Chapter II.

From equations (4.5) and (4.6), we can determine the distribution of particle volume concentration at steady state in any radial directions determined by the angle θ .

4.1.2 Time-Dependent Solutions

The time-dependent solutions of equation (4.1) are solved numerically by using the finite-difference method. The finite-difference method is a numerical method which solving differential equations, with some assigned initial and boundary conditions, for their approximated numerical solutions by approximating differentiations with some corresponding difference relations. In the finite-difference method, the continuous range of r_a and τ is replaced by corresponding discrete ranges composed of a finite set of uniformly distributed discrete points called grid as shown in Figure 4.1. In Figure 4.1, each points in the grid is specified by discrete coordinates $(r_a)_i$ and τ^n . The values of

$(r_a)_i$ and τ^n can be obtained from

$$(r_a)_i = 1 + i(\Delta r_a); \quad i = 0, 1, 2, 3, \dots, Q \quad (4.7)$$

and
$$\tau^n = n(\Delta \tau); \quad n = 0, 1, 2, 3, \dots, N, \quad (4.8)$$

where Q and N are some finite positive integers much larger than unity and variables Δr_a and $\Delta \tau$ are called grid steps.

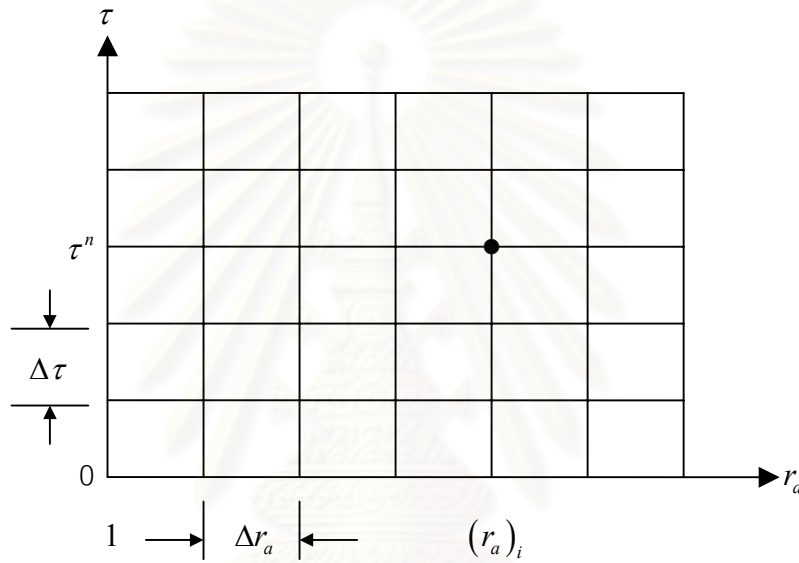


Figure 4.1: The grid in finite-difference method.

The approximated numerical value of particle volume concentration, denoted by C_i^n , are determined at every points in the grid.

To solved equation (4.1) numerically, we rewrite it as

$$\frac{\partial c}{\partial \tau} = \frac{\partial^2 c}{\partial r_a^2} - G_r \frac{\partial c}{\partial r_a} - c \frac{\partial G_r}{\partial r_a}. \quad (4.9)$$

All partial differentiations are approximated by some corresponding difference relations. The term $\partial c / \partial \tau$ is approximated by the first-order forward difference, the term $\partial c / \partial r_a$ is approximated by the first-order central difference, the term $\partial^2 c / \partial r_a^2$ is approximated by the second-order central difference. Some details on these approximations are presented in the Appendix C. Value of G_r and $\partial G_r / \partial r_a$

at every discrete radial positions $(r_a)_i$ are not necessary to be approximated since their analytical values can be calculated from their expressions and we obtain

$$(G_r)_i = G_r|_{(r_a)_i} \quad (4.10)$$

and

$$\left(\frac{\partial G_r}{\partial r_a} \right)_i = \frac{\partial G_r}{\partial r_a} \Big|_{(r_a)_i}, \quad (4.11)$$

where the expression of $\partial G_r / \partial r_a$ can be obtained from equation (2.27) of Chapter II as

$$\frac{\partial G_r(r_a, \theta)}{\partial r_a} = (-1) G_0^{ferro} \left[\frac{3 \cos(2\theta)}{r_a^4} + \frac{5K_W}{r_a^5} \right]. \quad (4.12)$$

By using finite-difference method, the partial differential equation (4.9) is approximated by its corresponding difference equation

$$\frac{C_i^{n+1} - C_i^n}{\Delta \tau} = \left(\frac{C_{i+1}^n - 2C_i^n + C_{i-1}^n}{(\Delta r_a)^2} \right) - (G_r)_i \left(\frac{C_{i+1}^n - C_{i-1}^n}{2(\Delta r_a)} \right) - \left(\frac{\partial G_r}{\partial r_a} \right)_i C_i^n. \quad (4.13)$$

It is seen from this equation that when approximated values of particle volume concentration at every discrete points are known at the n^{th} step of the discrete normalized time then we can compute new value of approximated particle volume concentration at every points at the $n+1^{th}$ step of the discrete normalized time.

The initial condition is assigned as

$$C_i^0 = C_0 \quad \text{for all } i \quad (4.14)$$

and the boundary condition is assigned as

$$C_Q^n = C_0 \quad \text{for all } n \quad (4.15)$$

where C_0 is a positive constant. Now we can see from equation (4.13) that we can

compute $\mathbb{C}_i^1, \mathbb{C}_i^2, \mathbb{C}_i^3, \dots, \mathbb{C}_i^n$ in succession for all i and approximated time-dependent solutions of the continuity equation (4.9) can be determined at various normalized times by the relation

$$\begin{aligned} \mathbb{C}_i^{n+1} = & \left[1 - \frac{2(\Delta\tau)}{(\Delta r_a)^2} - (\Delta\tau) \left(\frac{\partial G_r}{\partial r_a} \right)_i \right] \mathbb{C}_i^n + \left[\frac{(\Delta\tau)}{(\Delta r_a^2)} - \frac{(G_r)_i (\Delta\tau)}{2(\Delta r_a)} \right] \mathbb{C}_i^{n+1} \\ & + \left[\frac{(\Delta\tau)}{(\Delta r_a)^2} + \frac{(G_r)_i (\Delta\tau)}{2(\Delta r_a)} \right] \mathbb{C}_{i-1}^n. \end{aligned} \quad (4.16)$$

The capture of ultra-fine particles in one dimension by a single ferromagnetic cylindrical collector can be simulated by computing values of \mathbb{C}_i^n at every discrete radial positions $(r_a)_i$ at various normalized times (τ^n) .

4.1.2.1 Errors of the Computation

The finite-difference method gives us the approximated value of particle volume concentration at a given point in the computational grid. When the computation are performed, there exist some errors at every points in each cycle of computation.

To estimate the error of the computation, equation (4.13) is rewritten as

$$\frac{\mathbb{C}_i^{n+1} - \mathbb{C}_i^n}{\Delta\tau} - \left(\frac{\mathbb{C}_{i+1}^n - 2\mathbb{C}_i^n + \mathbb{C}_{i-1}^n}{(\Delta r_a)^2} \right) + (G_r)_i \left(\frac{\mathbb{C}_{i+1}^n - \mathbb{C}_{i-1}^n}{2(\Delta r_a)} \right) + \left(\frac{\partial G_r}{\partial r_a} \right)_i \mathbb{C}_i^n = 0. \quad (4.17)$$

Let's c_i^n denotes the value of analytical solution of equation (4.9) evaluated at a discrete radial position $(r_a)_i$, that is

$$c_i^n = c((r_a)_i, \tau^n). \quad (4.18)$$

When all approximated solutions in equation (4.17) are replaced by their corresponding analytical solutions we obtain

$$\frac{c_i^{n+1} - c_i^n}{\Delta\tau} - \left(\frac{c_{i+1}^n - 2c_i^n + c_{i-1}^n}{(\Delta r_a)^2} \right) + (G_r)_i \left(\frac{c_{i+1}^n - c_{i-1}^n}{2(\Delta r_a)} \right) + \left(\frac{\partial G_r}{\partial r_a} \right)_i c_i^n = \varepsilon_i^n, \quad (4.19)$$

where ε_i^n is a real number generally not equal to zero.

The value of ε_i^n indicates the error of the computation occurred at a discrete radial position $(r_a)_i$ at the n^{th} step of the computation. If the approximated solution \mathbb{C}_i^n approach to the analytical solution c_i^n then ε_i^n approach to zero. The maximum value of ε_i^n among all discrete radial positions at the n^{th} step of the computation can be estimated as (see Appendix D)

$$\max_{i,n} |\varepsilon_i^n| \leq \max_{i,n} \left| \left(\frac{\partial^2 c}{\partial \tau^2} \right)_i \right| \frac{(\Delta\tau)^2}{2} + \max_{i,n} \left| 2(G_r)_i \left(\frac{\partial^3 c}{\partial r_a^3} \right)_i - \left(\frac{\partial^4 c}{\partial r_a^4} \right)_i \right| \frac{(\Delta r_a)^2}{12}. \quad (4.20)$$

This equation shows us that the difference equation (4.13) can approximate the continuity equation (4.9) for its analytical solution $c(r_a, \tau)$, with the limited second-order partial derivative of c with respect to τ and the limited third and fourth-order partial derivative of c with respect to r_a . Equation (4.20) tells us that the approximation with respect to grid steps $\Delta\tau$ and Δr_a is of the first and second order, respectively, or we can write the order of the approximation as $O[(\Delta\tau) + (\Delta r_a)^2]$. It is seen from equation (4.20) that the approximate solution \mathbb{C}_i^n can approach the analytical solution c_i^n when grid steps $\Delta\tau$ and Δr_a are approach to zero.

4.1.2.2 Stability of the Computation

Suppose that at the n^{th} step of the discrete normalized time, $\tau^n = n(\Delta\tau)$, (and also the n^{th} step of the computation) the approximated solution \mathbb{C}_i^n differ from the analytical solution c_i^n with a certain quantity δc_i^n called the error of computation at the discrete radial position $(r_a)_i$ and at the n^{th} step of the discrete normalized time that is

$$\mathbb{C}_i^n = c_i^n + \delta c_i^n. \quad (4.21)$$

Similarly, at the $n + 1^{\text{th}}$ step of computation we have

$$\mathbb{C}_i^{n+1} = c_i^{n+1} + \delta c_i^{n+1}. \quad (4.22)$$

If the error made at any $n + 1^{\text{th}}$ step of computation, δc_i^{n+1} , not larger than the error made at the previous step, δc_i^n , then the computation is call stable. In other words, for the computation to be stable, the error made in one step of computation should not be increased by subsequent computations.

For the simulation of the capture of ultra-fine particles in one dimension by a single ferromagnetic cylindrical collector, conditions to achieve a stable computation are (see Appendix D)

$$(\Delta \tau) \max_i \left| \left(\frac{\partial G_r}{\partial r_a} \right)_i \right| \ll \xi, \quad (4.23a)$$

$$\frac{(\Delta \tau)}{2(\Delta r_a)} \max_i |(G_r)_i| \ll \xi, \quad (4.23b)$$

and
$$0 \leq \xi \leq \frac{1}{2}, \quad (4.23c)$$

where it is defined that

$$\xi \equiv \frac{(\Delta \tau)}{(\Delta r_a)^2}. \quad (4.24)$$

When all conditions in equation (4.23) are satisfied, the computation is stable and the maximum error occurred at the N^{th} step of computation can be determined as (see Appendix D)

$$\max_i |\delta c_i^N| \leq \max_i |\delta c_i^0| + N(\Delta\tau) \mathcal{O}\left[(\Delta\tau) + (\Delta r_a)^2\right], \quad (4.25)$$

where the term δc_i^0 denotes the error from the assignment of the initial condition. From equation (4.25), we can see that, with vanishing grid steps, $\Delta\tau$ and Δr_a , and all conditions in the equation (4.23) are satisfied, the approximated solution \mathbb{C}_i^n converge to the analytical solution c_i^n and the computation is stable.

4.1.2.3 Initial Condition of the Computation

The initial condition of the simulation of this case is assigned by setting the value of particle volume concentration at every discrete points $(r_a)_i$ at initial $(\tau = 0)$ equal to a constant denoted by C_0 that is

$$\mathbb{C}_i^0 = C_0 \quad \text{for all } i. \quad (4.26)$$

4.1.2.4 Saturation Condition

In practical, as particle volume concentration at a given point increase, inter-particle forces will limit this concentration to a finite value and the saturation is occurred. Experimental evidence [18] indicates that saturation occurs approximately at $c \approx 0.10$. This value is therefore used as a limit to the particle volume concentration. A discrete radial position $(r_a)_i$ with a concentration $\mathbb{C}_i^n \geq 0.10$ is assumed to be the saturation point. In this research, the point of saturation is considered to be the point that particles accumulate highly dense and the build-up of particles is considered to be static. All saturation points are excluded from the computation and values of particle volume concentration are held fixed at 0.10.

The saturation condition can be expressed as

$$0 \leq \mathbb{C}_i^n \leq 0.10 \quad \text{for all } i \text{ and } n. \quad (4.27)$$

4.1.2.5 Boundary Conditions of the Computation

4.1.2.5.1 Outer Boundary Condition

Since the capture of ultra-fine particles must be simulated in a finite computational domain. Let $(r_a)_Q = 1 + Q(\Delta r_a)$ be the outer boundary of the computational domain. From equation (2.20) of Chapter II, we can see that the magnitude of radial component of magnetic traction force decrease with increasing r_a . Consequently in the simulation, the outer boundary of the computational domain is chose to far from the collector. This make it is reasonably to approximate that the influence of the magnetic force can be neglected at the outer boundary. From this, the value of C_Q^n is maintained equal to the initial particle volume concentration C_0 for all steps of discrete normalized time τ^n . Consequently, the outer boundary condition of the computation can be expressed as

$$C_Q^n = C_0 \quad \text{for all } n. \quad (4.28)$$

4.1.2.5.2 Boundary Condition at the Impervious Surface

The impervious surface in this research is defined as the surface of the collector or the surface of the region of saturation concentration where particles accumulate highly dense. The particle volume flux in the radial direction at any points on the impervious surface is considered equal to zero. Let subscript I indicates the position of a point on the impervious surface. We can write the condition of particle volume flux in the radial direction on the impervious surface as

$$\left(\frac{\partial c}{\partial r_a} - G_r c \right)_I = 0. \quad (4.29)$$

In finite-difference method, the difference equation corresponds to the equation (4.29) can be written as

$$\left(\frac{C_I^n - C_{I-1}^n}{\Delta r_a} \right) - (G_r)_I C_I^n = 0. \quad (4.30)$$

In the simulation, the value of particle volume concentration at a given point on the surface of the collector can be computed at the n^{th} step of the computation by using the expression

$$C_I^n = \frac{C_{I+1}^n}{1 + (G_r)_I (\Delta r_a)}. \quad (4.31)$$

When the value of particle volume concentration at a point on the surface of the collector reaches the saturation concentration, that point will be excluded from the computation in the next cycle and equation (4.31) is applied for the point adjacent to the saturation point.

4.1.2.6 Parameters of Simulations

For the simulation of ultra-fine particle capture in one dimension by a single ferromagnetic cylindrical collector, parameters of the simulation are as follows:

- 1) The magnitude of applied uniform magnetic field (H_0),
- 2) The radius of ultra-fine particles (b_p).
- 3) The effective magnetic susceptibility ($\chi \equiv \chi_p - \chi_f$).

4.1.2.7 Procedures of the Simulation

Procedures of the simulation in one dimensional case can be separated into three main parts as shown schematically in Figure 4.2

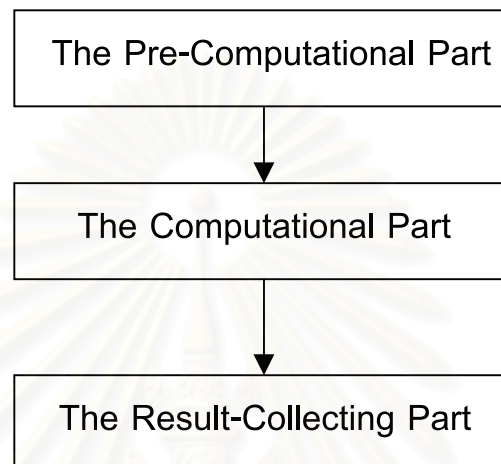


Figure 4.2: Three main procedures of the simulation.

The first main procedure, the pre-computational part, is the preparation before performing the computation. Sub-procedures contained in this part are

- 1.1) Describe some introductions and the objective of the simulation,
- 1.2) Set all constants and parameters those are used in the simulation,
- 1.3) Declare all output files and variables those are used in the simulation,
- 1.4) Construct the computational domain,
- 1.5) Set the initial condition of the computation.

In the second main procedure, the computational part, the numerical value of approximated particle volume concentration C_i^n is updated at every discrete radial positions $(r_a)_i$ in the computational domain at each step of discrete normalized time (τ^n) . Sub-procedures in this part are as follows:

- 2.1) Increase the step of the discrete normalized time (τ^n) by one,
- 2.2) Find and mark the position of the impervious point in the computational domain,
- 2.3) Set the outer boundary condition of the computation,
- 2.4) Update numerical value of the approximated particle volume concentration at every points in the computational domain by starting from the point at the outer boundary toward the impervious point,
- 2.5) Prepare for the next cycle of computation (τ^{n+1}) by treat the new values of particle volume concentration those are computed in the present cycle as the old values for the next cycle.

In the third main procedure, the result-collecting part, results of the simulation which are numerical values of particle volume concentration at every discrete points in the computational domain at some steps of normalized times those has early specified are sent to corresponding output files. When these results are saved in the output files, all output files are then closed and the simulation is terminated.

4.2 Two Dimensional Simulations of the Capture of Ultra-Fine Particles

From section 2.3.3 of Chapter II, we obtain the continuity equation describing the capture of ultra-fine particles in two dimensions as

$$\frac{\partial c}{\partial \tau} = \left\{ \frac{\partial^2 c}{\partial r_a^2} + \frac{1}{r_a} \frac{\partial c}{\partial r_a} + \frac{1}{r_a^2} \frac{\partial^2 c}{\partial \theta^2} \right\} - \left\{ \frac{G_r c}{r_a} + \frac{\partial}{\partial r_a} (G_r c) + \frac{1}{r_a} \frac{\partial}{\partial \theta} (G_\theta c) \right\}. \quad (4.32)$$

We can study the capture of ultra-fine particles in two dimensions by solving this equation when some initial and boundary conditions are given. The solution of this equation provides us the distribution of particle volume concentration in two dimensional area around the collector at various normalized times. In this research, the time-dependent solution of equation (4.32) is determined numerically by using the

finite-difference method.

4.2.1 The Two Dimensional Computational Domain

The analytical solution of equation (4.32) is a continuous function of two dimensional polar coordinates and normalized time denoted by $c(r_a, \theta, \tau)$. If this analytical solution can be determined by some methods then the particle volume concentration can be calculated, at any values of normalized time, at any points in a continuous range $1 \leq r_a \leq \infty$. In numerical method, numerical solutions of equation (4.32) are computed in a finite discrete computational domain in two dimensions as shown in Figure 4.3

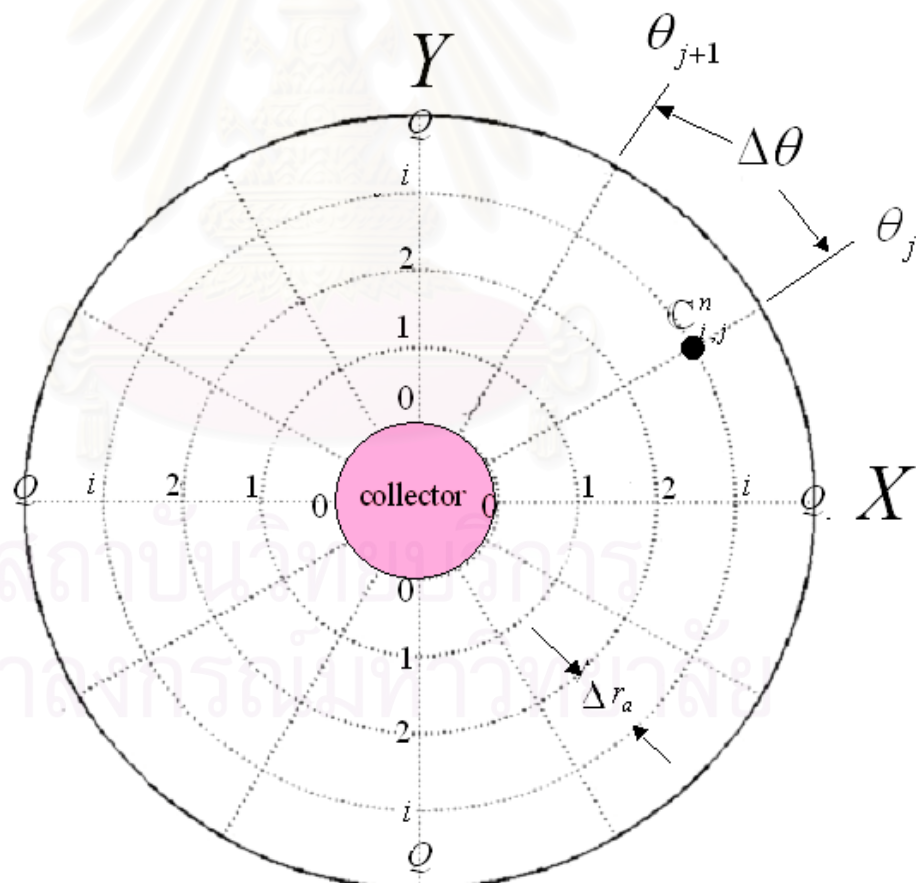


Figure 4.3: A two dimensional circular grid.

In Figure 4.3, the computational domain consists of a finite set of uniformly distributed discrete points $((r_a)_i, \theta_j)$ where discrete radial and angular coordinates are determined by

$$(r_a)_i = 1 + i(\Delta r_a) \quad 0 \leq i \leq Q, \quad (4.33)$$

and
$$\theta_j = j(\Delta \theta) \quad 0 \leq j \leq P, \quad (4.34)$$

where i and j are positive integers, Q and P are positive integers generally much larger than unity.

In the simulation of ultra-fine particles capture in two dimensions, some initial and boundary conditions are assigned to the computational domain and the numerical value of particle volume concentration is computed at every points at various normalized times. The numerical value of particle volume concentration at a discrete point $((r_a)_i, \theta_j)$ and at the n^{th} step of the discrete normalized time is denoted by $C_{i,j}^n$.

4.2.2 The Computation of Approximated Time-Dependent Solutions

The continuity equation (4.32) is solved numerically to obtain its approximated time-dependent solutions by using the finite-difference method. At the first step, the continuity equation (4.32) is rewritten in an alternative form as

$$\frac{\partial c}{\partial \tau} = \frac{\partial^2 c}{\partial r_a^2} + \frac{1}{r_a} \frac{\partial c}{\partial r_a} + \frac{1}{r_a^2} \frac{\partial^2 c}{\partial \theta^2} - \frac{G_r c}{r_a} - G_r \frac{\partial c}{\partial r_a} - c \frac{\partial G_r}{\partial r_a} - \frac{G_\theta}{r_a} \frac{\partial c}{\partial \theta} - \frac{c}{r_a} \frac{\partial G_\theta}{\partial \theta}. \quad (4.35)$$

Then, all partial differentiations in this equation are approximated by their corresponding difference relations. The term $\partial c / \partial \tau$ is approximated by the first-order forward difference, terms $\partial^2 c / \partial r_a^2$ and $\partial^2 c / \partial \theta^2$ are approximated by the second-order central difference, terms $\partial c / \partial r_a$ and $\partial c / \partial \theta$ are approximated by the first-order central difference (see Appendix C), terms $\partial G_r / \partial r_a$ and $\partial G_\theta / \partial \theta$ are not necessary to be

approximated since their analytical values can be determined at any discrete points $((r_a)_i, \theta_j)$ in the computational domain.

Expressions of $\partial G_r / \partial r_a$ and $\partial G_\theta / \partial \theta$ can be obtained as

$$\frac{\partial G_r}{\partial r_a} = -G_0 \left[\frac{3 \cos(2\theta)}{r_a^4} + \frac{5K}{r_a^5} \right], \quad (4.36)$$

and

$$\frac{\partial G_\theta}{\partial \theta} = \frac{2G_0 \cos(2\theta)}{r_a^3}, \quad (4.37)$$

where the value of the factor G_0 and K depend on the type of the magnetic collectors those are used.

The values of $\partial G_r / \partial r_a$ and $\partial G_\theta / \partial \theta$ evaluated at a discrete points $((r_a)_i, \theta_j)$ are defined as

$$\left(\frac{\partial G_r}{\partial r_a} \right)_{i,j} \equiv \frac{\partial G_r}{\partial r_a} \Big|_{((r_a)_i, \theta_j)}, \quad (4.38)$$

and

$$\left(\frac{\partial G_\theta}{\partial r_\theta} \right)_{i,j} \equiv \frac{\partial G_\theta}{\partial r_\theta} \Big|_{((r_a)_i, \theta_j)}. \quad (4.39)$$

The value of G_r and G_θ at a discrete point $((r_a)_i, \theta_j)$ are not necessary to be approximated and we define

$$(G_r)_{i,j} \equiv G_r \Big|_{((r_a)_i, \theta_j)}, \quad (4.40)$$

and

$$(G_\theta)_{i,j} \equiv G_\theta \Big|_{((r_a)_i, \theta_j)}. \quad (4.41)$$

After all approximations are performed, the continuity equation (4.35) is replaced by its corresponding difference equation

$$\begin{aligned}
\frac{\mathbb{C}_{i,j}^{n+1} - \mathbb{C}_{i,j}^n}{\Delta\tau} = & \left(\frac{\mathbb{C}_{i+1,j}^n - 2\mathbb{C}_{i,j}^n + \mathbb{C}_{i-1,j}^n}{(\Delta r_a)^2} \right) + \frac{1}{(r_a)_i} \left(\frac{\mathbb{C}_{i+1,j}^n - \mathbb{C}_{i-1,j}^n}{2(\Delta r_a)} \right) + \frac{1}{(r_a)_i^2} \left(\frac{\mathbb{C}_{i,j+1}^n - 2\mathbb{C}_{i,j}^n + \mathbb{C}_{i,j-1}^n}{(\Delta\theta)^2} \right) \\
& - \frac{(G_r)_{i,j}}{(r_a)_i} \mathbb{C}_{i,j}^n - (G_r)_{i,j} \left(\frac{\mathbb{C}_{i+1,j}^n - \mathbb{C}_{i-1,j}^n}{2(\Delta r_a)} \right) - \left(\frac{\partial G_r}{\partial r_a} \right)_{i,j} \mathbb{C}_{i,j}^n \\
& - \frac{(G_\theta)_{i,j}}{(r_a)_i} \left(\frac{\mathbb{C}_{i,j+1}^n - \mathbb{C}_{i,j-1}^n}{2(\Delta\theta)} \right) - \frac{\mathbb{C}_{i,j}^n}{(r_a)_i} \left(\frac{\partial G_\theta}{\partial \theta} \right)_{i,j}, \tag{4.42}
\end{aligned}$$

where $\mathbb{C}_{i,j}^n$ is the approximated numerical solution of the continuity equation (4.35) at the discrete point $((r_a)_i, \theta_j)$ and at the n^{th} step of discrete normalized time τ^n .

The value of $\mathbb{C}_{i,j}^{n+1}$ which is the updated value of particle volume concentration at the discrete point $((r_a)_i, \theta_j)$ at the $n+1^{\text{th}}$ step of the discrete normalized time τ^n can be computed from the equation

$$\begin{aligned}
\mathbb{C}_{i,j}^{n+1} = & \left[1 - \frac{2(\Delta\tau)}{(\Delta r_a)^2} - \frac{2}{(r_a)_i^2} \left(\frac{\Delta\tau}{(\Delta\theta)^2} \right) - \left(\frac{(G_r)_{i,j}}{(r_a)_i} + \left(\frac{\partial G_r}{\partial r_a} \right)_{i,j} + \frac{1}{(r_a)_i} \left(\frac{\partial G_\theta}{\partial \theta} \right)_{i,j} \right) (\Delta\tau) \right] \mathbb{C}_{i,j}^n \\
& + \left[\frac{\Delta\tau}{(\Delta r_a)^2} + \left(\frac{1}{2(r_a)_i} - \frac{(G_r)_{i,j}}{2} \right) \left(\frac{\Delta\tau}{\Delta r_a} \right) \right] \mathbb{C}_{i+1,j}^n \\
& + \left[\frac{\Delta\tau}{(\Delta r_a)^2} - \left(\frac{1}{2(r_a)_i} - \frac{(G_r)_{i,j}}{2} \right) \left(\frac{\Delta\tau}{\Delta r_a} \right) \right] \mathbb{C}_{i-1,j}^n \\
& + \left[\frac{1}{(r_a)_i^2} \left(\frac{\Delta\tau}{(\Delta\theta)^2} \right) - \frac{(G_\theta)_{i,j}}{2(r_a)_i} \left(\frac{\Delta\tau}{\Delta\theta} \right) \right] \mathbb{C}_{i,j+1}^n \\
& + \left[\frac{1}{(r_a)_i^2} \left(\frac{\Delta\tau}{(\Delta\theta)^2} \right) + \frac{(G_\theta)_{i,j}}{2(r_a)_i} \left(\frac{\Delta\tau}{\Delta\theta} \right) \right] \mathbb{C}_{i,j-1}^n. \tag{4.43}
\end{aligned}$$

We can see from this equation that if the initial value ($n=0$) of \mathbb{C} are given at every discrete points as $\mathbb{C}_{i,j}^0$ for all i and j then we can compute $\mathbb{C}_{i,j}^1$, $\mathbb{C}_{i,j}^2$, $\mathbb{C}_{i,j}^3$, ..., $\mathbb{C}_{i,j}^N$ in succession when some boundary conditions are assigned. Consequently, the approximated solutions of the continuity equation can be determined at various discrete normalized times and the simulation of the capture of ultra-fine particles in two dimensions can be performed.

4.2.3 Errors of the Computation

From equation (4.42) if all approximated solutions \mathbb{C} are replaced by their corresponding analytical solutions c at every discrete points at the n^{th} step of the discrete normalized time τ^n then we obtain

$$\begin{aligned} \frac{c_{i,j}^{n+1} - c_{i,j}^n}{\Delta\tau} = & \left(\frac{c_{i+1,j}^n - 2c_{i,j}^n + c_{i-1,j}^n}{(\Delta r_a)^2} \right) + \frac{1}{(r_a)_i} \left(\frac{c_{i+1,j}^n - c_{i-1,j}^n}{2(\Delta r_a)} \right) + \frac{1}{(r_a)_i^2} \left(\frac{c_{i,j+1}^n - 2c_{i,j}^n + c_{i,j-1}^n}{(\Delta\theta)^2} \right) \\ & - \frac{(G_r)_{i,j} c_{i,j}^n}{(r_a)_i} - (G_r)_{i,j} \left(\frac{c_{i+1,j}^n - c_{i-1,j}^n}{2(\Delta r_a)} \right) - \left(\frac{\partial G_r}{\partial r_a} \right)_{i,j} c_{i,j}^n \\ & - \frac{(G_\theta)_{i,j} \left(c_{i,j+1}^n - c_{i,j-1}^n \right)}{(r_a)_i} - \frac{c_{i,j}^n}{(r_a)_i} \left(\frac{\partial G_\theta}{\partial \theta} \right)_{i,j} + \varepsilon_{i,j}^n, \end{aligned} \quad (4.44)$$

where $\varepsilon_{i,j}^n$ is a real quantity, generally not equal to zero, which indicates the error of the computation. If the approximated solution at a given point, $\mathbb{C}_{i,j}^n$, is close to the analytical solution $c_{i,j}^n$ at the same point then the value of $\varepsilon_{i,j}^n$ is close to zero at that point.

For the simulation of ultra-fine particles capture in two dimensions, we can estimate the maximum value of $\varepsilon_{i,j}^n$ which occurred at the n^{th} step of the computation as (see Appendix E)

$$\begin{aligned} \max_{i,j} |\varepsilon_{i,j}^n| \leq & \max_{i,j} \left| \left(\frac{\partial^2 c}{\partial \tau^2} \right)_{i,j} \left| \left(\frac{\Delta\tau}{2} \right) \right| + \max_{i,j} \left| 2 \left((G_r)_{i,j} - \frac{1}{(r_a)_i} \right) \left(\frac{\partial^3 c}{\partial r_a^3} \right)_{i,j} - \left(\frac{\partial^4 c}{\partial r_a^4} \right)_{i,j} \right| \left| \left(\frac{\Delta r_a}{12} \right)^2 \right| \right. \\ & \left. + \max_{i,j} \left| \left(\frac{2(G_\theta)_{i,j}}{(r_a)_i} \right) \left(\frac{\partial^3 c}{\partial \theta^3} \right)_{i,j} - \frac{1}{(r_a)_i} \left(\frac{\partial^4 c}{\partial \theta^4} \right)_{i,j} \right| \left| \left(\frac{\Delta\theta}{12} \right)^2 \right| \right|. \end{aligned} \quad (4.45)$$

The expression (4.45) tell us that the difference equation (4.42) can approximate the continuity equation (4.35) for its analytical solution $c(r_a, \theta, \tau)$, with the limited second-order partial derivative of c with respect to τ and the limited third and fourth-order partial derivative of c with respect to r_a and θ , respectively.

The approximation with respect to grid steps $\Delta\tau$, Δr_a and $\Delta\theta$ are of the first, second and second order, respectively. It is said that the difference equation (4.42) approximate the continuity equation (4.35) for its solution within the order $O\left[(\Delta\tau)+(\Delta r_a)^2+(\Delta\theta)^2\right]$.

4.2.4 The Stability of the Simulation

The stability of the simulation of the capture of ultra-fine particles in two dimensional space is analyzed in the appendix E. Conditions those make the simulation stable are

$$0 < \max_{i,j} \left| \left(\frac{\xi}{\alpha^2 (r_a)_i^2} \right) - \left(\frac{(G_\theta)_{i,j} (\Delta\tau)}{2\alpha (r_a)_i (\Delta r_a)} \right) \right| < 1, \quad (4.46)$$

$$0 < \max_{i,j} \left| \left(\frac{\xi}{\alpha^2 (r_a)_i^2} \right) + \left(\frac{(G_\theta)_{i,j} (\Delta\tau)}{2\alpha (r_a)_i (\Delta r_a)} \right) \right| < 1, \quad (4.47)$$

$$\max_i \left| \frac{1}{\alpha^2 (r_a)_i^2} \right| \ll 1, \quad (4.48)$$

$$\max_{i,j} \left| \left\{ \frac{(G_r)_{i,j}}{(r_a)_i} + \left(\frac{\partial G_r}{\partial r_a} \right)_{i,j} + \frac{1}{(r_a)_i} \left(\frac{\partial G_\theta}{\partial \theta} \right)_{i,j} \right\} (\Delta\tau) \right| \ll 1, \quad (4.49)$$

$$\max_{i,j} \left| \left(\frac{(G_r)_{i,j}}{2} - \frac{1}{2(r_a)_i} \right) \left(\frac{\Delta\tau}{\Delta r_a} \right) \right| \ll \xi, \quad (4.50)$$

$$\text{and} \quad 0 \leq \xi \leq \frac{1}{2}, \quad (4.51)$$

where it is defined that

$$\alpha \equiv \frac{(\Delta\theta)}{(\Delta r_a)} \quad (4.52)$$

and ξ has been defined in the equation (4.24).

When these conditions are satisfied, the simulation in two dimensional space can be stable and the maximum error of the computation among all discrete points in the computational domain after N steps of computations can be expressed as

$$\max_{i,j} |\delta c_{i,j}^{n+1}| \leq \max_{i,j} |\delta c_{i,j}^0| + N(\Delta\tau) O \left[(\Delta\theta)^2 + (\Delta r_a)^2 + (\Delta\tau) \right]. \quad (4.53)$$

This expression means that if all grid steps ($\Delta\tau$, Δr_a and $\Delta\theta$) are approach to zero and all stability conditions are satisfied then the computed numerical approximated solution \mathbb{C} converge to the analytical solution c and the simulation is stable.

4.2.5 Initial Condition of the Simulation

The initial condition for the simulation in the two dimensional space can be assigned as

$$\mathbb{C}_{i,j}^0 = C_0 \quad \text{for all } i \text{ and } j, \quad (4.54)$$

where C_0 is a numerical constant greater than zero.

4.2.6 Saturation Condition

The saturation condition in this two dimensional case is similar to the one dimensional case and can be assigned as

$$0 < \mathbb{C}_{i,j}^n \leq 0.1 \quad \text{for all } i, j \text{ and } n. \quad (4.55)$$

4.2.7 Boundary Conditions

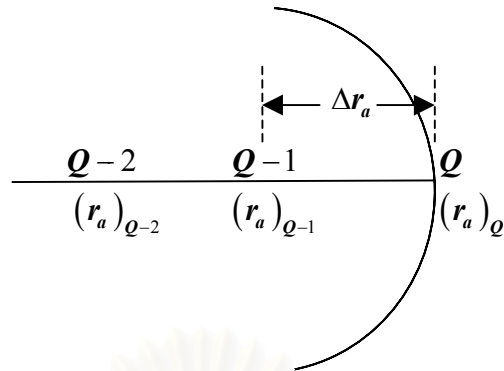
4.2.7.1 Outer Boundary Condition

The outer boundary condition for the case of single cylindrical collector is assigned similar to the case of one dimensional simulation. Since the magnitude of magnetic traction force decrease with increasing r_a , if we set the outer boundary of the computational domain at $(r_a)_Q \gg 1$ then the magnetic force can be neglected at the outer boundary. Consequently, the outer boundary condition can be assigned as

$$C_{Q,j}^n = C_0 \text{ for all } j \text{ and } n, \quad (4.56)$$

where C_0 is the initial particle volume concentration.

In another case where ultra-fine particles are captured by an assemblage of random cylindrical paramagnetic collectors, the effective medium model allows us to study the capture process of overall system (collectors + fluid) by consider only in a cylindrical representative cell. In this research, the capture of ultra-fine particles by an assemblage of random cylindrical paramagnetic collectors is studied for the case of static fluid. This means that no particle volume flux flow through the overall system. Consequently, the total amount of ultra-fine particles in the system can be considered to be constant. Since the representative cell is the representation of the system, we then impose a constraint on the simulation that the total amount of ultra-fine particles in the representative cell should be constant. Consequently, the net particle volume flux in all directions perpendicular to the outer boundary of the representative cell must equal to zero. From this, we will approximate that the outer boundary of the representative cell is equivalent to an impervious surface as shown in Figure 4.4.



the outer boundary of the representative cell

Figure 4.4: The outer boundary of the representative cell as an impervious surface.

The continuity equation at all points on the outer boundary can be approximated as (see Appendix F)

$$\left(\frac{\partial c}{\partial \tau}\right)_{(r_a)_Q} \approx \frac{1}{(r_a)_Q^2} \left(\frac{\partial^2 c}{\partial \theta^2}\right)_{(r_a)_Q} - \frac{1}{(r_a)_Q} \left(\frac{\partial(G_\theta c)}{\partial \theta}\right)_{(r_a)_Q} + \frac{1}{(\Delta r_a)} \left(G_r c - \frac{\partial c}{\partial r_a}\right)_{(r_a)_{Q-1}}, \quad (4.57)$$

where Q denotes the position of a point on the outer boundary of the representative cell. From the expression (4.57), the approximated numerical value of particle volume concentration at various points on the outer boundary of the representative cell can be computed from

$$\begin{aligned} \mathbb{C}_{Q,j}^{n+1} = & \left[1 - \frac{2(\Delta \tau)}{(r_a)_Q^2 (\Delta \theta)^2} - \frac{(\Delta \tau)}{(r_a)_Q} \left(\frac{\partial G_\theta}{\partial \theta}\right)_{Q,j} - \frac{(\Delta \tau)}{2(\Delta r_a)^2} \right] \mathbb{C}_{Q,j}^n \\ & + \left[\frac{(\Delta \tau)}{(r_a)_Q^2 (\Delta \theta)^2} - \frac{(G_\theta)_{Q,j} (\Delta \tau)}{(r_a)_Q (\Delta \theta)} \right] \mathbb{C}_{Q,j+1}^n \\ & + \left[\frac{(\Delta \tau)}{(r_a)_Q^2 (\Delta \theta)^2} + \frac{(G_\theta)_{Q,j} (\Delta \tau)}{(r_a)_Q (\Delta \theta)} \right] \mathbb{C}_{Q,j-1}^n \\ & + \left[\frac{(G_r)_{Q-1,j} (\Delta \tau)}{(\Delta r_a)} \right] \mathbb{C}_{Q-1,j}^n + \left[\frac{(\Delta \tau)}{2(\Delta r_a)^2} \right] \mathbb{C}_{Q-2,j}^n. \end{aligned} \quad (4.58)$$

4.2.7.2 Boundary Condition at the Surface of the Collector or at the Surface of the Saturation Region

In this research, the surface of the collector and the surface of the saturation region, composed from many saturation points, are considered as an impervious surface as shown in the Figure 4.5

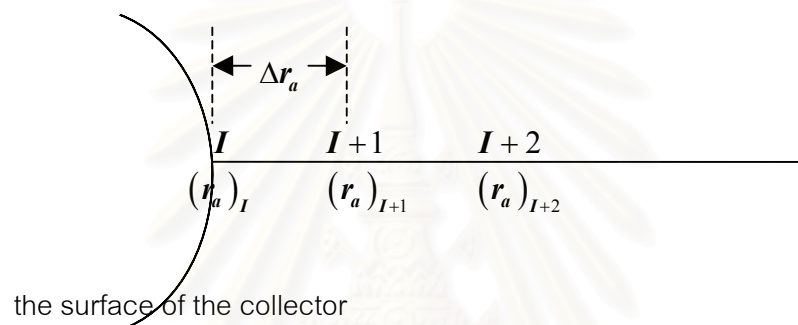


Figure 4.5: Surface of the collector or the saturation region as an impervious surface.

The continuity equation for a given point which is adjacent to the surface of the collector or the surface of the saturation region can be approximated as (see Appendix F)

$$\left(\frac{\partial c}{\partial \tau}\right)_{(r_a)_I} \approx \frac{1}{(r_a)_I^2} \left(\frac{\partial^2 c}{\partial \theta^2}\right)_{(r_a)_I} - \frac{1}{(r_a)_I} \left(\frac{\partial(G_\theta c)}{\partial \theta}\right)_{(r_a)_I} + \frac{1}{(\Delta r_a)} \left(G_r c - \frac{\partial c}{\partial r_a}\right)_{(r_a)_{I+1}}, \quad (4.59)$$

where the index I denotes the position of a point on the impervious surface.

From the expression (4.59), the approximated numerical value of particle volume concentration at various points on the surface of the collector can be computed from

$$\begin{aligned}
C_{I,j}^{n+1} = & \left[1 - \frac{2(\Delta\tau)}{(r_a)_I^2(\Delta\theta)^2} - \frac{(\Delta\tau)}{(r_a)_I} \left(\frac{\partial G_\theta}{\partial \theta} \right)_{I,j} \right] C_{I,j}^n \\
& + \left[\frac{(\Delta\tau)}{(r_a)_I^2(\Delta\theta)^2} - \frac{(G_\theta)_{I,j}(\Delta\tau)}{2(r_a)_I(\Delta\theta)} \right] C_{I,j+1}^n \\
& + \left[\frac{(\Delta\tau)}{(r_a)_I^2(\Delta\theta)^2} + \frac{(G_\theta)_{I,j}(\Delta\tau)}{2(r_a)_I(\Delta\theta)} \right] C_{I,j-1}^n \\
& - \left[\frac{(\Delta\tau)}{(\Delta r_a)^2} + \frac{(G_r)_{I+1,j}(\Delta\tau)}{(\Delta r_a)} \right] C_{I+1,j}^n + \left[\frac{(\Delta\tau)}{(\Delta r_a)^2} \right] C_{I+2,j}^n. \tag{4.60}
\end{aligned}$$

When the impervious surface is the surface of saturation, equation (4.60) is used for compute the value of particle concentration at the point adjacent to the saturation point.

4.2.8 Parameters of Simulations

Simulations of ultra-fine particle capture in two dimensions are separated into two categories. The first is the case of single ferromagnetic cylindrical collector and the second is the case of an assemblage of random paramagnetic cylindrical collectors. Parameters of these simulations are as follows:

- 1) In the case of single collector, the parameter is the magnitude of the applied uniform magnetic field (H_0),
- 2) In the case of an assemblage of random paramagnetic cylindrical collectors, parameters are the packing fraction (F) of the cylindrical collectors in the system and the magnitude of the applied uniform magnetic field (H_0).

4.2.9 Procedures of the Simulation

Procedures of the simulation for this two dimensional case are the same as the one dimensional case and are already described in the section 4.1.2.7

In Chapter V, capture of ultra-fine particles is simulated in various cases.

CHAPTER V

Results of Simulations and Discussions

In this chapter, results of simulations of HGMS capture of ultra-fine particles in various cases are presented with discussions. The simulation begins with the capture of ultra-fine particles in one dimension by a single ferromagnetic cylindrical collector. Next, the simulation is extended to the capture of ultra-fine particles in two dimensions by a single ferromagnetic cylindrical collector. Finally, results of two dimensional simulations of HGMS capture of ultra-fine particles by an assemblage of random paramagnetic cylindrical collectors are presented. From all of these results, the capture of ultra-fine particles in various situations can be investigated.

5.1 One Dimensional Simulations of the Capture of Ultra-Fine Particles by a Single-Ferromagnetic Cylindrical Collector

In one dimensional case, HGMS capture of ultra-fine particles is simulated in two situations and results of these simulations are categorized into two sections.

5.1.1 Paramagnetic Mode of the Capture

In the first situation, the ultra-fine particle is paramagnetic $\text{Mn}_2\text{P}_2\text{O}_7$ particle of radius $b_p = 1.2 \times 10^{-8}$ m. An assembly of $\text{Mn}_2\text{P}_2\text{O}_7$ particles dispersed in a static water. The effective magnetic susceptibility of the system (water + $\text{Mn}_2\text{P}_2\text{O}_7$ particle) is $\chi = +4.73 \times 10^{-3}$. This situation which $\chi > 0$ is called the paramagnetic mode of the capture. The ferromagnetic collector is considered to be homogeneous saturate magnetized perpendicular to its axis by a uniform external magnetic field $H_0 = 1.0 \times 10^6$ A/m points in the positive X direction and its saturate magnetization is $M_s = 1.6 \times 10^6$ A/m. Let the absolute temperature equal to 300 K. From these parameters, we can calculate the value of factor G_0^{ferro} , from equation(2.28)

of Chapter II, as -16.62 and the value of the factor K_w , from equation (2.14) as 0.80 . The value of initial particle concentration at every points in the computational domain is set equal to $C_0 = 1.0 \times 10^{-3}$ and the saturation concentration is set equal to $C_{sat} = 0.10$. From equation (2.20) of Chapter II, we can see that, for the paramagnetic mode, the radial component of the magnetic force is strongest attractive at $\theta = 0, \pi$ radian whereas the strongest repulsive magnetic force occur at $\theta = \pi/2, 3\pi/2$ radian. The position of the outer boundary is assigned at $r_{dl} = 10.00$ where the magnetic force is assumed neglected. The value of particle concentration at the outer boundary is held fixed equal to the initial value for all normalized times.

Figure 5.1 shows the distribution of concentration in the paramagnetic mode at $\theta = 0$ radian at various normalized times.

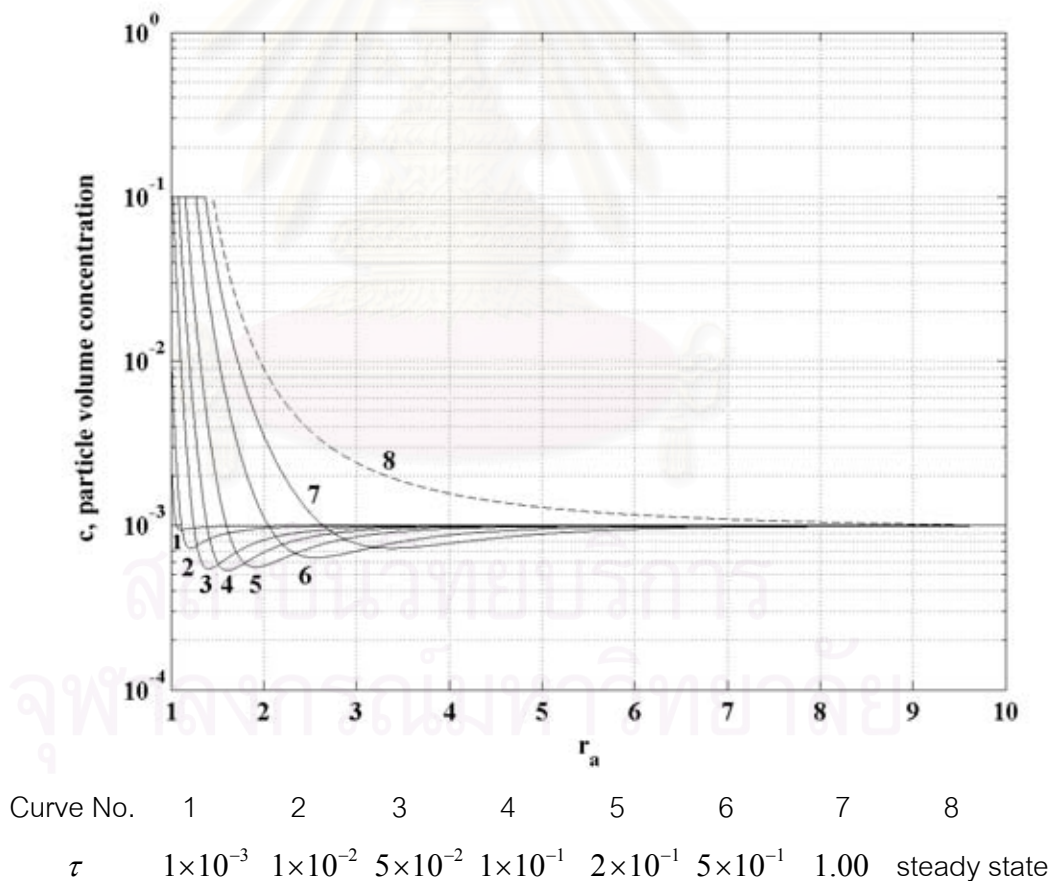


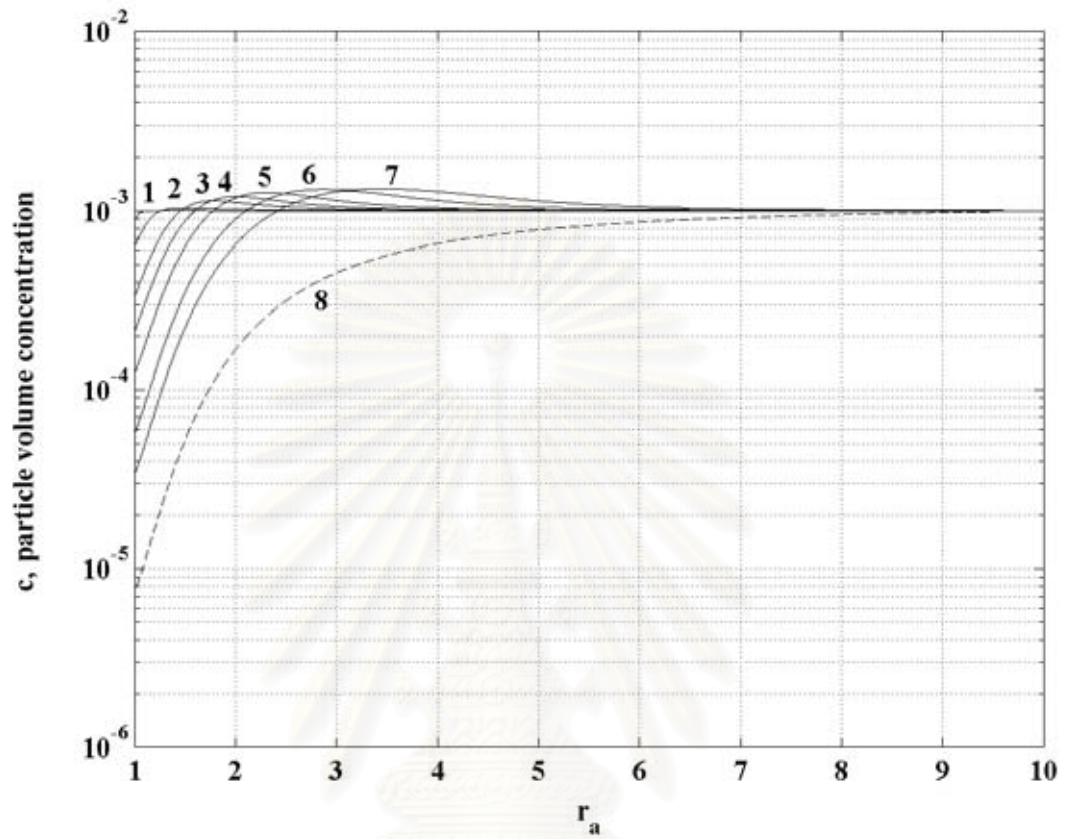
Figure 5.1: Time evolution of concentration distribution at $\theta = 0$ radian in paramagnetic mode, $G_0^{ferro} = -16.62$, $K_w = 0.80$.

In Figure 5.1, at small τ , particles accumulate dynamically on the surface of the collector and saturation does not occur. As τ increase, concentration on the surface of the collector increase which corresponds to the attractive magnetic force at $\theta = 0$ radian. As τ increase continuously, particles accumulate densely on the surface of the collector, inter-particle forces (both electric and magnetic types) will limit the concentration of particles to a finite value called the saturation concentration. Consequently, when τ is larger than a certain value, saturation concentration take places on the surface of the collector. The saturation region extends with increasing τ . The dash line in the figure represents the analytical steady-state solution of this situation which is the theoretical limit of numerical time-dependent solutions in curves number 1 to 7. The expression of steady-state solution for this situation is determined in the Appendix G.

The result in Figure 5.1 is obtained by using the same set of parameters as the former work produced in 1998 by R. Gerber and coworkers [3]. These two results are compared and we find that they are consistent. This consistency indicates that our simulation methodology is reliable.

The former work of R. Gerber and coworkers consider the capture in paramagnetic mode at $\theta = 0$ radian only. In our work, ultra-fine particle capture in paramagnetic mode at $\theta = \pi/2$ radian is also considered. Figure 5.2 shows the distribution of particle concentration at $\theta = \pi/2$ radian at various normalized times, the radial magnetic force become repulsive at this angle.

In Figure 5.2, we can see that, at $\theta = \pi/2$ radian, particle concentration on the surface of the collector decreases with increasing normalized time. These features is opposite to those in Figure 5.1, this is because the directions of magnetic forces in these two cases are opposite. From equation (2.20) of Chapter II, radial magnetic force becomes repulsive at $\theta = \pi/2$ radian. Ultra-fine particles in the region near to surface of the collector are repelled, by the magnetic force, to other regions faraway from the collector. As τ increase, amount of ultra-fine particles in the region near to the collector surface more rare. The dash line in the Figure 5.2 represents the analytical steady-state solution of this situation.



Curve No.	1	2	3	4	5	6	7	8
τ	1×10^{-3}	1×10^{-2}	5×10^{-2}	1×10^{-1}	2×10^{-1}	5×10^{-1}	1.00	steady state

Figure 5.2: Time evolution of concentration distribution at $\theta = \pi/2$ radian in paramagnetic mode, $G_0^{ferro} = -16.62$, $K_w = 0.80$.

5.1.2 Diamagnetic Mode of the Capture

In the second situation, the ultra-fine particle is diamagnetic gold particle of radius $b_p = 6.92 \times 10^{-8}$ m. An assembly of gold particles dispersed in a static water. The effective magnetic susceptibility of the system (water + gold particles) is $\chi = -2.55 \times 10^{-5}$. This situation which $\chi < 0$ is called the diamagnetic mode of the capture. Properties of ferromagnetic collector and the uniform external magnetic field in this situation are all the same as the paramagnetic mode in previous section. The value of factors G_0^{ferro} and K_w in this situation are $G_0^{ferro} = +17.18$, $K_w = 0.80$. The value of initial particle concentration is set equal to $C_0 = 8 \times 10^{-4}$ and the saturation concentration is set equal to $C_{sat} = 0.10$. The position of the outer boundary is at $r_{al} = 10.00$ and the value of concentration at the outer boundary is held fixed equal to initial concentration for all normalized times. For the diamagnetic mode, the radial component of the magnetic force is strongest attractive at $\theta = \pi/2, 3\pi/2$ radian whereas the strongest repulsive magnetic force occur at $\theta = 0, \pi$ radian (see equation (2.20) of Chapter II). Figure 5.3 shows the distribution of concentration in the diamagnetic mode at $\theta = \pi/2$ radian at various normalized times.

In Figure 5.3, we can see that, since the radial magnetic force is attractive at $\theta = \pi/2$ radian, the concentration on the surface of the collector increases with τ . When two results in Figure 5.1 and 5.3 are compared, we can see that, at the same value of τ , the increasing of particle concentration on the surface of the collector in diamagnetic mode is slower than that of the paramagnetic mode. At $\tau = 1.00$, saturation concentration take place on the surface of the collector in paramagnetic mode but dose not take place in the diamagnetic mode. This can be understood by consider equation (2.27) of Chapter II. We consider on the surface of the collector so $r_a = 1.00$, in paramagnetic mode at $\theta = 0$ radian the absolute value of the function G_r is 29.92 whereas in diamagnetic mode at $\theta = \pi/2$ radian the absolute value of the function G_r is 3.44 which is much smaller. The dash line in the figure represents the analytical steady-state solution of this situation. We can see that saturation concentration take place on the surface of the collector at steady state in this situation.

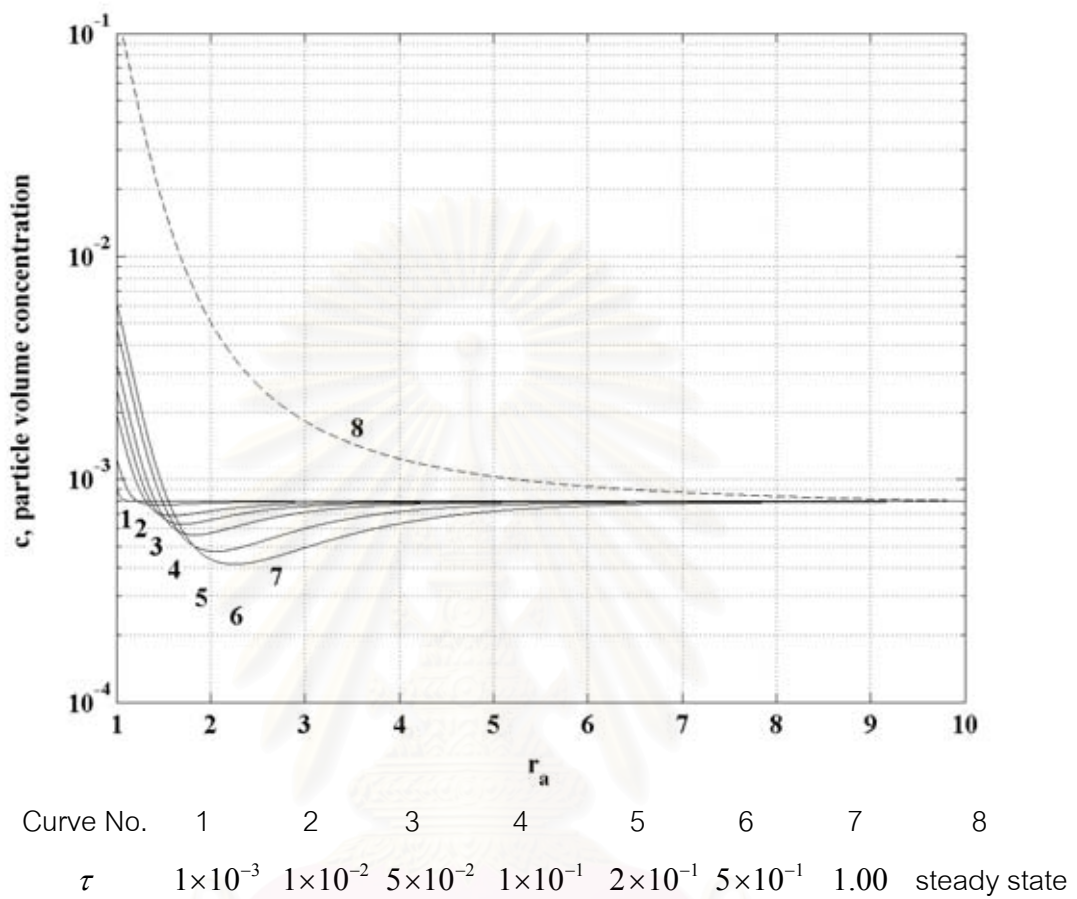


Figure 5.3: Time evolution of concentration distribution at $\theta = \pi/2$ radian in diamagnetic mode, $G_0^{ferro} = +17.18$, $K_w = 0.80$.

The result in Figure 5.3 obtained by using the same set of parameters as a former work published in 1998 by R. Gerber and coworkers [3]. These two results are compared and the consistency is found. This consistency confirms the reliability of our simulation methodology.

Figure 5.4 shows the distribution of concentration in the diamagnetic mode at $\theta = 0$ radian at various normalized times. At this angle, the radial magnetic force becomes repulsive. In Figure 5.4, we can see that the value of particle concentration on the surface of the collector decreases with increasing normalized times. When two results in Figures 5.2 and 5.4 are compared, we see that the decreasing of concentration on the surface of the collector in diamagnetic mode is faster than that in the paramagnetic mode. This is because the absolute value of the function G_r on the surface of the collector at $\theta = 0$ radian in this situation is 30.92 whereas in the paramagnetic mode, at $\theta = \pi/2$ radian, the absolute value of the function G_r is 3.32 which is much smaller. The dash line in the figure represents the analytical steady-state solution of this situation.

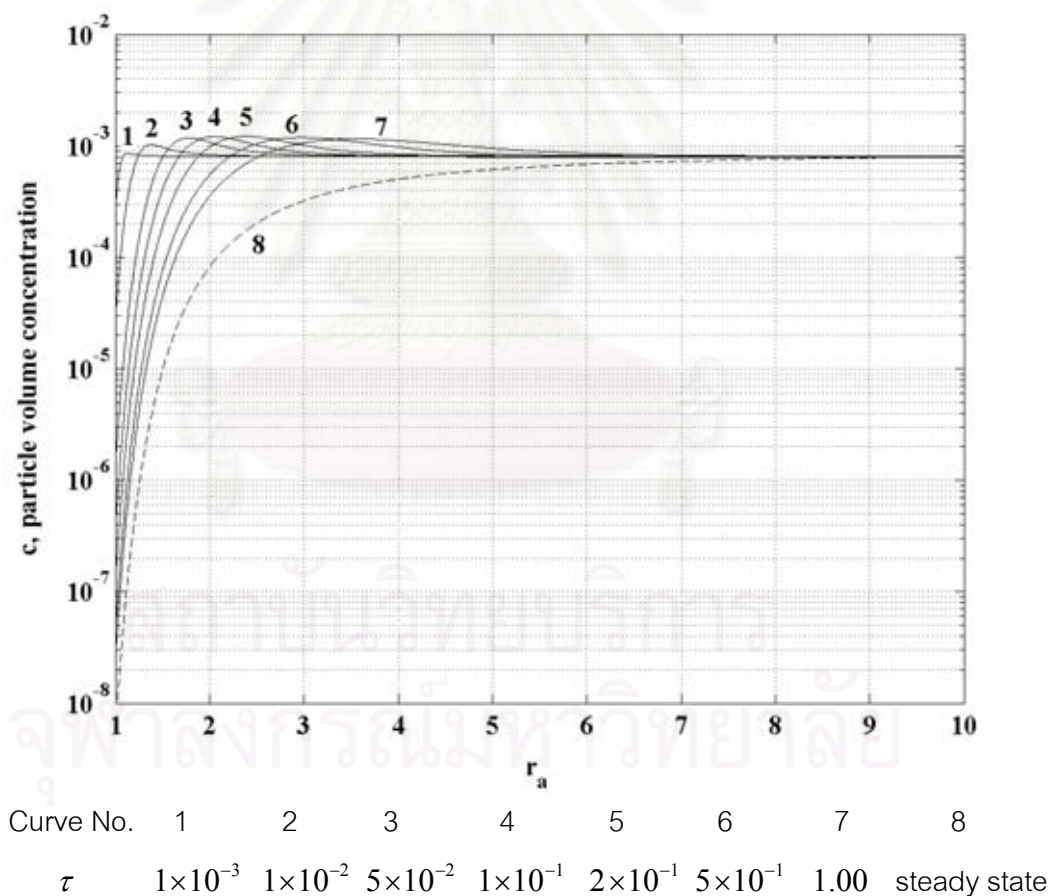


Figure 5.4: Time evolution of concentration distribution at $\theta = 0$ radian in diamagnetic mode, $G_0^{ferro} = +17.18$, $K_w = 0.80$.

From Figure 5.1, we have seen that saturation concentration take place on the surface of the collector in HGMS capture of $Mn_2P_2O_7$ particles. It is interested to investigate how the occurrence of the saturation concentration on the surface of the collector depends on the magnitude of the uniform external magnetic field H_0 . Figure 5.5 shows the variation of τ_{sat} with H_0 where τ_{sat} is defined as the value of normalized time that saturation concentration begins to take place on the surface of the collector. In Figure 5.1, at $\tau = 5 \times 10^{-2}$ the saturation concentration take places on the surface of the collector then we obtain $\tau_{sat} \approx 5 \times 10^{-2}$ for the situation in Figure 5.1.

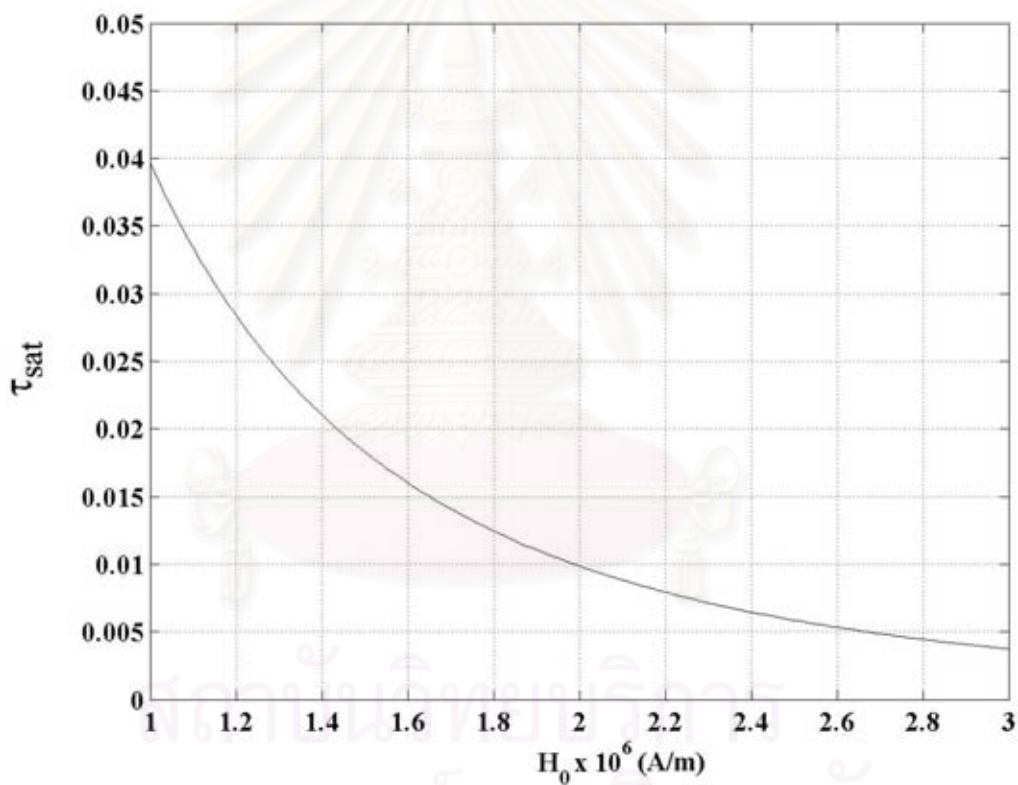


Figure 5.5: Variation of τ_{sat} with H_0 in paramagnetic mode of one dimensional capture of $Mn_2P_2O_7$ particle.

From Figure 5.5, at the value of $H_0 = 1 \times 10^6$ A/m, the value of $\tau_{sat} \approx 0.040$ which is close to the value 0.050 given by approximating curve number 3 in Figure 5.1.

In Figure 5.5, we see that the value of τ_{sat} decreases rapidly with increasing H_0 . If the variation of τ_{sat} with H_0 is plotted in semi-logarithmic scale, the result is given in Figure 5.6. From Figure 5.6, we can approximate that the value of $\log_{10}(\tau_{sat})$ decreases linearly with H_0 , Consequently, we may approximate that the value of τ_{sat} decrease ,with increasing H_0 , by the factor which is the negative power of 10.

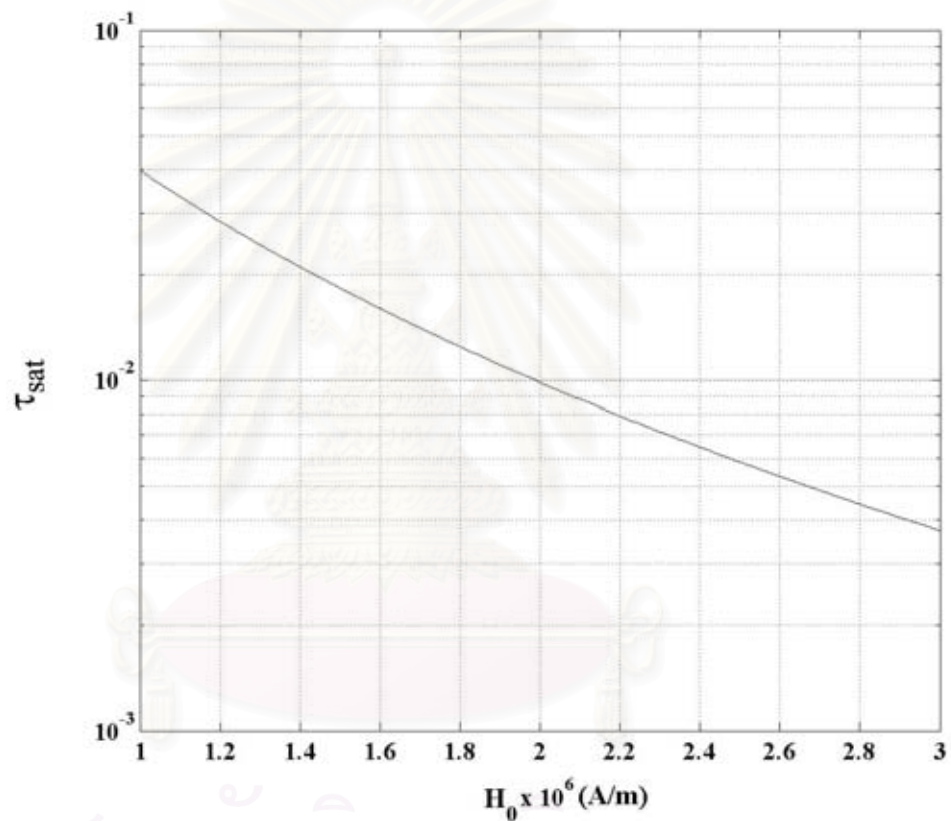


Figure 5.6: Variation of τ_{sat} with H_0 in paramagnetic mode of one dimensional capture of $Mn_2P_2O_7$ particles plotted in semi-logarithmic scale.

All results of simulations shown in Figures 5.1 to 5.6 achieved by using values of grid steps $\Delta r_a = 4 \times 10^{-3}$ and $\Delta \tau = 2 \times 10^{-7}$. From equation (4.25) of chapter IV, we can estimate that the maximum error of the computation generated at $\tau = 1.00$ is in the order of 10^{-5} .

5.2 Two Dimensional Simulations of the Capture of Ultra-Fine Particle by a Single-Ferromagnetic Cylindrical Collector

In this section, HGMS capture of ultra-fine particles by a single ferromagnetic cylindrical collector is simulated in all the same situations as the previous section of one dimensional case but all simulations here are performed in two dimensions.

5.2.1 Paramagnetic Mode of the Capture

The first situation is the paramagnetic mode of the capture. The ultra-fine particle is paramagnetic $\text{Mn}_2\text{P}_2\text{O}_7$ particle of radius $b_p = 1.2 \times 10^{-8}$ m. An assembly of $\text{Mn}_2\text{P}_2\text{O}_7$ particles dispersed in a static water. The effective magnetic susceptibility of the system (water + $\text{Mn}_2\text{P}_2\text{O}_7$ particle) is $\chi = +4.73 \times 10^{-3}$. The ferromagnetic collector is considered to be homogeneous saturate magnetized perpendicular to its axis by a uniform external magnetic field $H_0 = 1.0 \times 10^6$ A/m points in the positive X direction and its saturate magnetization is $M_s = 1.6 \times 10^6$ A/m. Let the absolute temperature equal to 300 K. The values of factors $G_0^{ferro} = -16.62$ and $K_w = 0.80$. The value of initial concentration at every points in the computational domain is set equal to $C_0 = 1.0 \times 10^{-3}$ and the saturation concentration is set equal to $C_{sat} = 0.10$. Grid steps used in this two-dimensional simulation are $\Delta r_a = 1 \times 10^{-2}$, $\Delta \theta = 1 \times 10^{-1}$, and $\Delta \tau = 1 \times 10^{-5}$. The outer boundary of the computational domain is set at $r_{al} = 10.00$ and the boundary condition is assigned that the value of particle concentration at all points on the outer boundary are held fixed at the initial concentration for all normalized times. The results of the simulation are presented to illustrate the behavior of the build-up of ultra-fine particles on the collector.

Figure 5.7 shows the family of concentration contours in various regions around the collector those describing the build-up features of ultra-fine particles on the surface of the collector.

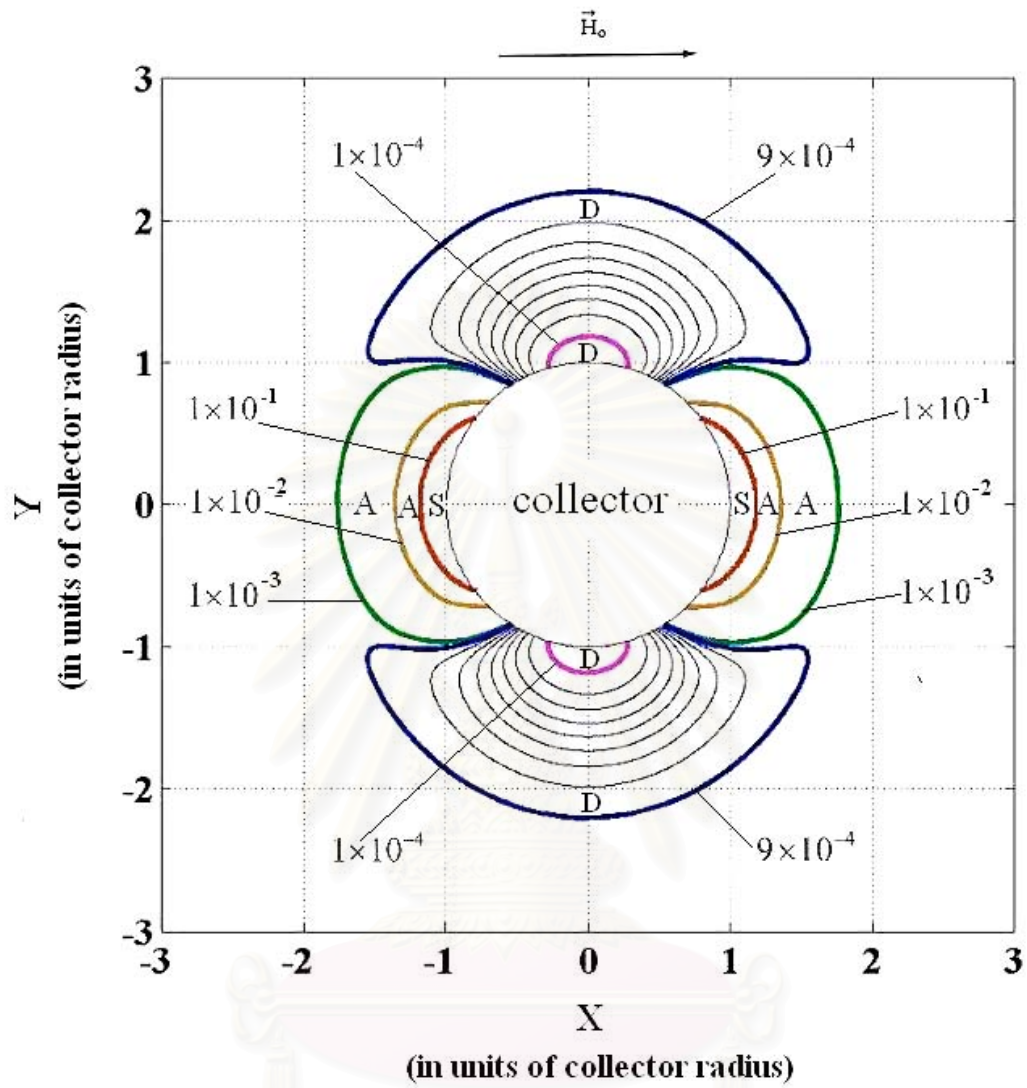


Figure 5.7: A family of concentration contours around the ferromagnetic collector in paramagnetic mode, $G_0^{ferro} = -16.62$, $K_w = 0.80$.

จุฬาลงกรณ์มหาวิทยาลัย

In Figure 5.7, we can see the feature of the build-up of ultra-fine particles on the ferromagnetic collector. Regions around the collector can be specified in three zones. The first zone is called the saturation region where concentration at all points equal to the saturation concentration $C_{sat} = 0.10$. Saturation regions in the figure are labeled by the symbol \boxed{S} . The second zone is called the accumulation region where the value of concentration is larger than the initial concentration but less than the saturation concentration that is $C_0 < c < C_{sat}$. Particles accumulate dynamically in the accumulation region. Accumulation regions in the figure are labeled by the symbol \boxed{A} . The radial magnetic force is attractive in both saturation and accumulation regions. The third zone is called the depletion region where the value of concentration is less than the initial value that is $0 < c < C_0$. The radial magnetic force is repulsive in the depletion region. Depletion regions in the figure are labeled by the symbol \boxed{D} .

In Figure 5.7, we see that, in paramagnetic mode, the build-up of ultra-fine particles on the ferromagnetic collector occur in the direction parallel to the direction of uniform external magnetic field \vec{H}_0 which is the X -direction in the figure. Particles depleted in the direction that perpendicular to the direction of \vec{H}_0 since, due to magnetic force, they are repelled to other regions.

Figure 5.8 shows concentration distribution at $\theta = 0, \pi$ radian at various normalized times and Figure 5.9 shows concentration distribution at $\theta = \pi/2, 3\pi/2$ radian at the same normalized times. The dash line in the each figure represents the analytical steady-state solution at that angle. From these figures, we can see that when capture process proceeds, ultra-fine particles are transferred, by the action of the magnetic force, from depletion regions to accumulation and saturation regions. In the saturation region, particles accumulate highly dense and all particles contained in this region are separated from the fluid. When the capture process is terminated, the external magnetic field is shutdown and particles those are captured in saturation regions can be washed from the collector.

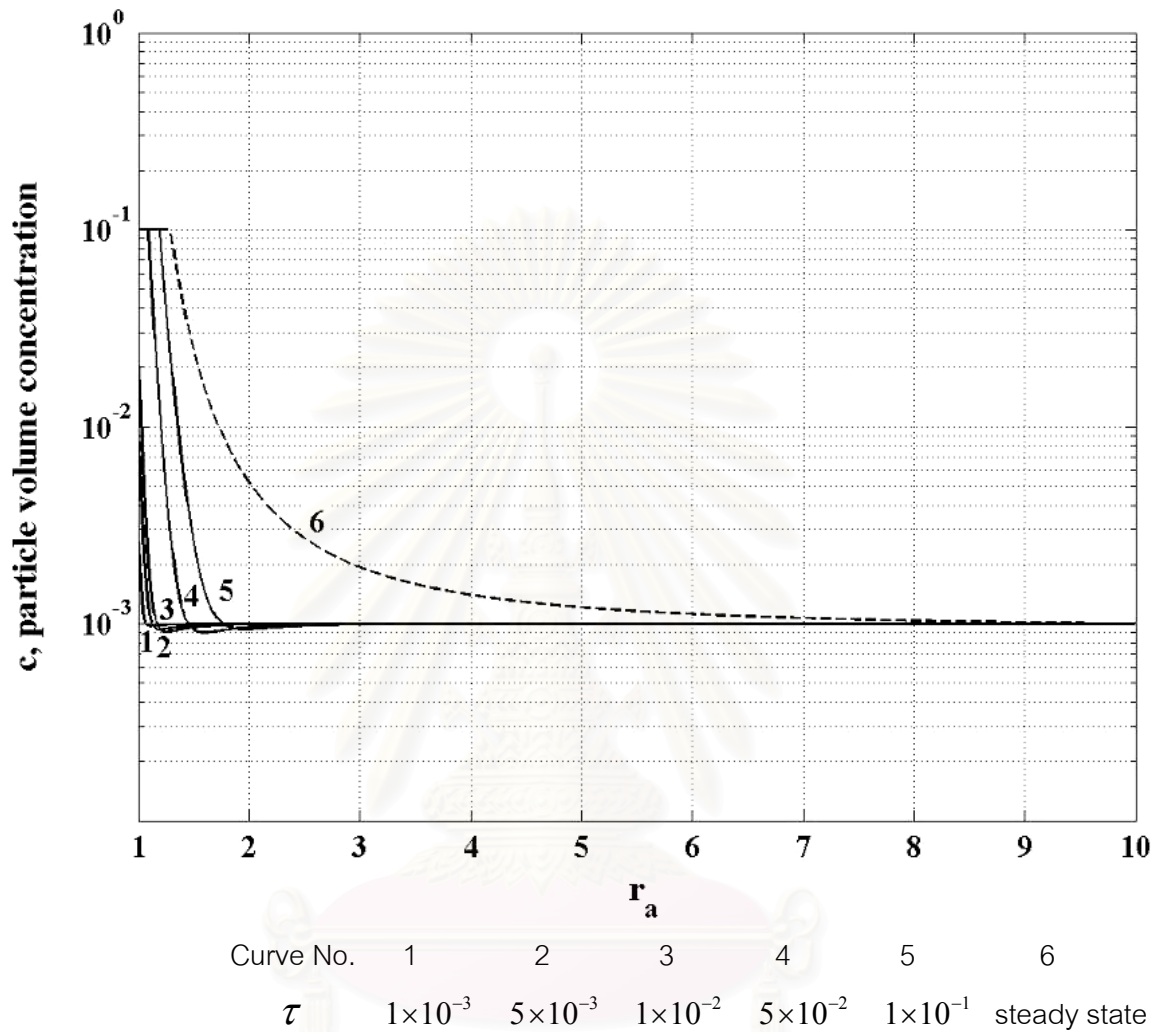
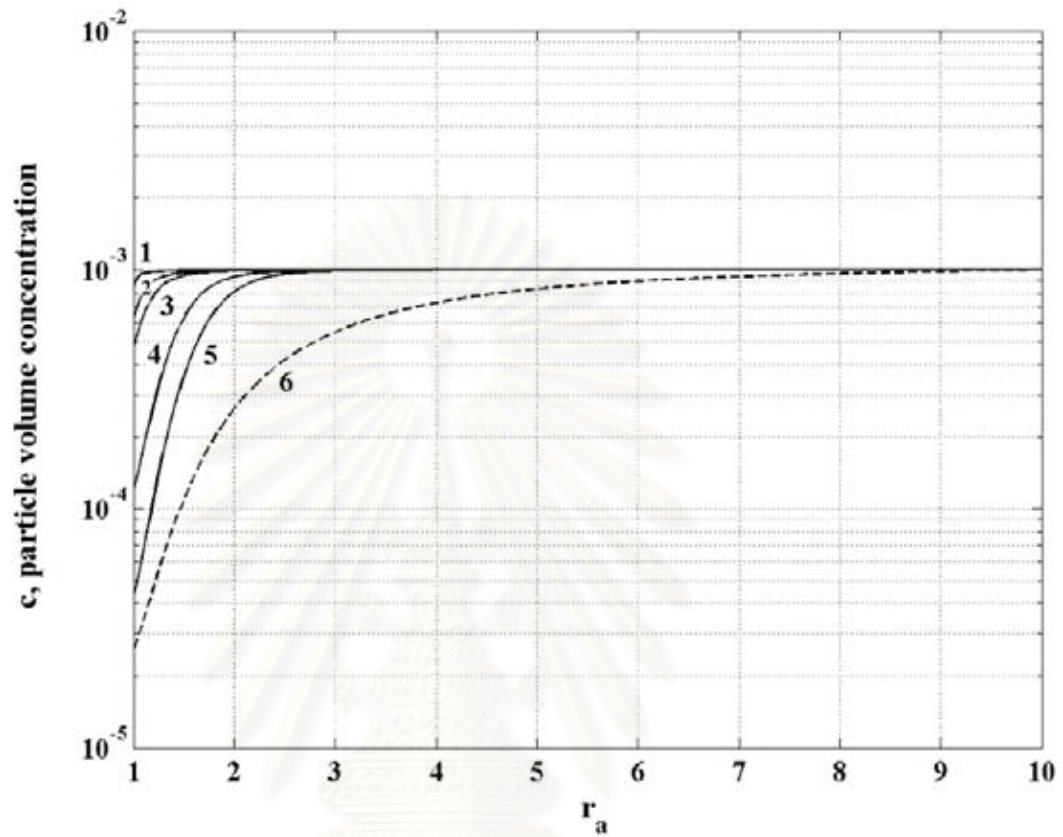


Figure 5.8: Concentration distribution at $\theta = 0, \pi$ radian at various normalized times in paramagnetic mode, $G_0^{ferro} = -16.62, K_w = 0.80$.



Curve No.	1	2	3	4	5	6
τ	1×10^{-3}	5×10^{-3}	1×10^{-2}	5×10^{-2}	1×10^{-1}	steady state

Figure 5.9: Concentration distribution at $\theta = \pi/2, 3\pi/2$ radian at various normalized times in paramagnetic mode,

$$G_0^{ferro} = -16.62, K_w = 0.80.$$

Figure 5.10 shows a comparison between steady-state concentration distribution at $\theta = 0$ radian and $\theta = \pi/2$ radian. From this comparison, we see that the maximum concentration ($C_{sat} = 0.10$) is about 5000 times of the minimum concentration. Consequently, almost total amounts of ultra-fine particles in depletion regions are transferred to saturation and accumulation regions.

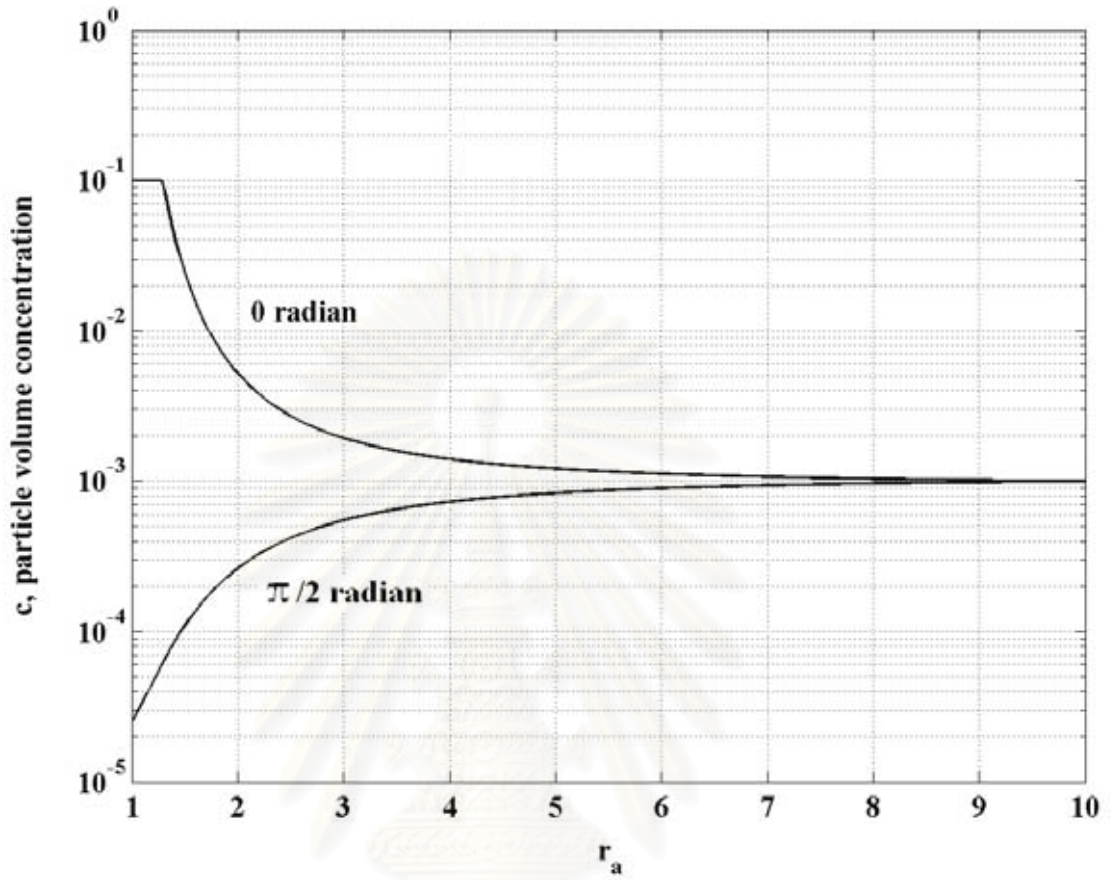


Figure 5.10: Comparison between steady-state concentration distribution at

$\theta = 0$ and $\pi/2$ radian in paramagnetic mode,

$$G_0^{ferro} = -16.62, K_w = 0.80.$$

The family of concentration contours shown in Figure 5.7 is compared with the result of the former work published by L. P. Davies and R. Gerber in 1990 [8]. In their work, HGMS capture of $Mn_2P_2O_7 \cdot 3H_2O$ particles ($b_p = 1.2 \times 10^{-8}$ m, $\chi = 2.03 \times 10^{-3}$) in aqueous suspension by a thin stainless steel wire of radius $a = 5 \times 10^{-5}$ m and saturate magnetization $M = 8.61 \times 10^5$ A/m is simulated in paramagnetic mode. The uniform external magnetic field is $H_0 = 1 \times 10^7$ A/m. The factors $G_0^{ferro} = -38.4$, $K_w = 0.04305$ and the initial concentration is $C_0 = 1 \times 10^{-3}$. The capture process was simulated until $\tau = 0.20$. We find that the features the build-up of ultra-fine particles on the surface of the collector in these two results are consistent. Consequently, our simulation methodology in this two-dimensional case can be considered reliable.

All results of two dimensional simulations shown in Figures 5.7 to 5.10 are achieved by using values of grid steps $\Delta r_a = 1 \times 10^{-2}$, $\Delta \theta = 1 \times 10^{-1}$ and $\Delta \tau = 1 \times 10^{-5}$. From equation (4.53) of Chapter IV, we can estimate that the maximum error of the computation generated at $\tau = 0.10$ is in the order of 10^{-3} .

All results shown in Figure 5.7 to 5.9 are simulated from $\tau = 0$ to $\tau = 0.10$. Now we will consider steady state of HGMS capture process in two dimensions. From the original continuity equation (2.5) of Chapter II, we assume that the magnetic force is only the force that dominates the capture process. The outer boundary condition is assigned that the value of particle concentration at every points on the outer boundary is held fix equal to the initial concentration for all normalized times. From these assumptions we can determine the steady-state solution of the original continuity equation (2.5) in two dimensions as (see Appendix G)

$$c_s(r_a, \theta) = \lambda(\theta) \exp \left[\frac{U_m(r_a, \theta)}{k_B T} \right], \quad (5.1)$$

where U_m is the magnetic potential energy of the system of particles and fluid,

$$U_m(r_a, \theta) = \frac{1}{2} \mu_0 (\chi_p - \chi_f) H^2(r_a, \theta) \quad (5.2)$$

and $\lambda(\theta)$ is a function of θ which make the value of $c_s(r_a, \theta)$ satisfy the outer boundary condition at all points on the outer boundary of the computational domain,

$$\lambda(\theta) = \frac{C_0}{\left[\frac{U_m(r_{aL}, \theta)}{k_B T} \right]}, \quad (5.3)$$

where C_0 is the initial concentration.

For this situation where the collector is a ferromagnetic one, from equation (2.13) of Chapter II, we can determine the expression of $U_m(r_a, \theta)$ as

$$U_m(r_a, \theta) = \frac{1}{2} \mu_0 (\chi_p - \chi_f) \left[H_0^2 + \frac{MH_0 \cos(2\theta)}{r_a^2} + \frac{M^2}{4r_a^2} \right], \quad (5.4)$$

where M is the magnetization of the ferromagnetic collector.

From equations (5.1) to (5.4), we can generate the steady-state concentration contours in the paramagnetic mode as shown in Figure 5.11.

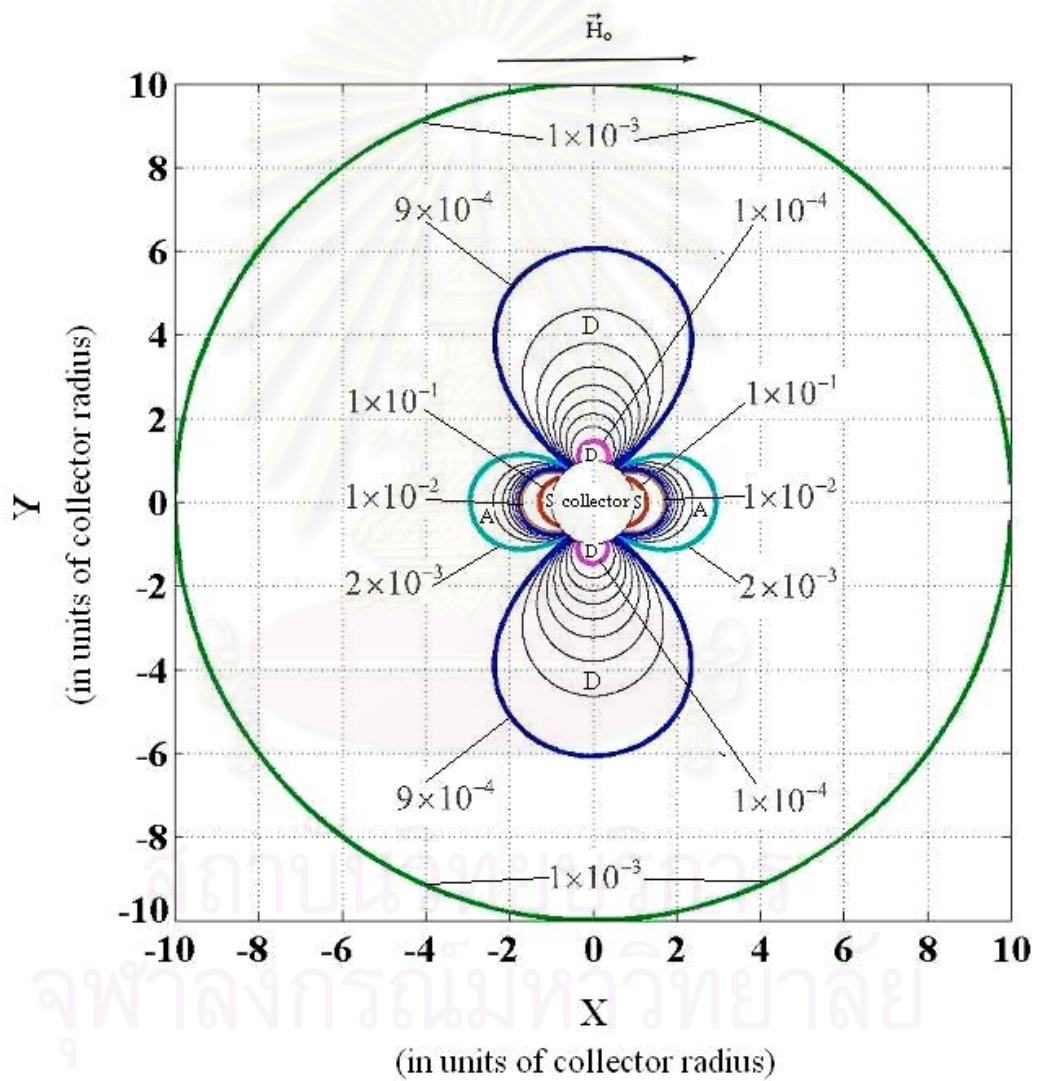


Figure 5.11: Steady-state concentration contours around the ferromagnetic collector in paramagnetic mode, $G_0^{ferro} = -16.62$, $K_w = 0.80$.

In the Figure 5.11, we generate the steady-state concentration contours in capture process of the ultra-fine paramagnetic $\text{Mn}_2\text{P}_2\text{O}_7$ particle of radius $b_p = 1.2 \times 10^{-8}$ m. An assembly of $\text{Mn}_2\text{P}_2\text{O}_7$ particles dispersed in a static water. The effective magnetic susceptibility of the system (water + $\text{Mn}_2\text{P}_2\text{O}_7$ particle) is $\chi = +4.73 \times 10^{-3}$. The ferromagnetic collector is considered to be homogeneous saturate magnetized perpendicular to its axis by a uniform external magnetic field $H_0 = 1.0 \times 10^6$ A/m points in the positive X direction and its saturate magnetization is $M_s = 1.6 \times 10^6$ A/m. The absolute temperature equal to 300 K. The factor $G_0^{ferro} = -16.62$ and the factor $K_W = 0.80$. The value of initial concentration at every points in the computational domain is set equal to $C_0 = 1.0 \times 10^{-3}$ and the saturation concentration is set equal to $C_{sat} = 0.10$.

Figure 5.11 depicts the feature of the build-up of ultra-fine particles on the collector at steady state. Locations of saturation, accumulation and depletion regions are specified.

In this research, we define a variable denoted by P_{sat} as the percent of the volume of ultra-fine particles those captured in saturation regions from total volume of ultra-fine particles in the computational domain,

$$P_{sat} = \frac{\text{volume of ultra-fine particles captured in saturation regions}}{\text{total volume of ultra-fine particles in the computational domain}} \times 100 . \quad (5.5)$$

From the family of concentration contours in Figure 5.7, we can determine the variation of P_{sat} with normalized time τ as shown in Figure 5.12. In Figure 5.12, we can see that, for this paramagnetic mode, the saturation concentration take places at about $\tau = 0.020$. When $\tau = 0.10$ the value of P_{sat} is about 10%.

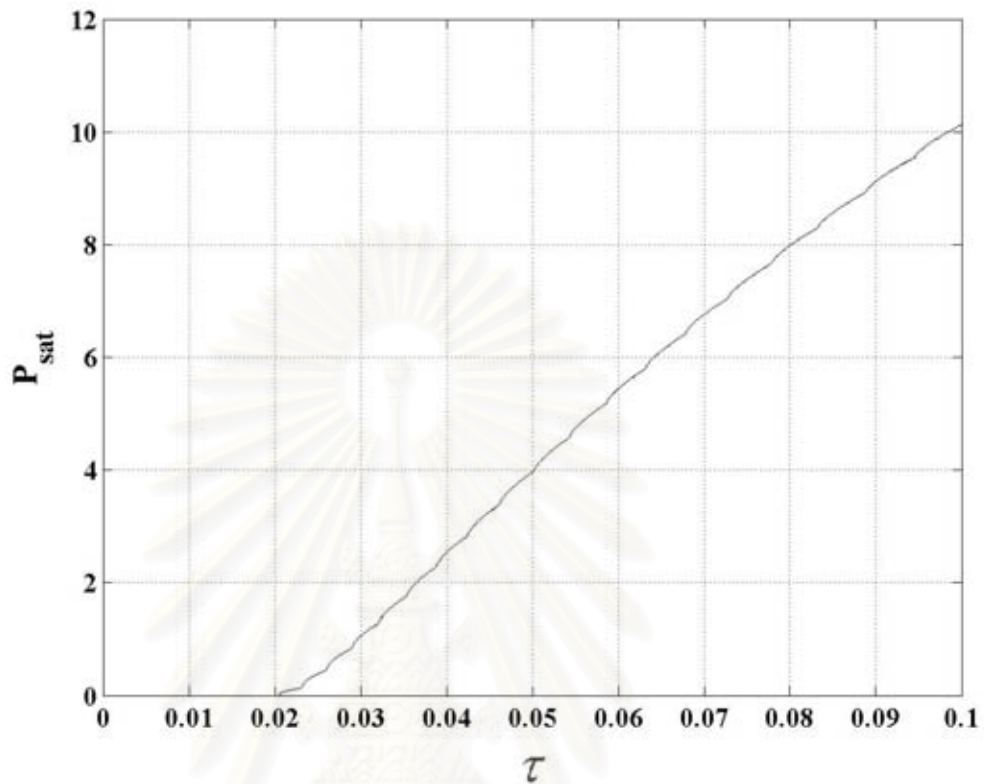


Figure 5.12: Variation of P_{sat} with τ in the paramagnetic mode,

$$G_0^{ferro} = -16.62, K_W = 0.80.$$

Since we can determine the steady-state solution $c_s(r_a, \theta)$, It is interested to determine how the value of P_{sat} at steady state vary with the magnitude of uniform external magnetic field H_0 . This result is shown in Figure 5.13.

In Figure 5.13, if we consider at $H_0 = 1.0 \times 10^6$ A/m which equal to the value of uniform external magnetic field used in our simulation then we find that the steady-state value of P_{sat} for this value of H_0 equal to about 12.5%. When this data is compared with the result of simulation in Figure 5-12, we can estimate that , for the value of $H_0 = 1.0 \times 10^6$ A/m , the capture process reach the steady state at normalized time τ small amount greater than 0.10.

Figure 5.13 can help us for adjustment the optimum value of the uniform external magnetic field when the certain amount of ultra-fine particles to be separated from the fluid is specified.

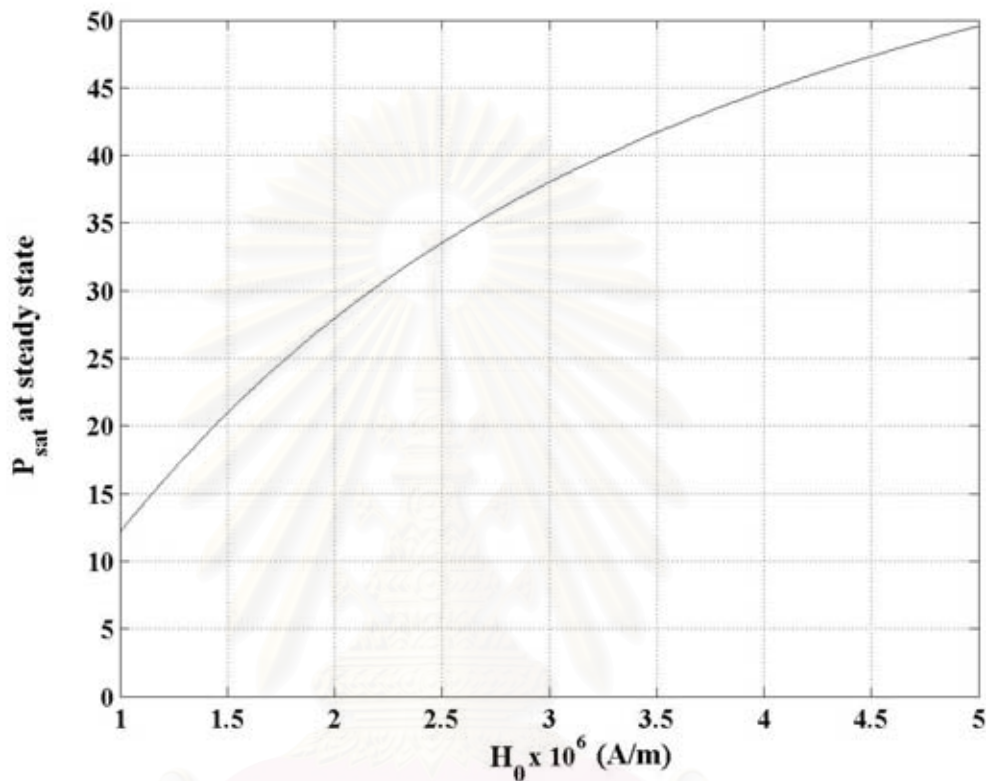


Figure 5.13: Variation of steady-state P_{sat} with H_0 in paramagnetic mode, $G_0^{ferro} = -16.62$, $K_w = 0.80$.

5.2.2 Diamagnetic Mode of the Capture

In the diamagnetic mode, the ultra-fine particle is diamagnetic gold particle of radius $b_p = 6.92 \times 10^{-8}$ m. An assembly of gold particles dispersed in a static water. The effective magnetic susceptibility is $\chi = -2.55 \times 10^{-5}$. The ferromagnetic collector is considered to be homogeneous saturate magnetized perpendicular to its axis by a uniform external magnetic field $H_0 = 1.0 \times 10^6$ A/m points in the positive X direction and its saturate magnetization is $M_s = 1.6 \times 10^6$ A/m. The value of initial concentration is set equal to $C_0 = 8 \times 10^{-4}$ and the saturation concentration is set equal

to $C_{sat} = 0.10$. The position of the outer boundary is at $r_{al} = 10.00$ and the value of concentration at the outer boundary is held fixed equal to $C_0 = 8 \times 10^{-4}$ for all normalized times. For this diamagnetic mode, the factors $G_0^{ferro} = +17.18$ and $K_W = 0.80$.

Figure 5.14 shows the family of concentration contours around the collector at $\tau = 0.10$.

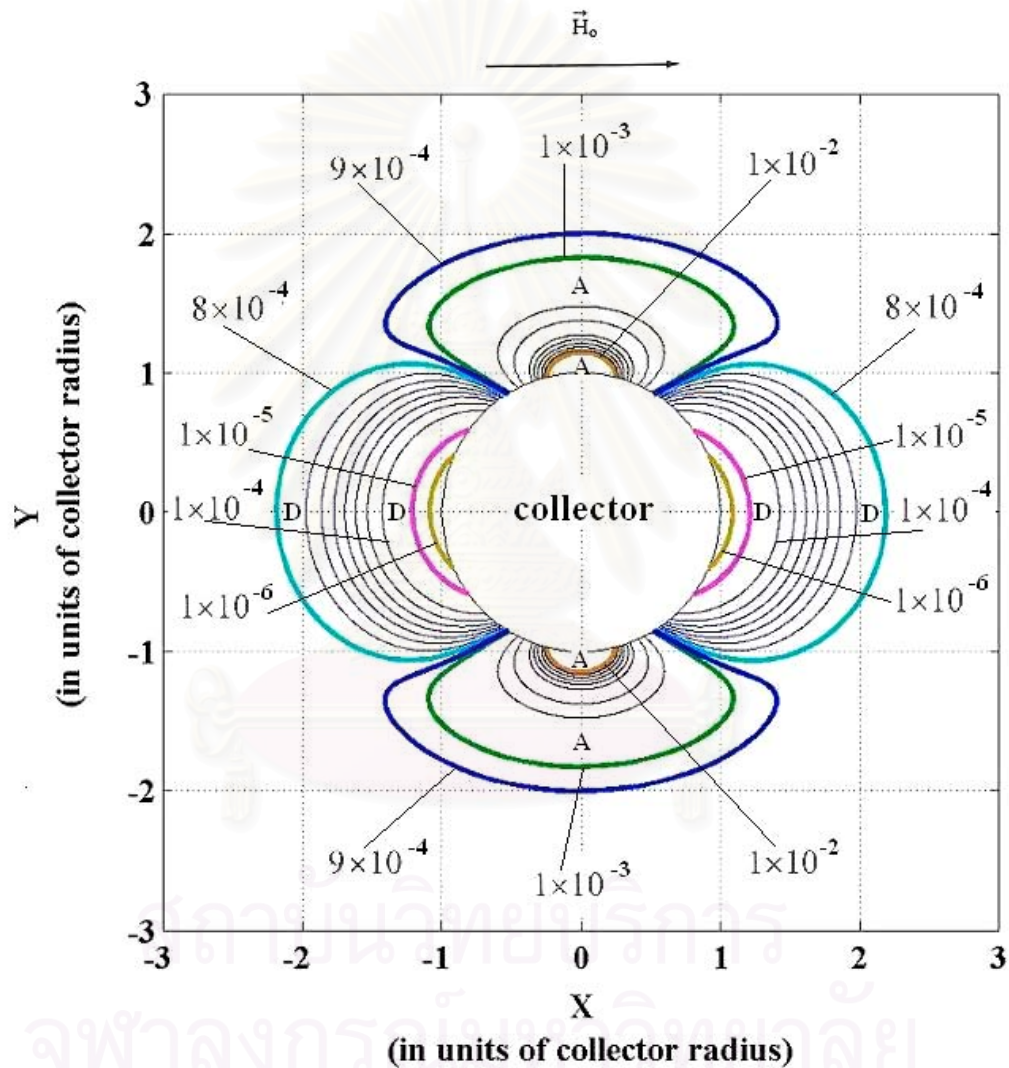
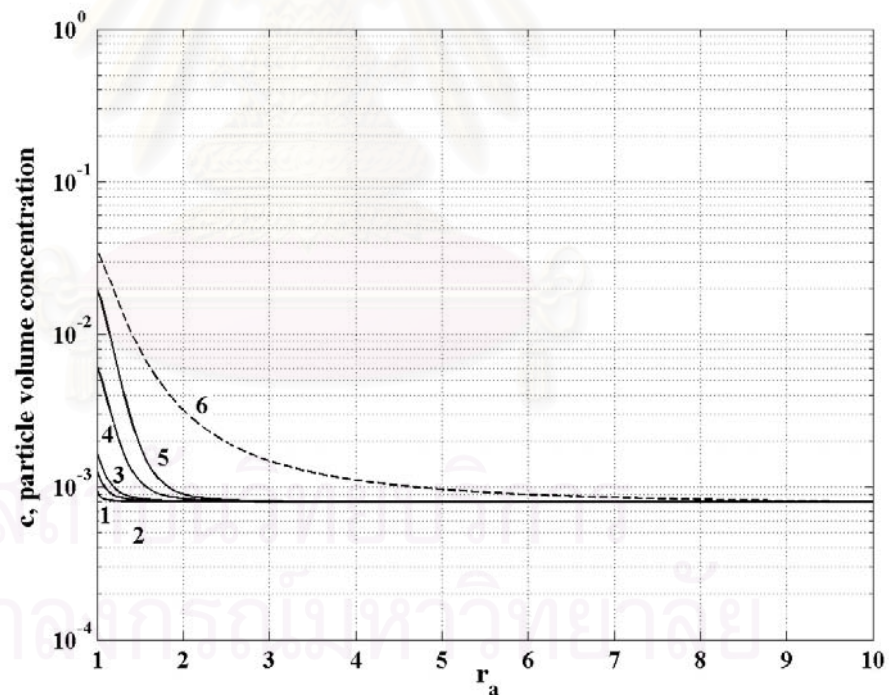


Figure 5.14: A family of concentration contours around ferromagnetic collector in diamagnetic mode, $G_0^{ferro} = +17.18$, $K_W = 0.80$, $\tau = 0.10$.

From this figure, we see that the location of accumulation regions and depletion regions in diamagnetic mode are opposite to those of paramagnetic mode.

This is because the directions of magnetic traction force between paramagnetic mode and diamagnetic mode are opposite. We see in Figure 5.14 that the saturation region does not exist on the surface of the collector, this tell us that, at $\tau = 0.10$, ultra-fine particles accumulate around the collector as a cloud but they are not retained statically on the surface of the collector. Consequently, ultra-fine particles are not separated from the fluid. The higher value of H_0 is required to achieve a successful separation in this diamagnetic mode.

Figure 5.15 shows the distribution of concentration in the diamagnetic mode at $\theta = \pi/2, 3\pi/2$ radian at various normalized times. The dash line in the figure represents the analytical steady-state solution at these angles. From this figure, we see that the concentration on the surface of the collector at $\theta = \pi/2, 3\pi/2$ radian increases with τ since the magnetic force is attractive at these angles.



Curve No.	1	2	3	4	5	6
τ	1×10^{-3}	5×10^{-3}	1×10^{-2}	5×10^{-2}	1×10^{-1}	steady state

Figure 5.15: Time evolution of concentration distribution at $\theta = \pi/2, 3\pi/2$ radian in diamagnetic mode, $G_0^{ferro} = +17.18$, $K_w = 0.80$.

Figure 5.16 shows the distribution of concentration in the diamagnetic mode at $\theta = 0, \pi$ radian at various normalized times. The dash line in the figure represents the analytical steady-state solution at these angles. From this figure, we see that the concentration on the surface of the collector at $\theta = 0, \pi$ radian decrease with τ since the magnetic force is repulsive at these angles.

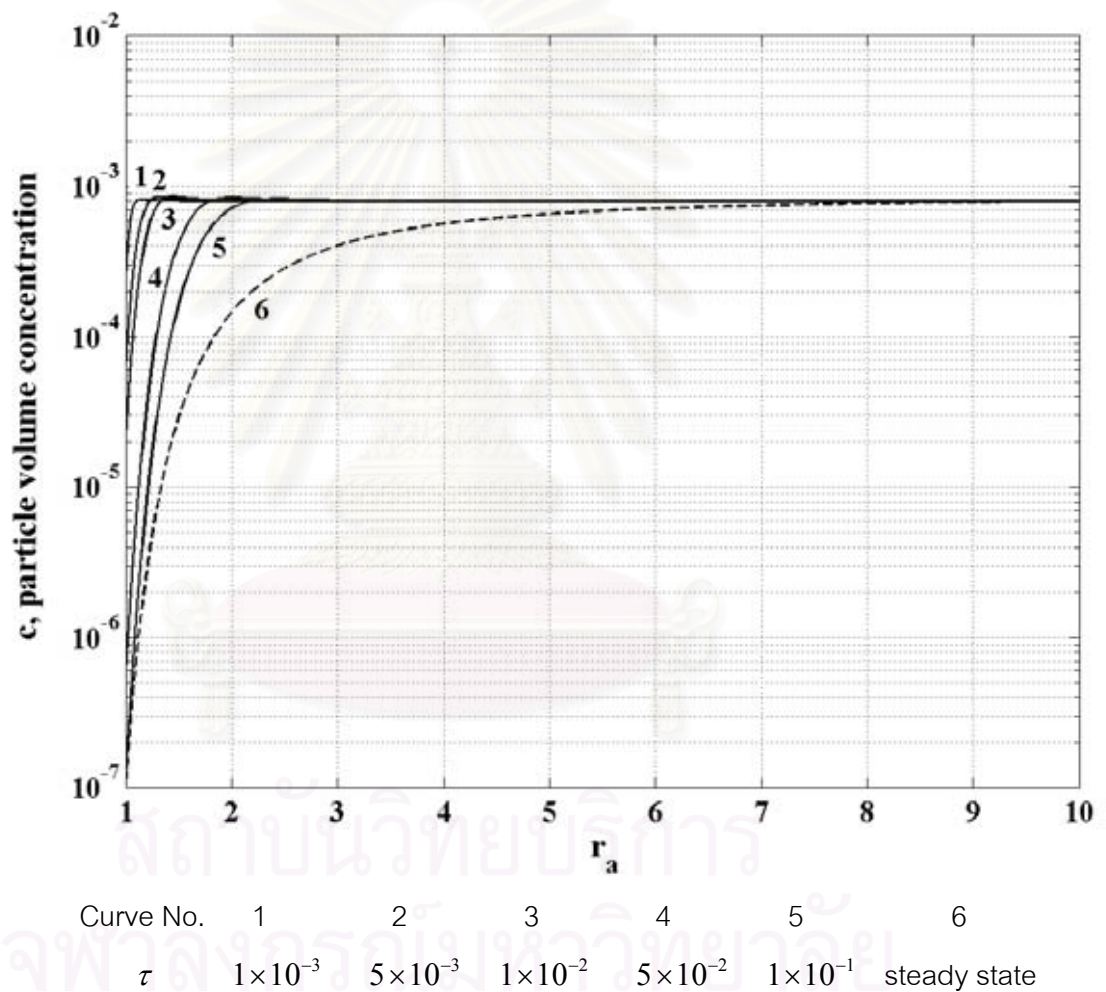


Figure 5.16: Time evolution of concentration distribution at $\theta = 0, \pi$ radian in diamagnetic mode, $G_0^{ferro} = +17.18$, $K_W = 0.80$.

Figure 5.17 shows concentration contours around the collector in diamagnetic mode at steady state. These contours are generated by using equations (5.1) to (5.4) where parameters are specified in pages 66 to 67. Contours in Figure 5.17 show us that, in the diamagnetic mode, particles accumulate in the direction perpendicular to the applied uniform external magnetic field (\vec{H}_0) and particles deplete in the direction parallel to the applied uniform external magnetic field. This result is opposite to the case of paramagnetic mode. In Figure 5.17, we see that no saturation region take place in this situation as we can see from the curve number 6 in Figure 5.15.

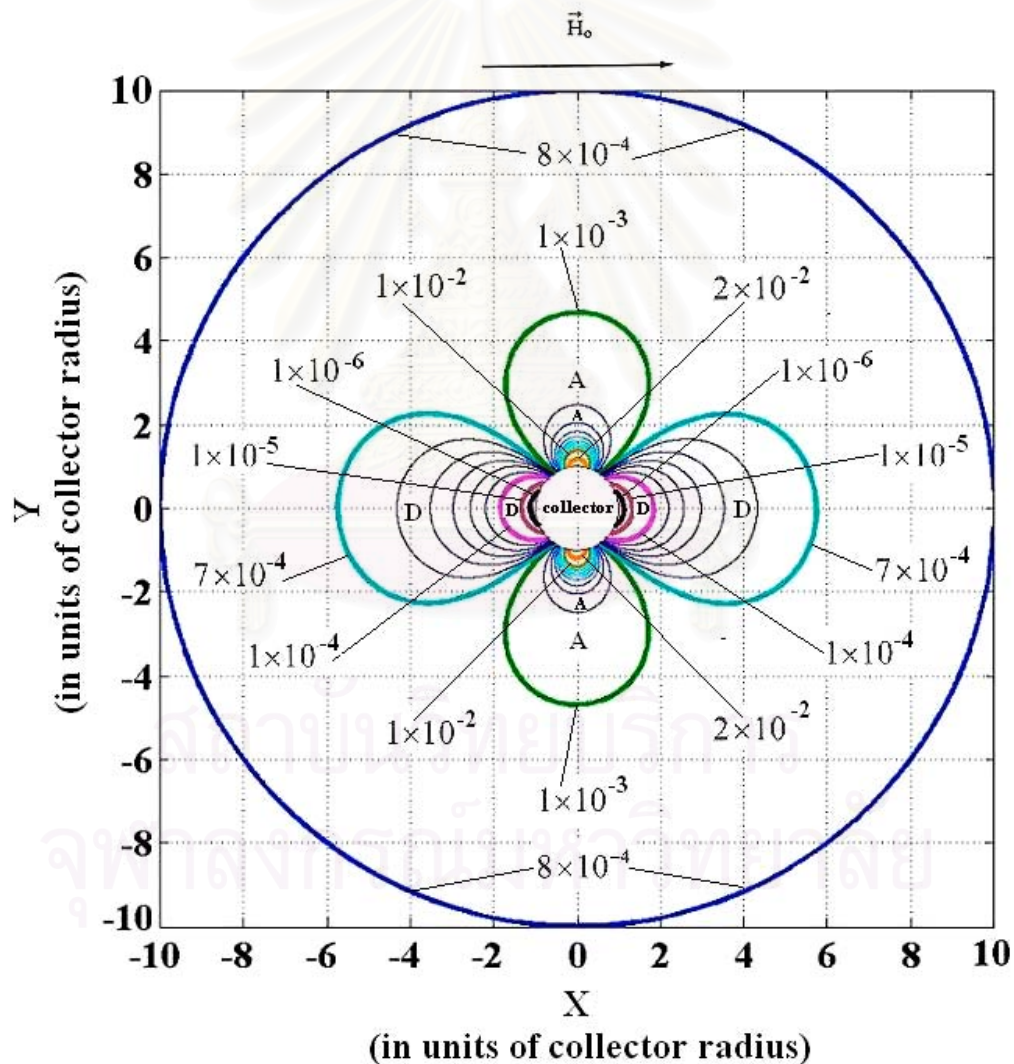


Figure 5.17: Steady-state concentration contours around the ferromagnetic collector in diamagnetic mode, $G_0^{ferro} = +17.18$, $K_W = 0.80$.

The absence of the saturation region at steady state in Figure 5.17 tell us that ultra-fine particles accumulate around the collector as a cloud but are not retained statically on the surface of the collector. Consequently, at steady state, ultra-fine particles are not separated from the fluid. The higher value of H_0 is required to achieve a successful separation in this diamagnetic mode. Figure 5.18 shows the variation of P_{sat} at steady state with H_0 in diamagnetic mode.

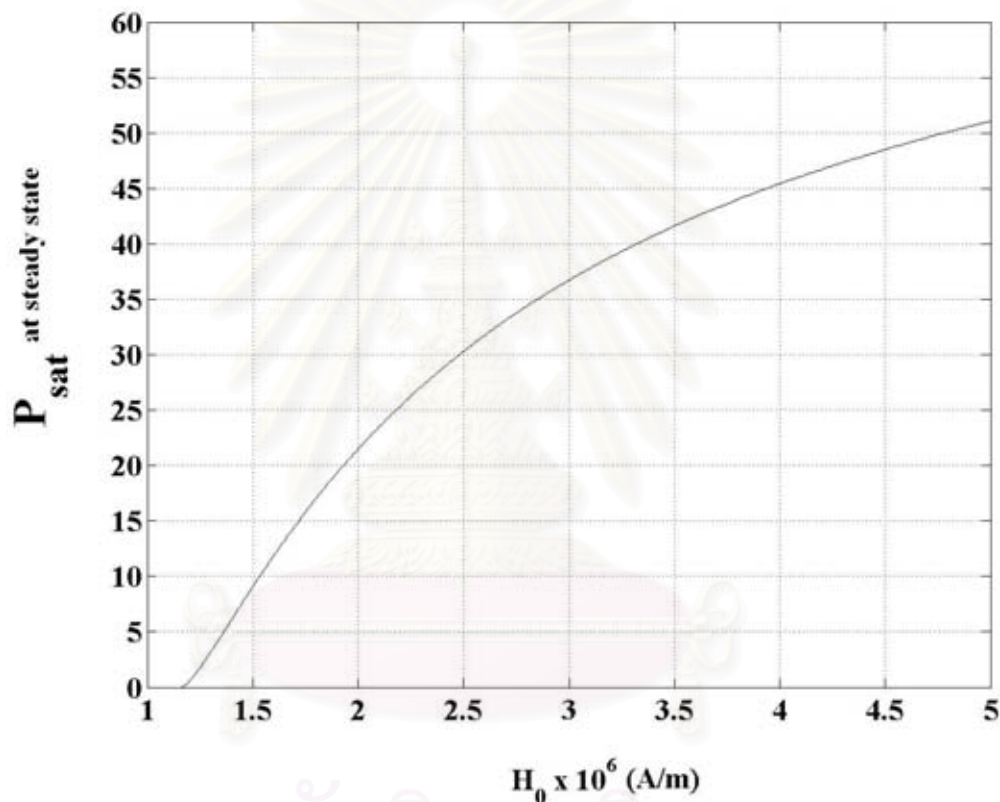


Figure 5.18: Variation of steady-state P_{sat} with H_0 in diamagnetic mode,

$$G_0^{ferro} = +17.18, K_w = 0.80.$$

In Figure 5.18, we see that, for $H_0 = 1 \times 10^6$ A/m, the value of steady-state P_{sat} equal to zero which corresponds to the result in Figure 5.17. The result in Figure 5.18 can help us for adjustment the optimum value of the uniform external magnetic field in diamagnetic mode when the certain amount of ultra-fine particles to be separated from the fluid is specified.

5.3 Two Dimensional Simulations of the Capture of Ultra-Fine Particles by an Assemblage of Random Paramagnetic Cylindrical Collectors

In this research, two dimensional simulations of the capture of ultra-fine particles by an assemblage of random paramagnetic cylindrical collectors in static fluid are performed in paramagnetic mode. Our first objective is to investigate the effect of variation of packing fraction of cylindrical collectors in the fluid to the feature of the build-up of ultra-fine particles on the surface of the collector and the distribution of concentration around the collector in the representative cell. The second objective is to investigate the effect of variation of packing fraction of cylindrical collectors in the fluid to the volume of ultra-fine particles captured in the saturation regions on the surface of the collector in the same interval of normalized time. The third and final objective is to investigate the effect of varying the magnitude of uniform external magnetic field to the volume of ultra-fine particles captured in the saturation regions on the surface of the collector in the same interval of normalized time.

5.3.1 The Effect of Variation of Packing Fraction to Features of Concentration Distributions in the Representative Cell

In every simulations of this section, the ultra-fine particle is paramagnetic $\text{Mn}_2\text{P}_2\text{O}_7$ particle of radius $b_p = 1.2 \times 10^{-8}$ m. An assembly of $\text{Mn}_2\text{P}_2\text{O}_7$ particle dispersed in a static water. The effective magnetic susceptibility of the system (water + $\text{Mn}_2\text{P}_2\text{O}_7$ particles) is $\chi = +4.73 \times 10^{-3}$. The uniform external magnetic field has its magnitude $H_0 = 2.0 \times 10^6$ A/m and points in the positive X direction which perpendicular to axes of all cylindrical collectors. The parameter K_C defined in the equation (2.17) of Chapter II is equal to 0.20. The absolute temperature is set equal to 300 K. The value of initial concentration at every points in the representative cell is set equal to $C_0 = 1.0 \times 10^{-3}$ and the saturation concentration is set equal to $C_{sat} = 0.10$. Three values of packing fractions of cylindrical collectors in fluid are used as

$F = 5\%$, 8% and 10%. For all value of packing fractions, simulations are perform in the same interval of normalized time as $0 \leq \tau \leq 0.10$.

In the first case, $F = 5\%$ the value of factor G_0^{random} for this case is equal to -16.95 . Figure 5.19 shows the feature of the build-up of ultra-fine particles on the surface of the collector and the distribution of concentration around the collector in the representative cell. The concentration contours are shown only in the first quadrant, ($0 \leq \theta \leq \pi/2$), since the distribution of concentration has symmetry about X and Y axes.

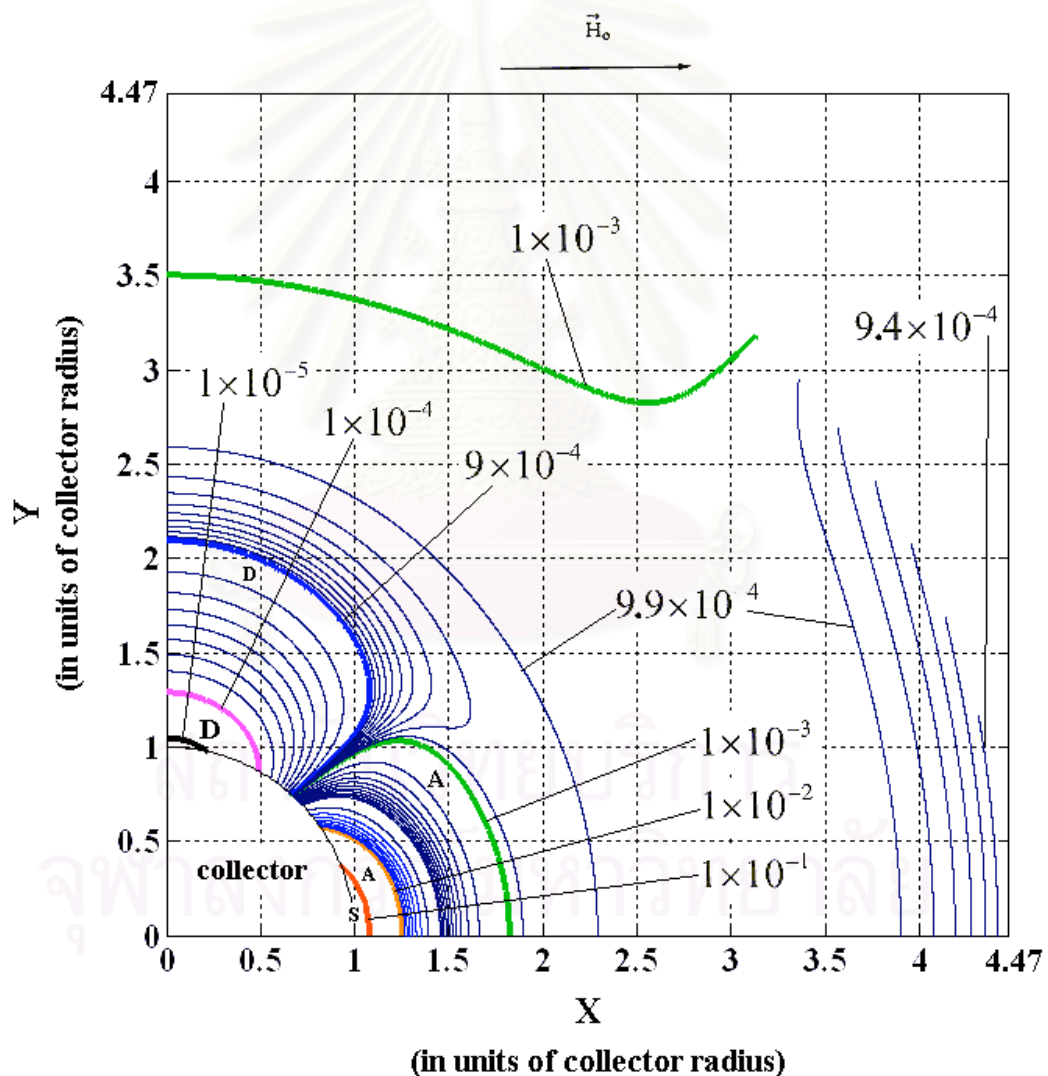


Figure 5.19: A family of concentration contours around the paramagnetic collector in the representative cell, $F = 5\%$, $G_0^{random} = -16.95$, $\tau = 0.10$.

From concentration contours in Figure 5.19, we see that at $\tau = 0.10$ saturation concentration take place on the surface of the paramagnetic collector in the representative cell. The features of the build-up and depletion of ultra-fine particles in regions close to the surface of the collector are similar to those in the case of single ferromagnetic collector in Figure 5.7. This is because the forms of the equations of functions $G_r(r_a, \theta)$ and $G_\theta(r_a, \theta)$ are the same for these two cases but the forms of the factors G_0^{ferro} and G_0^{random} are different. In the case of single collector, we assign the outer boundary condition by fix the concentration on the outer boundary of the computational domain equal to initial concentration for all normalized times. In this case of random cylindrical collectors, the capture of ultra-fine particles is considered only in a representative cell. The outer boundary of the representative cell is considered as an impervious surface. We can see the variation of concentration on the outer boundary of the representative cell. In the range of θ that radial magnetic force is attractive, the concentration on the outer boundary decreases lower than the initial concentration. This is because ultra-fine particles in regions near to the outer boundary are transferred to other regions more closed to the collector. In the range of θ that radial magnetic force is repulsive, the concentration on the outer boundary increases higher than the initial concentration. This is because ultra-fine particles in regions near to the surface of the collector are transferred to other regions faraway from the collector.

Figure 5.20 shows the distribution of concentration at $\theta = 0$ radian at various normalized times for this case of $F = 5\%$. In Figure 5.20, note that the value of concentration at the outer boundary is lower than initial concentration ($C_0 = 1 \times 10^{-3}$) since the magnetic force is attractive at this angle.

Figure 5.21 shows the distribution of concentration at $\theta = \pi/2$ radian at various normalized times for this case of $F = 5\%$. In Figure 5.21, note that the value of concentration at the outer boundary is higher than initial concentration ($C_0 = 1 \times 10^{-3}$) since the magnetic force is repulsive at this angle.

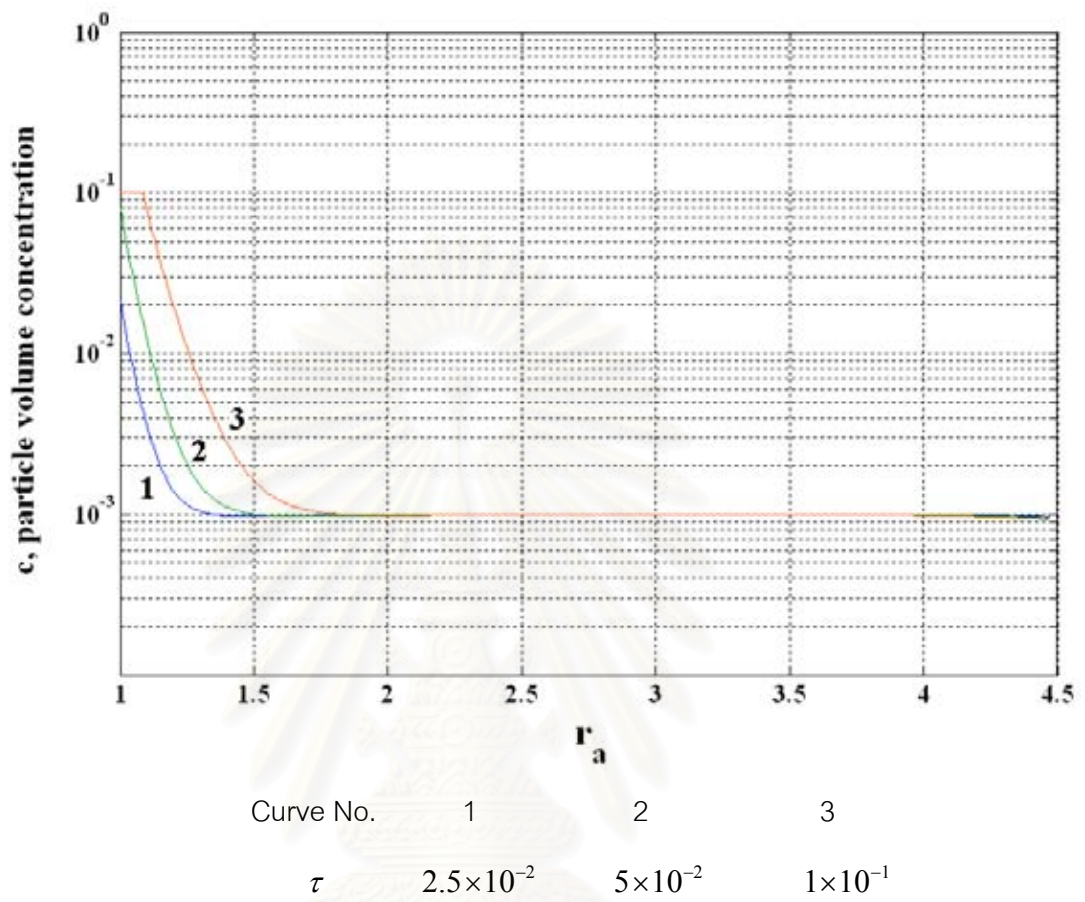
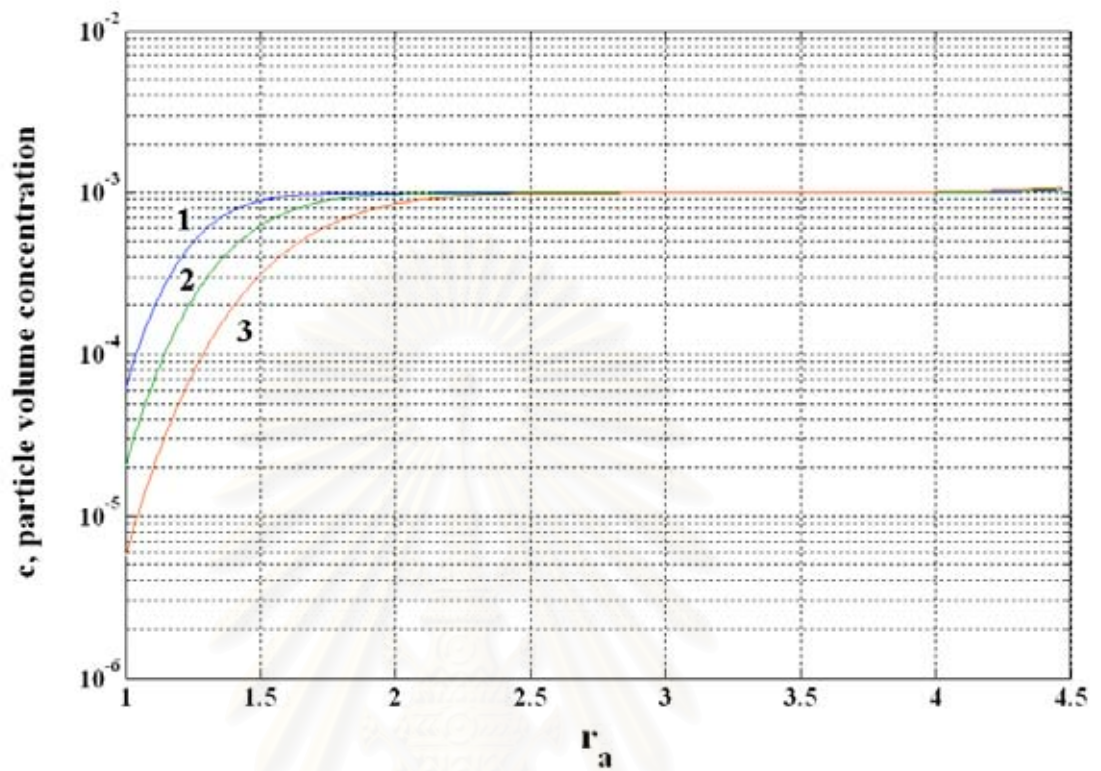


Figure 5.20: Time evolution of concentration distribution at $\theta = 0$ radian in the representative cell, $F = 5\%$, $G_0^{random} = -16.95$.

สถาบันวิทยบริการ
จุฬาลงกรณ์มหาวิทยาลัย



Curve No.	1	2	3
τ	2.5×10^{-2}	5×10^{-2}	1×10^{-1}

Figure 5.21: Time evolution of concentration distribution at $\theta = \pi/2$ radian in the representative cell, $F = 5\%$, $G_0^{random} = -16.95$.

สถาบันวิทยบริการ
จุฬาลงกรณ์มหาวิทยาลัย

Figure 5.22 shows the feature of the build-up of ultra-fine particles on the surface of the collector and the distribution of concentration around the collector in the representative cell for the case of $F = 8\%$. In this case the value of factor G_0^{random} is equal to -17.16 .

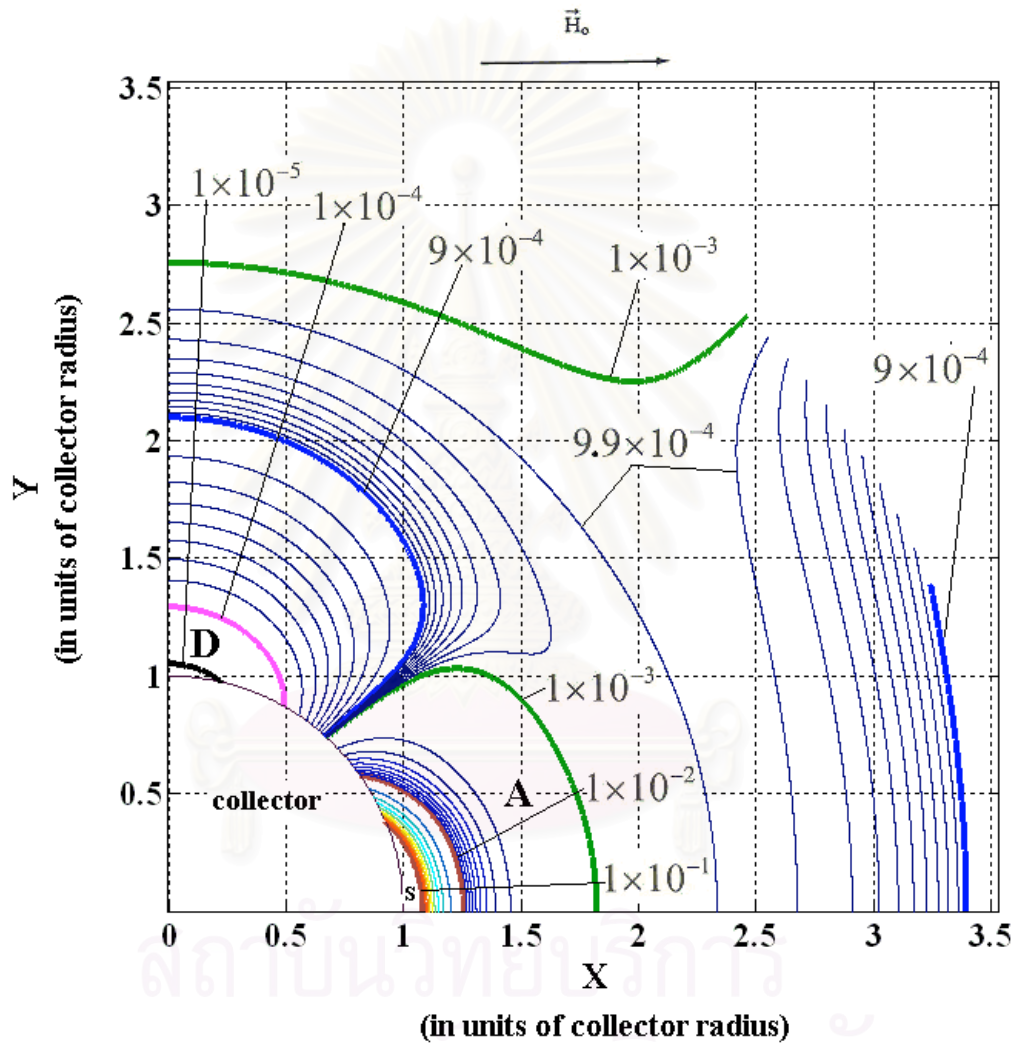


Figure 5.22: A family of concentration contours around the paramagnetic collector in the representative cell, $F = 8\%$, $G_0^{random} = -17.16$, $\tau = 0.10$.

Figure 5.23 shows the distribution of concentration at $\theta = 0$ radian at various normalized times for this case of $F = 8\%$.

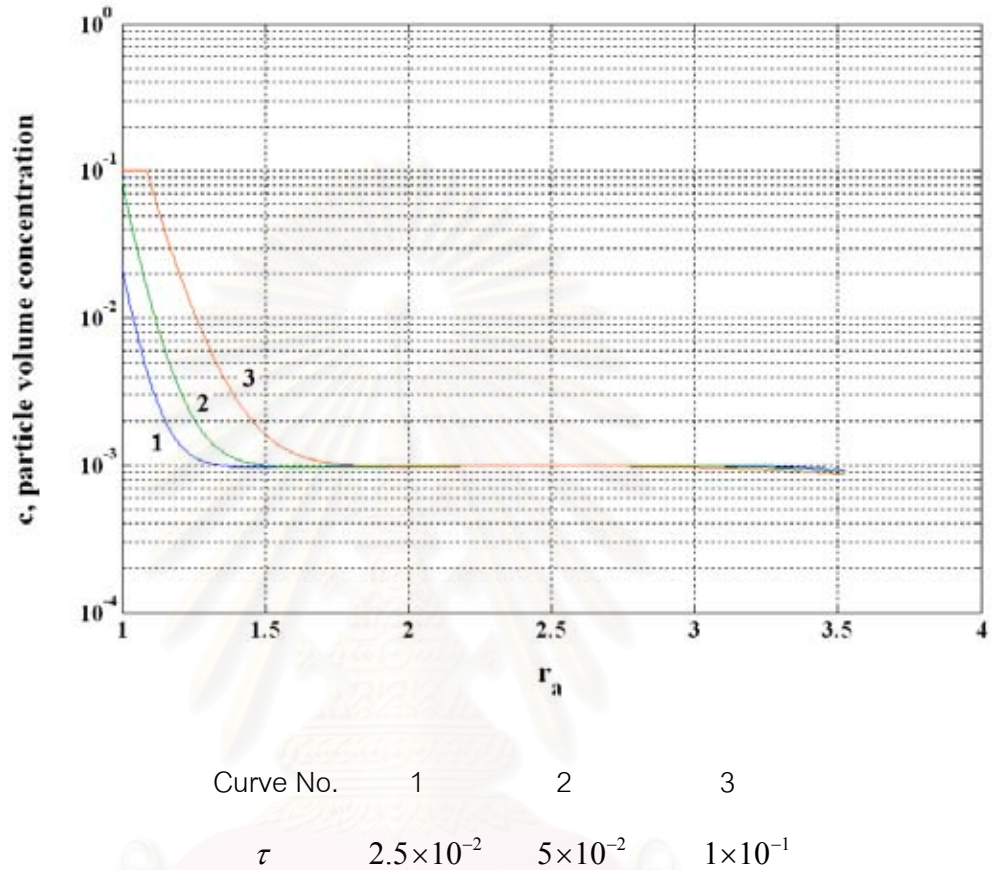
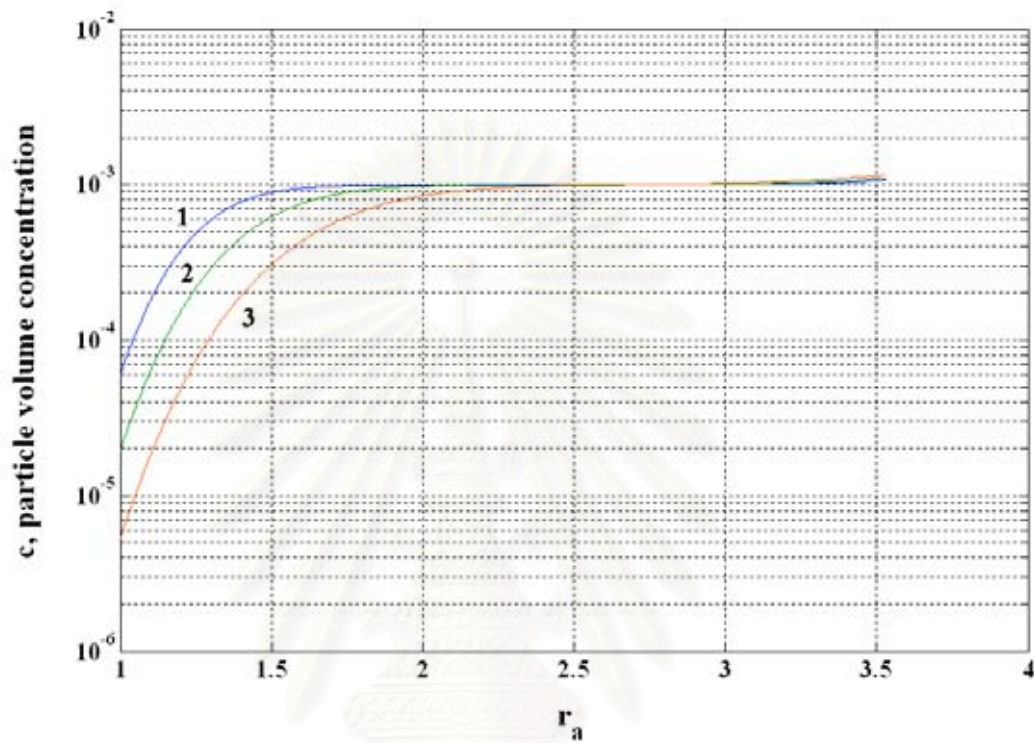


Figure 5.23: Time evolution of concentration distribution at $\theta = 0$ radian in the representative cell, $F = 8\%$, $G_0^{random} = -17.16$.

สถาบันวิทยบริการ
จุฬาลงกรณ์มหาวิทยาลัย

Figure 5.24 shows the distribution of concentration at $\theta = \pi/2$ radian at various normalized times for this case of $F = 8\%$.



Curve No.	1	2	3
τ	2.5×10^{-2}	5×10^{-2}	1×10^{-1}

Figure 5.24: Time evolution of concentration distribution at $\theta = \pi/2$ radian in the representative cell, $F = 8\%$, $G_0^{random} = -17.16$.

Figure 5.25 shows the feature of the build-up of ultra-fine particles on the surface of the collector and the distribution of concentration around the collector in the representative cell for the case of $F = 10\%$. In this case the value of factor G_0^{random} is equal to -17.30 .

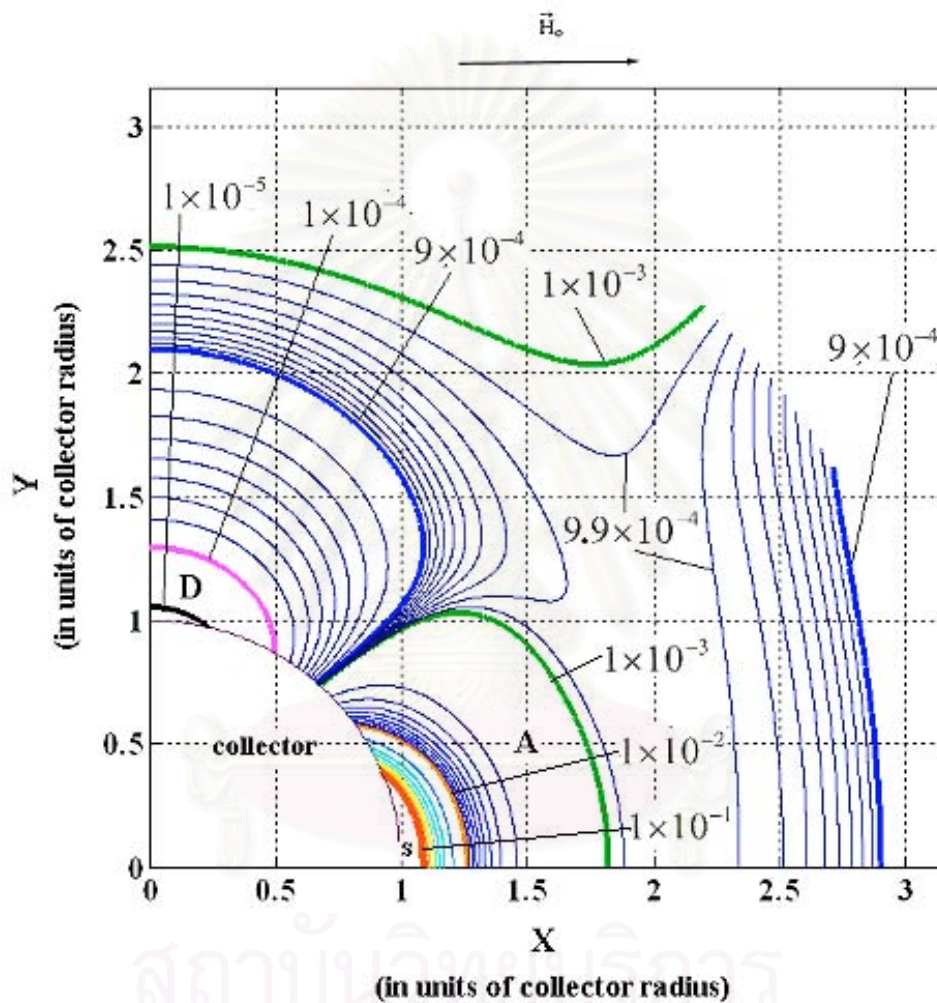
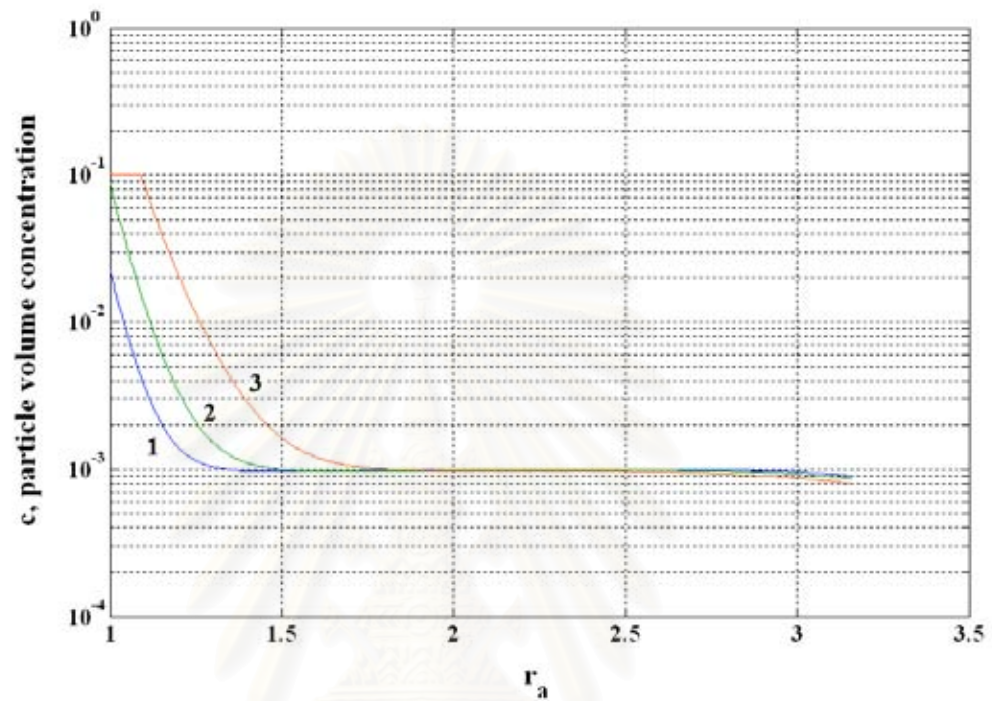


Figure 5.25: A family of concentration contours around the paramagnetic collector in the representative cell,

$$F = 10\%, G_0^{random} = -17.30, \tau = 0.10.$$

Figure 5.26 shows the distribution of concentration at $\theta = 0$ radian at various normalized times for this case of $F = 10\%$.

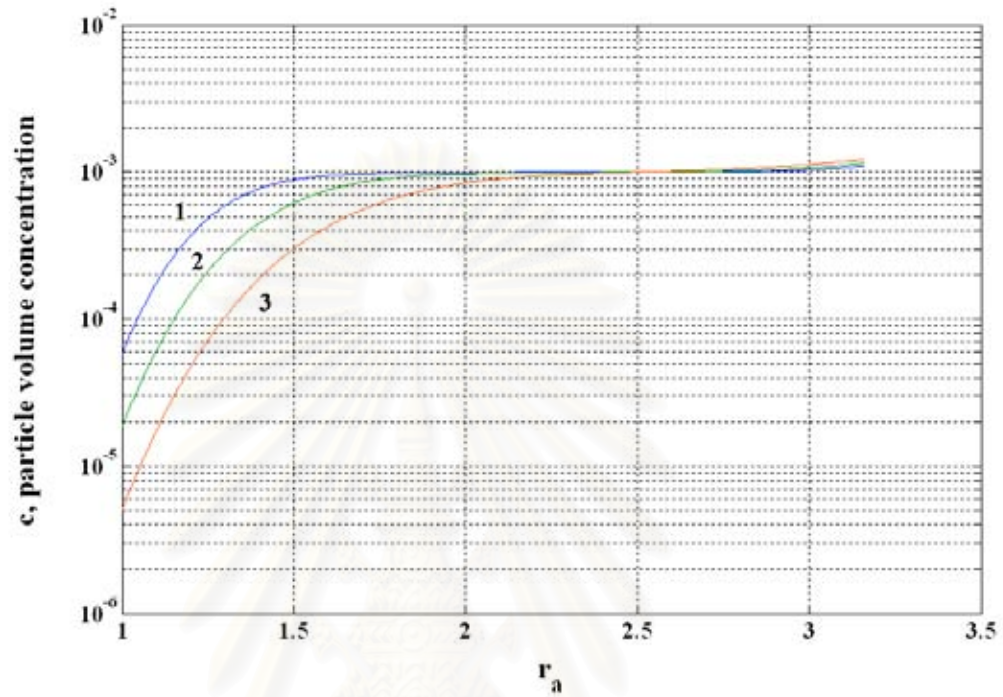


Curve No.	1	2	3
τ	2.5×10^{-2}	5×10^{-2}	1×10^{-1}

Figure 5.26: Time evolution of concentration distribution at $\theta = 0$ radian in the representative cell, $F = 10\%$, $G_0^{random} = -17.30$.

สถาบันวิทยบริการ
จุฬาลงกรณ์มหาวิทยาลัย

Figure 5.27 shows the distribution of concentration at $\theta = \pi/2$ radian at various normalized times for this case of $F = 10\%$.



Curve No.	1	2	3
τ	2.5×10^{-2}	5×10^{-2}	1×10^{-1}

Figure 5.27: Time evolution of concentration distribution at $\theta = \pi/2$ radian in the representative cell, $F = 10\%$, $G_0^{random} = -17.30$.

สถาบันวิทยบริการ
จุฬาลงกรณ์มหาวิทยาลัย

From all results in Figures 5.19 to 5.27, we can conclude that variation of packing fraction of cylindrical collectors in fluid has no significant effect to the feature of the build-up of ultra-fine particles on the surface of the paramagnetic collector in the representative cell. The variation of packing fraction of cylindrical collectors in fluid also has no significant to the feature of concentration distribution in various regions around the collector in the representative cell. These are because, features of concentration contours in every case, $F = 5\%$, 8% , 10% are very similar and features of concentration distributions at $\theta = 0$ radian and $\theta = \pi/2$ radian of all values of packing fraction are also very similar.

5.3.2 The Effect of Variation of Packing Fraction to the Amounts of Particles Captured in Saturation Regions

In this section, we investigate the effect of variation of packing fraction of cylindrical collectors in fluid to the amounts of ultra-fine particles captured in saturation regions on the surface of the paramagnetic collector in the representative cell.

We compare the variation of variable P_{sat} , defined in equation (5.5), with normalized time among three values of packing fraction, $F = 5\%$, 8% , 10% .

For every values of packing fraction, the ultra-fine particle is paramagnetic $Mn_2P_2O_7$ particle of radius $b_p = 1.2 \times 10^{-8}$ m. An assembly of $Mn_2P_2O_7$ particle dispersed in the static water. The effective magnetic susceptibility of the system (water + $Mn_2P_2O_7$ particles) is $\chi = +4.73 \times 10^{-3}$. The uniform external magnetic field has its magnitude $H_0 = 2.0 \times 10^6$ A/m and points in the positive X direction. The parameter K_C defined in the equation (2.17) of Chapter II is equal to 0.20. The absolute temperature is set equal to 300 K. The value of initial concentration at every points in the representative cell is set equal to $C_0 = 1.0 \times 10^{-3}$ and the saturation concentration is set equal to $C_{sat} = 0.10$. The values of factor G_0^{random} for packing fraction $F = 5\%$, 8% , 10% are -16.95 , -17.16 and -17.30 , respectively. The interval of normalized time is $0 \leq \tau \leq 0.10$ for all values of packing fraction.

Figure 5.28 shows the comparison of variation of P_{sat} with τ in the interval $0 \leq \tau \leq 0.10$ for three values of packing fraction.

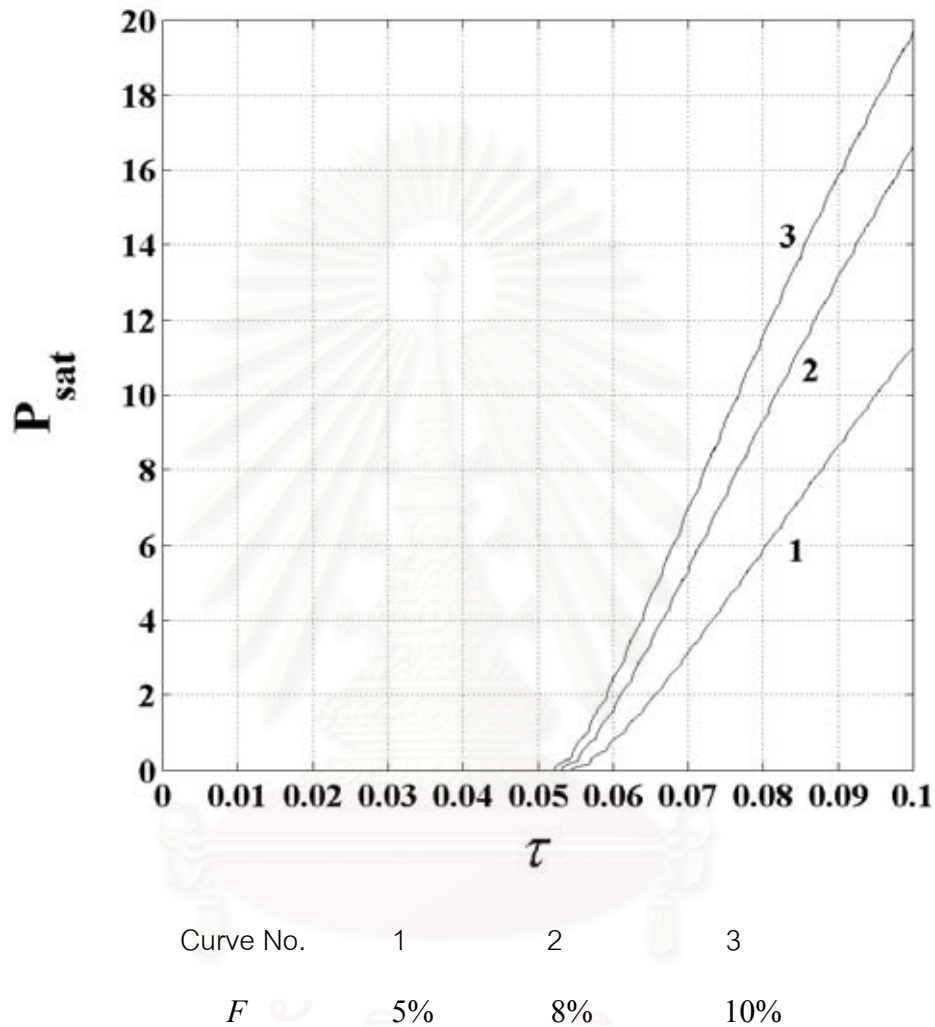


Figure 5.28: Comparison of variations of P_{sat} with τ between $F = 5\%$, 8% , 10% .

From the result shown in Figure 5.28, we see that the evolution of P_{sat} with τ is faster when packing fraction is increased. In the same interval of normalized time, the value of P_{sat} is proportional to the value of packing fraction. This can be understood by a simple consideration, when packing fraction is increased, number of paramagnetic collectors in the system is increased. Consequently, more collectors can capture more amounts of ultra-fine particles in the same interval of τ .

5.3.3 The Effect of Variation of Uniform External Magnetic Field to the Amounts of Particles Captured in Saturation Regions

In this section, we investigate the effect of variation of uniform external magnetic field (H_0) to the amounts of ultra-fine particles captured in saturation regions on the surface of the paramagnetic collector in the representative cell.

We compare the variation of variable P_{sat} , with normalized time among three values of H_0 , $H_0 = 1.0 \times 10^6$ A/m, 2.0×10^6 A/m, 3.0×10^6 A/m.

For every values of H_0 , the ultra-fine particle is paramagnetic $Mn_2P_2O_7$ particle of radius $b_p = 1.2 \times 10^{-8}$ m. An assembly of $Mn_2P_2O_7$ particle dispersed in the static water. The effective magnetic susceptibility of the system (water + $Mn_2P_2O_7$ particles) is $\chi = +4.73 \times 10^{-3}$. The uniform external magnetic field ($\overline{H_0}$) points in the positive X direction. The parameter K_C is equal to 0.20. The absolute temperature is set equal to 300 K. The value of initial concentration at every points in the representative cell is set equal to $C_0 = 1.0 \times 10^{-3}$ and the saturation concentration is set equal to $C_{sat} = 0.10$. The values of packing fraction is $F = 5\%$ and the value of factor G_0^{random} is -16.95 . The interval of normalized time is $0 \leq \tau \leq 0.10$ for all values of H_0 .

Figure 5.29 shows the comparison of variations of P_{sat} with τ in the interval $0 \leq \tau \leq 0.10$ for three values of H_0 .

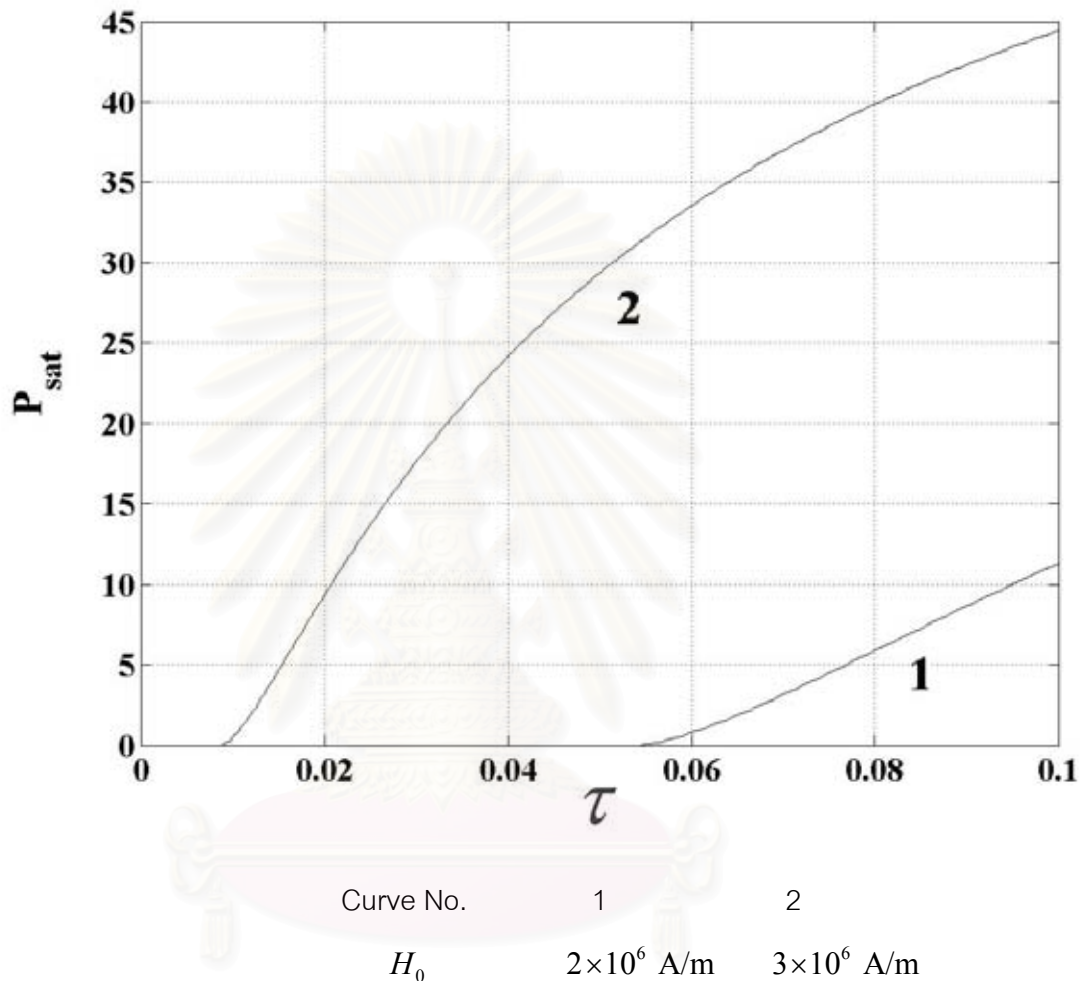


Figure 5.29: Comparison of variations of P_{sat} with τ between $H_0 = 2.0 \times 10^6$ A/m, 3.0×10^6 A/m.

From the result shown in Figure 5.29, we see that the evolution of P_{sat} with τ is increased rapidly with increased H_0 . The curve of $H_0 = 1.0 \times 10^6$ A/m is not shown since the value of P_{sat} equal to zero at every τ in the interval shown in the figure. The obtained result can be understood by consider equation (3.14) of Chapter III. We can see, in equation (3.14), that the factor G_0^{random} is proportional to H_0^2 . Consequently, when H_0 is increased, the amounts of particles captured in saturation regions on the surface of the collector in representative cell increase rapidly.

CHAPTER VI

CONCLUSIONS

In this research, HGMS capture of ultra-fine weakly magnetic particles in various situations both in one dimension and two dimensions are investigated. For the case of single collector, former published researches are studied and more analyses are given in details. Furthermore, we develop a simple two dimensional theoretical model for describing the capture of ultra-fine particles by an assemblage of randomly distributed parallel cylindrical collectors. We use the effective medium treatment to construct the model mentioned. We simulate HGMS capture of ultra-fine particles in various physical situations by solving the continuity equation describing dynamics of the system of particles both analytically and numerically. Both time-dependent and steady-state features of the capture of ultra-fine particles are obtained.

For the case of a single collector, Results of simulations can predict the features of the build-up of ultra-fine particles on the surface of the collector both in paramagnetic and diamagnetic modes of the capture. These results show that the build-up of paramagnetic and diamagnetic particles on the collector have the opposite features. The assembly of paramagnetic particles accumulate in the direction parallel to the uniform external magnetic field whereas the assembly of diamagnetic particles accumulate in the direction perpendicular to the uniform external magnetic field. In addition, our results provide a basic guide for setting the strength of external magnetic field to achieve the required amount of particles to be separated from the fluid at steady state.

For the case of an assemblage of randomly distributed parallel cylindrical collectors, we study the effect of collector packing fraction to the feature of the build-up of ultra-fine particles on the collector and to the feature of particle concentration distribution around the collector. Results of simulations show us that the packing fraction has insignificant effect to those features. Furthermore, we study the effect of packing fraction to the amount of particles captured in saturation regions on the

surface of the collector in the same interval of normalized time. Results of simulation show us that, in the same interval of normalized time, amount of particles captured in saturation regions on the surface of the collector is proportional to the packing fraction. Finally, we study the effect of the strength of magnetic field to the amount of particles captured in saturation regions on the collector in the same interval of normalized time. Results of simulation also show us that the amount of particles captured in saturation regions on the surface of the collector increases rapidly when the strength of external magnetic field is increased.

The theoretical model developed in this research can be used to predict the separation process of very small particles in many field of works for example, separation of blood component from whole blood, .etc.

The model developed in this research is for the capture of ultra-fine particles in static fluid. In the future, this model can be developed further to the case of the capture of ultra-fine particles in flowing fluid which more close to industrial applications of high gradient magnetic separation.



สถาบันวิทยบริการ
จุฬาลงกรณ์มหาวิทยาลัย

REFERENCES

1. J. H. Watson. Magnetic Filtraion. J. Appl. Phys. 44(1973): 4209-4213.
2. R. Gerber. Theory of particle capture in axial filters for high gradient magnetic Separation. J. Phys. D: Appl. Phys. 11(1978): 2119-2129.
3. R. Gerber, M. Takayasu and F. J. Friedlaender. Generalization of HGMS Theory: The Capture of Ultra-Fine Particles. IEEE Trans. Magn. MAG –19 (1983): 2115-2117.
4. M. Takayasu, R. Gerber and F. J. Friedlaender. Magnetic Separation of Submicron Particles. IEEE Trans. Magn. MAG –19 (1983): 2112-2114.
5. Derrick Fletcher. Fine Particle High Gradient Magnetic Entrapment. IEEE Trans. Magn. 27(1991): 3655-3677.
6. A. J. Kramer, J.J.M. Janssen and J.A.A.J. Perenboon. Single-Wire HGMS of Colloidal Particles: The Evolution of Concentration Profiles. IEEE Trans. Magn. 26 (1990): 1858-1860.
7. J. P. Glew and M. R. Parker. The Influence of Interparticle Force in the Magnetic Separation of Submicron Particles. IEEE Trans. Magn. MAG –20(1984): 1165-1167.
8. L. P. Davies and R. Gerber. 2-D Simulation of Ultra-Fine Particle Capture by a Single-Wire Magnetic Collector. IEEE Trans. Magn. Vol 26(1990): 1867-1869.
9. website hikwww1.fzk.de/itc-wgt/2/deutsch/prinzip.htm
10. J. Crank. The Mathematic of Diffusion. 2nd ed. Oxford: Clarendon Press, 1975.
11. E. L. Cussler. Diffusion Mass Transfer in Fluid Systems. 2nd ed. Cambridge: Cambridge University Press, 1997.
12. D. J. Amit, Y. Verbin. Statistical Physics an Introductory Course. 1st ed. Singapore: World Scientific, 1999.
13. M. Natenapit. Magnetic Field for an Assemblage of Cylinders. J. Sci. Res. Chula. Univ. 13:1(1988): 23-27.
14. Z. Hashin. Assessment of the Selt Consistent Scheme Approximation: Conductivity of Particulate Composites. J. Comp. Mat. 2(1968): 284-298.
15. E. F. Nogotov, B. M. Berkovsky, W. J. Minkowycz. Applications of Numerical Heat Transfer. 1st ed. London: McGraw-Hill Book Company.

16. A. R. Mitchell and D. F. Griffiths. The Finite Difference Method in Partial Differential Equations. 1st ed. Norwich: John Wiley & sons, 1980.
17. M. Takayasu, D. R. Kelland, and J. V. Minervini. Continuous Magnetic Separation of Blood Components from Whole Blood. IEEE Trans. Magn. 10, (2000): 927-930.
18. Richard Gerber. Magnetic Filtration of Ultra-Fine Particles. IEEE Trans. Magn. 20, (1984): 1159-1164.



สถาบันวิทยบริการ
จุฬาลงกรณ์มหาวิทยาลัย



APPENDICES

สถาบันวิทยบริการ
จุฬาลงกรณ์มหาวิทยาลัย

APPENDIX A

Magnetic Field Around a Ferromagnetic Cylindrical Collector

Consider a long magnetic cylindrical collector of radius a immersed in a magnetic medium of permeability μ_f . Both collector and medium are placed in a uniform magnetic field of magnitude H_0 perpendicular to the axis of the collector. Let the Z axis of the Cartesian coordinate coincide with the axis of the collector. The geometry of the situation can be shown in Figure A.1.

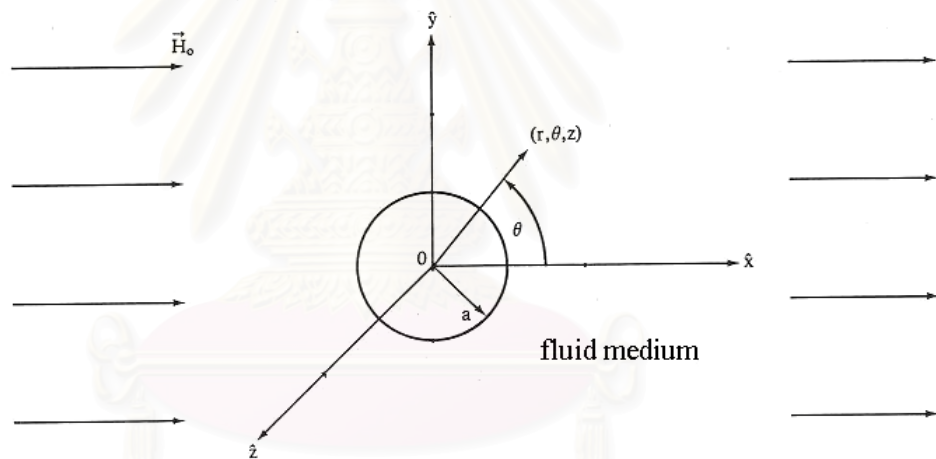


Figure A.1: A magnetic collector and surrounding medium in a uniform magnetic field.

The magnetic field in and around the collector can be determined by solving the Laplace's equation

$$\nabla^2 \Phi_M = 0, \quad (\text{A.1})$$

where Φ_M is the magnetic scalar potential.

Equation (A.1) can be solved by using these boundary conditions

- 1) The magnetic field very far from the collector is a uniform one of magnitude H_0 and point in the positive X – direction as shown in Figure A.1.
- 2) Magnetic field at the origin of Cartesian coordinate must finite
- 3) The component of magnetic field in the direction that parallel to the collector surface must continuous at the surface of the collector.
- 4) The component of magnetic induction in the direction that perpendicular to the collector surface must continuous at the surface of the collector.

Since the collector is long, we can approximate that the value of Φ_M dose not depend on the z coordinate and the problem will be solved in two dimensions. By the geometry in Figure A.1, it is convenient to solve this problem by using two dimensional circular cylindrical coordinate (r, θ) . Consequently, equation (A.1) becomes

$$\frac{1}{r} \frac{\partial}{\partial r} \left(r \frac{\partial \Phi_M}{\partial r} \right) + \frac{1}{r^2} \frac{\partial^2 \Phi_M}{\partial \theta^2} = 0 \quad (\text{A.2})$$

This equation has the general solution in the form

$$\Phi(r, \theta) = \sum_{n=1}^{\infty} \left[A_n r^{-n} \cos(n\theta) + B_n r^n \cos(n\theta) \right], \quad (\text{A.3})$$

where A_n and B_n are constants would be determined.

Let Φ_1 and Φ_2 is magnetic scalar potential in the fluid and collector, respectively. From the first and the second boundary condition we obtain

$$\Phi_1(r, \theta) = -H_0 r \cos \theta + \sum_{n=1}^{\infty} A_n r^{-n} \cos(n\theta) \quad (\text{A.4})$$

and

$$\Phi_2(r, \theta) = \sum_{n=1}^{\infty} B_n r^n \cos(n\theta). \quad (\text{A.5})$$

From the relation between magnetic scalar potential and the magnetic field,

$$\vec{H} = -\vec{\nabla}\Phi_M, \quad (\text{A.6})$$

and the third boundary condition we obtain

$$\left(-\frac{1}{r} \frac{\partial \Phi_1}{\partial \theta} \right) \Big|_{r=a} = \left(-\frac{1}{r} \frac{\partial \Phi_2}{\partial \theta} \right) \Big|_{r=a}. \quad (\text{A.7})$$

When the magnetic collector is a ferromagnetic one with magnetization \vec{M} points in the same direction as the uniform external magnetic field \vec{H}_0 then we obtain

$$\mu_0 \left(-\frac{\partial \Phi_2}{\partial r} \right) \Big|_{r=a} + \mu_0 M \cos \theta = \mu_f \left(-\frac{\partial \Phi_1}{\partial r} \right) \Big|_{r=a}. \quad (\text{A.8})$$

When equations (A.4) and (A.5) are substituted in the equation (A.8), and by using orthogonality property of cosine function,

$$\int_0^{\pi} \cos(n\theta) \cos(m\theta) d\theta = \frac{\pi}{2} \delta_{nm}, \quad (\text{A.9})$$

we obtain

$$\mu_f a^{-2} A_1 + \mu_0 B_1 = \mu_0 M - \mu_f H_0, \quad (\text{A.10})$$

and

$$A_n = 0, \quad B_n = 0 \quad \text{for } n \neq 1. \quad (\text{A.11})$$

When equations (A.4) and (A.5) are substituted in the equation (A.7), and by using orthogonality property of sine function,

$$\int_0^{\pi} \sin(n\theta) \sin(m\theta) d\theta = \frac{\pi}{2} \delta_{nm}, \quad (\text{A.12})$$

we obtain
$$a^{-2} A_1 - B_1 = H_0, \quad (\text{A.13})$$

From the system of linear equations (A.10) and (A.13), we can obtain

$$A_1 = \frac{\mu_0 M a^2 + (\mu_0 - \mu_f) a^2 H_0}{\mu_0 + \mu_f} \quad (\text{A.14})$$

and
$$B_1 = \frac{\mu_0 M - 2\mu_f H_0}{\mu_0 + \mu_f}. \quad (\text{A.15})$$

Since $\mu_f = \mu_0 (1 + \chi_f)$, where χ_f is the magnetic susceptibility of the fluid, in general the value of χ_f is in the order of 10^{-3} to 10^{-5} , consequently, we can approximate that $\mu_f \approx \mu_0$ and we obtain

$$A_1 \approx \frac{M a^2}{2} \quad \text{and} \quad B_1 \approx \frac{M}{2} - H_0. \quad (\text{A.16})$$

From this equation, we can determine magnetic scalar potentials as

$$\Phi_1^{ferro}(r, \theta) = -H_0 r \cos \theta + \frac{M a^2}{2} \left(\frac{\cos \theta}{r} \right) \quad (\text{A.17})$$

and

$$\Phi_2^{ferro}(r, \theta) = \left(\frac{M}{2} - H_0 \right) r \cos \theta. \quad (\text{A.18})$$

From equation (A.17), we can determine the magnetic field in the fluid around the ferromagnetic collector as

$$\vec{H}_1^{ferro}(r_a, \theta) = H_0 \left[\left(1 + \frac{K_w}{r_a^2} \right) \cos \theta \hat{r} - \left(1 - \frac{K_w}{r_a^2} \right) \sin \theta \hat{\theta} \right], \quad (\text{A.19})$$

where

$$K_w = \frac{M}{2H_0}, \quad (\text{A.20})$$

and

$$r_a = \frac{r}{a}. \quad (\text{A.21})$$



สถาบันวิทยบริการ
จุฬาลงกรณ์มหาวิทยาลัย

APPENDIX B

Magnetic Field for an Assemblage of Random Cylindrical Paramagnetic Collectors

In 1998, Natenapit [13] determined the magnetic field around parallel cylindrical paramagnetic collectors which are randomly distributed in the formerly uniform external magnetic field. In that work, the effective medium approach originally conceived by Hashin [ref] was used.

In the effective medium approach, the system of paramagnetic collectors and surrounding medium is considered to be composed of cylindrical composite cells, each containing exactly one of the collectors. The ratio of the collector to the cell volume (a^2/b^2) is set equal to the packing fraction of collectors in the medium denoted by F . Adjacent to each collector (permeability μ_2) is the surrounding medium (permeability μ_1). In the effective medium model, only a representative cell is considered, while the neighbor cells are considered equivalent to a homogeneous medium with effective permeability μ^* to be determined. Figure B.1 shows a representative cell.

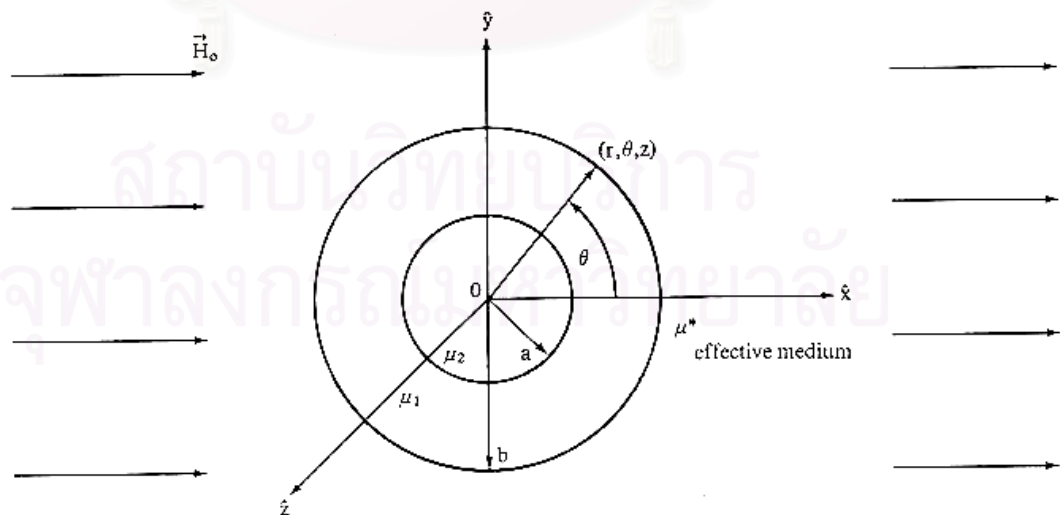


Figure B.1: A representative cylindrical composite cell.

To determine the magnetic field in the cell, the boundary value problem of coaxial magnetic cylinders subject to the boundary condition of uniform magnetic field at far away from the representative cell is solved. By taking z axis of the circular cylindrical coordinate along the collector axis and let Φ be the magnetic scalar potential satisfying Laplace's equation for each region in Figure B.1.

$$\bar{\nabla}^2 \Phi_0 = 0 \quad b \leq r \leq \infty \quad (\text{B.1})$$

$$\bar{\nabla}^2 \Phi_1 = 0 \quad a \leq r \leq b \quad (\text{B.2})$$

$$\bar{\nabla}^2 \Phi_2 = 0 \quad 0 \leq r \leq a \quad (\text{B.3})$$

with these boundary conditions

$$\Phi_0(r, \theta) = -H_0 r \cos \theta \quad \text{at } r \rightarrow \infty \quad (\text{B.4})$$

$$\frac{\partial \Phi_0(b, \theta)}{\partial \theta} = \frac{\partial \Phi_1(b, \theta)}{\partial \theta} \quad (\text{B.5})$$

$$\frac{\partial \Phi_1(a, \theta)}{\partial \theta} = \frac{\partial \Phi_2(a, \theta)}{\partial \theta} \quad (\text{B.6})$$

$$\mu^* \frac{\partial \Phi_0(r, \theta)}{\partial r} \Big|_{r=b} = \mu_1 \frac{\partial \Phi_1(r, \theta)}{\partial r} \Big|_{r=b} \quad (\text{B.7})$$

and

$$\mu_1 \frac{\partial \Phi_1(r, \theta)}{\partial r} \Big|_{r=a} = \mu_2 \frac{\partial \Phi_2(r, \theta)}{\partial r} \Big|_{r=a} \quad (\text{B.8})$$

From equation (B.1) to (B.3), the general solutions, with boundary condition in equations (B.4) assigned, of these equations are

$$\Phi_0(r, \theta) = -H_0 r \cos \theta + \sum_{n=1}^{\infty} A_n r^{-n} \cos(n\theta), \quad (\text{B.9})$$

$$\Phi_1(r, \theta) = \sum_{n=1}^{\infty} [B_n r^n + C_n r^{-n}] \cos(n\theta), \quad (\text{B.10})$$

and
$$\Phi_2(r, \theta) = \sum_{n=1}^{\infty} D_n r^n \cos(n\theta). \quad (\text{B.11})$$

When the boundary condition in equation (B.5) is imposed, we obtain

$$-H_0 b + \frac{A_1}{b} - B_1 b - \frac{C_1}{b} = 0 \quad \text{for } n = 1 \quad (\text{B.12})$$

and

$$A_n b^{-n} - B_n b^n - C_n b^{-n} = 0 \quad \text{for } n \neq 1. \quad (\text{B.13})$$

When the boundary conditions in equations (B.6) to (B.8) are imposed, we obtain

$$B_n a^n + C_n a^{-n} - D_n a^n = 0, \quad \text{for all } n \quad (\text{B.14})$$

$$-\mu^* H_0 - \mu^* A_1 b^{-2} + \mu_1 C_1 b^{-2} - \mu_1 B_1 = 0, \quad \text{for } n = 1 \quad (\text{B.15})$$

$$\mu^* A_n b^{-n-1} + \mu_1 (B_n b^{n-1} - C_n b^{-n-1}) = 0, \quad \text{for } n \neq 1 \quad (\text{B.16})$$

$$\mu_2 D_n a^{n-1} - \mu_1 B_n a^{n-1} + \mu_1 C_n a^{-n-1} = 0, \quad \text{for all } n \quad (\text{B.17})$$

By solving the system of linear equations (B.12) to (B.17), we can determine coefficients A_n , B_n , C_n and D_n as

$$A_n = B_n = C_n = D_n = 0 \quad \text{for all } n \neq 1 \quad (\text{B.18})$$

$$A_1 = \frac{H_0 a^2}{IF} \left[F(\nu^* + 1)(\nu - 1) - (\nu^* - 1)(\nu + 1) \right] \quad (\text{B.19})$$

$$B_1 = -\frac{2H_0 \nu^*}{I} (\nu + 1) \quad (\text{B.20})$$

$$C_1 = \frac{2H_0 a^2 \nu^*}{I} (\nu - 1) \quad (\text{B.21})$$

$$D_1 = -\frac{4H_0 \nu^*}{I} \quad (\text{B.22})$$

where $\nu^* = \mu^* / \mu_1$, $\nu = \mu_2 / \mu_1$, and $I = \left[(\nu^* + 1)(\nu + 1) - F(\nu - 1)(\nu^* - 1) \right]$.

The magnetic field in various regions in the representative cell can be determined from

$$\vec{H} = -\vec{\nabla}\Phi. \quad (\text{B.23})$$

However, the results are given in term of the unknown effective permeability μ^* . We can determine μ^* by using the consistency of the effective medium model that the magnetic induction averaged over the representative cell (collector plus medium) to be the volume average of the magnetic induction over the effective medium. That is

$$F\mu_2 \langle \vec{H}_2 \rangle_i + (1-F)\mu_1 \langle \vec{H}_1 \rangle_i = \mu^* \langle \vec{H}_{Eff} \rangle_i, \quad \left(\langle \vec{H}_{Eff} \rangle = -\vec{\nabla}\Phi_0 \right) \quad (\text{B.24})$$

where i referred to x , y or z . Substituting the magnetic field into equation (B.24) and taking the x component of the magnetic field, we obtain the relative effective permeability

$$\nu^* = \frac{\nu(1+F) + (1-F)}{\nu(1-F) + (1+F)} \quad (\text{B.25})$$

where $\nu^* = \mu^*/\mu_1$, $\nu = \mu_2/\mu_1$.

Then we can determine the magnetic field in the medium in the representative cell as

$$\vec{H}_1(r_a, \theta) = AH_0 \left[\left(1 + \frac{K_C}{r_a^2} \right) \cos \theta \hat{r} - \left(1 - \frac{K_C}{r_a^2} \right) \sin \theta \hat{\theta} \right], \quad 1 < r_a < \frac{b}{a} \quad (\text{B.26})$$

$$\vec{H}_{\text{eff}} = \vec{H}_0, \quad \frac{b}{a} < r_a < \infty \quad (\text{B.27})$$

where

$$A = \frac{1}{1 - FK_C}, \quad (\text{B.28})$$

$$K_C = \frac{\nu - 1}{\nu + 1} \quad (\text{B.29})$$

and $r_a = r/a$.

We note that in the limit of $F \left(= \frac{a^2}{b^2} \right) \rightarrow 0$, $\nu^* \rightarrow 1$ (or $\mu^* = \mu_1$), equation (B.26) is reduced to the case of single paramagnetic collector. For $\mu_2 = \mu_1$ (i.e. $K_C = 0$, $A = 1$), the homogeneous magnetic field $\vec{H} = \vec{H}_0$ is obtained.

สถาบันวิทยบริการ
จุฬาลงกรณ์มหาวิทยาลัย

APPENDIX C

Approximating Derivatives of Functions by Finite-Difference Relations

Consider a continuous function of real variable x denoted by $f(x)$, the derivative of this function with respect to x at a certain value of its argument, x_i , is defined as

$$\frac{dy}{dx} \equiv \lim_{\Delta x \rightarrow 0} \frac{f(x_i + \Delta x) - f(x_i)}{\Delta x} . \quad (\text{C.1})$$

Let us assume that f is a well-behaved function, then the derivative of f with respect to x can be determined in any order. Consequently, we can write Taylor's expansion of $f(x)$ at a point x_{k+1} which advance a point x_k with an amount Δx in the domain of f as

$$f(x_{k+1}) = f(x_k) + (\Delta x) f'(x_k) + \frac{(\Delta x)^2}{2!} f''(x_k) + \dots , \quad (\text{C.2})$$

where $\Delta x = x_{k+1} - x_k$.

From equation (C.2), we can determine the first-order derivative of f with respect to x at the point x_k as

$$f'(x_k) = \frac{f(x_{k+1}) - f(x_k)}{\Delta x} - \frac{(\Delta x)}{2!} f''(x_k) + \dots . \quad (\text{C.3})$$

The equation (C.3) can rewritten more compactly as

$$f'(x_k) = \frac{f(x_{k+1}) - f(x_k)}{\Delta x} + O(\Delta x) , \quad (\text{C.4})$$

where $O(\Delta x)$ represent the terms of order (Δx) and higher. We can approximate the first-order derivative of f with respect to x at the point x_k as

$$f'(x_k) \approx \frac{f(x_{k+1}) - f(x_k)}{\Delta x}, \quad (\text{C.5})$$

where the error of approximation is in the order (Δx) .

The equation (C.5) is called the first-order forward difference approximation. Now if we write Taylor's expansion of $f(x)$ at a point x_{k-1} which lag a point x_k with an amount Δx in the domain of f as

$$f(x_{k-1}) = f(x_k) - (\Delta x)f'(x_k) + \frac{(\Delta x)^2}{2!}f''(x_k) - \dots, \quad (\text{C.6})$$

where $\Delta x = x_k - x_{k-1}$.

From equation (C.6), we can determine the first-order derivative of f with respect to x at the point x_k as

$$f'(x_k) = \frac{f(x_k) - f(x_{k-1})}{\Delta x} + \frac{(\Delta x)}{2!}f''(x_k) - \dots \quad (\text{C.7})$$

The equation (C.7) can be rewritten more compactly as

$$f'(x_k) = \frac{f(x_k) - f(x_{k-1})}{\Delta x} + O[(\Delta x)]. \quad (\text{C.8})$$

Then we obtain an alternative way to approximate the first-order derivative of f with respect to x at the point x_k as

$$f'(x_k) \approx \frac{f(x_k) - f(x_{k-1})}{\Delta x}, \quad (\text{C.9})$$

where the error of approximation is also in the order (Δx) .

The equation (C.9) is called the first-order backward difference approximation.

If equation (C.6) is subtracted from equation (C.2) we obtain

$$f(x_{k+1}) - f(x_{k-1}) = 2(\Delta x)f'(x_k) + \frac{2}{3!}(\Delta x)^3 f'''(x_k) + \dots \quad (C.10)$$

From this equation we can determine the first-order derivative of f with respect to x at the point x_k as

$$f'(x_k) = \frac{f(x_{k+1}) - f(x_{k-1})}{2(\Delta x)} - \frac{(\Delta x)^2}{3!} f'''(x_k) + \dots, \quad (C.11)$$

or

$$f'(x_k) = \frac{f(x_{k+1}) - f(x_{k-1})}{2(\Delta x)} + O[(\Delta x)^2]. \quad (C.12)$$

From equation (C.12), we obtain an alternative way to approximate the first-order derivative of f with respect to x at the point x_k as

$$f'(x_k) \approx \frac{f(x_{k+1}) - f(x_{k-1})}{2(\Delta x)}, \quad (C.13)$$

where the error of approximation is also in the order $(\Delta x)^2$.

The equation (C.9) is called the first-order central difference approximation.

When equations (C.2) and (C.6) are added we obtain

$$f(x_{k+1}) + f(x_{k-1}) = 2f(x_k) + (\Delta x)^2 f''(x_k) + \frac{f^{(4)}(x_k)}{12} (\Delta x)^4 + \dots \quad (C.14)$$

This equation can be rewritten as

$$f''(x_k) = \frac{f(x_{k+1}) - 2f(x_k) + f(x_{k-1}))}{(\Delta x)^2} + O[(\Delta x)^2], \quad (C.15)$$

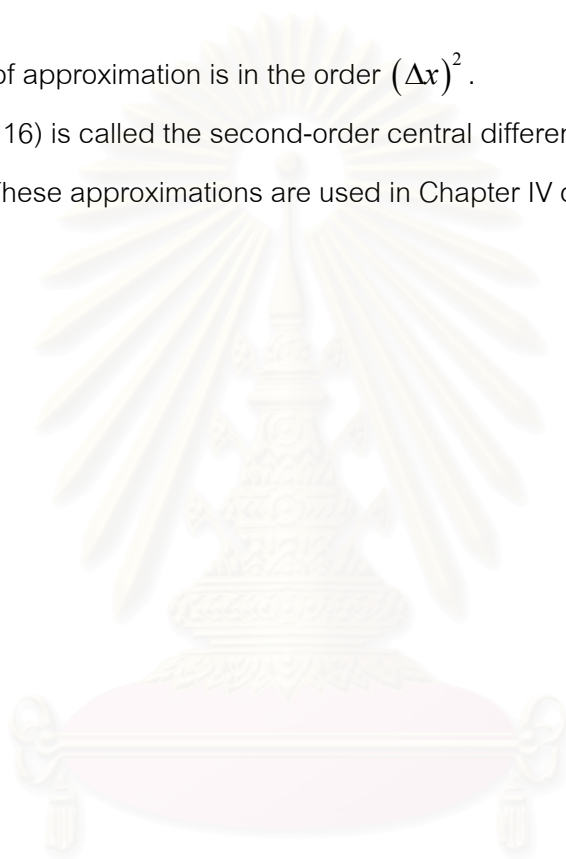
where $O[(\Delta x)^2]$ represent the terms of order $(\Delta x)^2$ and higher. We can approximate the second-order derivative of f with respect to x at the point x_k as

$$f''(x_k) \approx \frac{f(x_{k+1}) - 2f(x_k) + f(x_{k-1}))}{(\Delta x)^2}, \quad (\text{C.16})$$

where the error of approximation is in the order $(\Delta x)^2$.

The equation (C.16) is called the second-order central difference approximation.

These approximations are used in Chapter IV of this research.



สถาบันวิทยบริการ
จุฬาลงกรณ์มหาวิทยาลัย

APPENDIX D

Errors and Stability of the Computation for Simulations of the Capture of Ultra-Fine Particles in One Dimension

D.1 Errors of the Computation

We start with equation (4.19) of Chapter IV,

$$\frac{c_i^{n+1} - c_i^n}{\Delta \tau} - \left(\frac{c_{i+1}^n - 2c_i^n + c_{i-1}^n}{(\Delta r_a)^2} \right) + (G_r)_i \left(\frac{c_{i+1}^n - c_{i-1}^n}{2(\Delta r_a)} \right) + \left(\frac{\partial G_r}{\partial r_a} \right)_i c_i^n = \varepsilon_i^n, \quad (D.1)$$

where ε_i^n is a real number generally not equal to zero.

The value of ε_i^n indicate the error of the computation occurred at a discrete radial position $(r_a)_i$ at the n^{th} step of the computation. If the approximated solution C_i^n approach to the analytical solution c_i^n then ε_i^n approach to zero.

From equation (D.1), by using Taylor's expansions, we can approximate the analytical solution at each grid points as

$$c_i^{n+1} \approx c_i^n + (\Delta \tau) \left(\frac{\partial c}{\partial \tau} \right)_i + \frac{(\Delta \tau)^2}{2} \left(\frac{\partial^2 c}{\partial \tau^2} \right)_i, \quad (D.2)$$

$$c_{i+1}^n \approx c_i^n + (\Delta r_a) \left(\frac{\partial c}{\partial r_a} \right)_i + \frac{(\Delta r_a)^2}{2} \left(\frac{\partial^2 c}{\partial r_a^2} \right)_i + \frac{(\Delta r_a)^3}{3!} \left(\frac{\partial^3 c}{\partial r_a^3} \right)_i + \frac{(\Delta r_a)^4}{4!} \left(\frac{\partial^4 c}{\partial r_a^4} \right)_i, \quad (D.3)$$

$$c_{i-1}^n \approx c_i^n - (\Delta r_a) \left(\frac{\partial c}{\partial r_a} \right)_i + \frac{(\Delta r_a)^2}{2} \left(\frac{\partial^2 c}{\partial r_a^2} \right)_i - \frac{(\Delta r_a)^3}{3!} \left(\frac{\partial^3 c}{\partial r_a^3} \right)_i + \frac{(\Delta r_a)^4}{4!} \left(\frac{\partial^4 c}{\partial r_a^4} \right)_i. \quad (D.4)$$

When these approximations are substituted in equation (D.1), we obtain

$$\begin{aligned} \varepsilon_i^n \approx & \left[\left(\frac{\partial c}{\partial \tau} \right)_i^n - \left(\frac{\partial^2 c}{\partial r_a^2} \right)_i^n + (G_r)_i \left(\frac{\partial c}{\partial r_a} \right)_i^n - \left(\frac{\partial G_r}{\partial r_a} \right)_i c_i^n \right] \\ & + \left[\frac{(\Delta \tau)}{2} \left(\frac{\partial^2 c}{\partial \tau^2} \right)_i^n - \frac{(\Delta r_a)^2}{12} \left(\frac{\partial^4 c}{\partial r_a^4} \right)_i^n + \frac{(G_r)_i}{6} \left(\frac{\partial^3 c}{\partial r_a^3} \right)_i^n (\Delta r_a)^2 \right]. \end{aligned} \quad (D.5)$$

From this expression, we can see that the first part on the right hand side equal to zero and we have

$$\varepsilon_i^n \approx \left(\frac{\partial^2 c}{\partial \tau^2} \right)_i^n \frac{(\Delta \tau)}{2} + \left[2(G_r)_i \left(\frac{\partial^3 c}{\partial r_a^3} \right)_i^n - \left(\frac{\partial^4 c}{\partial r_a^4} \right)_i^n \right] \frac{(\Delta r_a)^2}{12}. \quad (D.6)$$

From equation (D.6), we can conclude that

$$\max_{i,n} |\varepsilon_i^n| \leq \max_{i,n} \left| \left(\frac{\partial^2 c}{\partial \tau^2} \right)_i^n \right| \frac{(\Delta \tau)}{2} + \max_{i,n} \left| 2(G_r)_i \left(\frac{\partial^3 c}{\partial r_a^3} \right)_i^n - \left(\frac{\partial^4 c}{\partial r_a^4} \right)_i^n \right| \frac{(\Delta r_a)^2}{12}. \quad (D.7)$$

D.2 Stability of the Computation

From equation (4.13) of Chapter IV

$$\frac{C_i^{n+1} - C_i^n}{\Delta \tau} = \left(\frac{C_{i+1}^n - 2C_i^n + C_{i-1}^n}{(\Delta r_a)^2} \right) - (G_r)_i \left(\frac{C_{i+1}^n - C_{i-1}^n}{2(\Delta r_a)} \right) - \left(\frac{\partial G_r}{\partial r_a} \right)_i C_i^n. \quad (D.8)$$

We write the approximated solutions at grid points as

$$C_i^{n+1} = c_i^{n+1} + \delta c_i^{n+1}, \quad (D.9a)$$

$$C_i^n = c_i^n + \delta c_i^n, \quad (D.9b)$$

$$\mathbb{C}_{i+1}^n = c_{i+1}^n + \delta c_{i+1}^n, \quad (\text{D.9c})$$

and
$$\mathbb{C}_{i-1}^n = c_{i-1}^n + \delta c_{i-1}^n. \quad (\text{D.9d})$$

When all expressions in equations (D.9a) to (D.9d) are substituted in equation (D.8) we obtain

$$\begin{aligned} \frac{\delta c_i^{n+1} - \delta c_i^n}{\Delta \tau} = & \left[\left(\frac{\delta c_{i+1}^n - 2\delta c_i^n + \delta c_{i-1}^n}{(\Delta r_a)^2} \right) - (G_r)_i \left(\frac{\delta c_{i+1}^n - \delta c_{i-1}^n}{2(\Delta r_a)} \right) - \left(\frac{\partial G_r}{\partial r_a} \right)_i \delta c_i^n \right] \\ & - \left[\left(\frac{c_i^{n+1} - c_i^n}{\Delta \tau} \right) - \left(\frac{c_{i+1}^n - 2c_i^n + c_{i-1}^n}{(\Delta r_a)^2} \right) + (G_r)_i \left(\frac{c_{i+1}^n - c_{i-1}^n}{2(\Delta r_a)} \right) + \left(\frac{\partial G_r}{\partial r_a} \right)_i c_i^n \right]. \quad (\text{D.10}) \end{aligned}$$

From section 4.1.2.1 of Chapter IV, the second term on the right hand side of equation (D.10) can be replaced by $O[(\Delta \tau) + (\Delta r_a)^2]$ and we obtain

$$\begin{aligned} \frac{\delta c_i^{n+1} - \delta c_i^n}{\Delta \tau} = & \left[\left(\frac{\delta c_{i+1}^n - 2\delta c_i^n + \delta c_{i-1}^n}{(\Delta r_a)^2} \right) - (G_r)_i \left(\frac{\delta c_{i+1}^n - \delta c_{i-1}^n}{2(\Delta r_a)} \right) - \left(\frac{\partial G_r}{\partial r_a} \right)_i \delta c_i^n \right] \\ & + O[(\Delta \tau) + (\Delta r_a)^2]. \quad (\text{D.11}) \end{aligned}$$

Solving equation (D.11) for δc_i^{n+1} , we obtain

$$\begin{aligned} \delta c_i^{n+1} = & \left[1 - \frac{2(\Delta \tau)}{(\Delta r_a)^2} - \left(\frac{\partial G_r}{\partial r_a} \right)_i (\Delta \tau) \right] \delta c_i^{n+1} + \left[\frac{(\Delta \tau)}{(\Delta r_a)^2} - \frac{(G_r)_i (\Delta \tau)}{2(\Delta r_a)} \right] \delta c_{i+1}^n \\ & + \left[\frac{(\Delta \tau)}{(\Delta r_a)^2} + \frac{(G_r)_i (\Delta \tau)}{2(\Delta r_a)} \right] \delta c_{i-1}^n + (\Delta \tau) O[(\Delta \tau) + (\Delta r_a)^2]. \quad (\text{D.12}) \end{aligned}$$

In the simulation, grid steps $\Delta \tau$ and Δr_a are set to make these following expressions become true

$$\max_i \left| \left(\frac{\partial G_r}{\partial r_a} \right)_i \right| (\Delta \tau) \ll \xi, \quad (\text{D.13})$$

$$\max_i |(G_r)_i| \frac{(\Delta \tau)}{2(\Delta r_a)} \ll \xi, \quad (\text{D.14})$$

where the variable ξ is defined in the equation (4.24) of Chapter IV.

With two expressions in equations (D.13) and (D.14) satisfied, we can approximate equation (D.12) as

$$\delta c_i^{n+1} \approx (1-2\xi) \delta c_i^n + \xi (\delta c_{i+1}^n + \delta c_{i-1}^n) + (\Delta \tau) \mathcal{O} \left[(\Delta \tau) + (\Delta r_a)^2 \right]. \quad (\text{D.15})$$

When the condition

$$0 \leq \xi \leq \frac{1}{2} \quad (\text{D.16})$$

is satisfied, all coefficients of δc_i^n , δc_{i+1}^n and δc_{i-1}^n are positive and we can obtain

$$|\delta c_i^{n+1}| \leq (1-2\xi) |\delta c_i^n| + \xi (|\delta c_{i+1}^n| + |\delta c_{i-1}^n|) + (\Delta \tau) \mathcal{O} \left[(\Delta \tau) + (\Delta r_a)^2 \right]. \quad (\text{D.17})$$

Equation (D.17) can be rewritten as

$$|\delta c_i^{n+1}| \leq \max \left(|\delta c_i^n|, |\delta c_{i+1}^n|, |\delta c_{i-1}^n| \right) + (\Delta \tau) \mathcal{O} \left[(\Delta \tau) + (\Delta r_a)^2 \right]. \quad (\text{D.18})$$

Since the inequality (D.18) hold for all indices i then we can write

$$\max_i |\delta c_i^{n+1}| \leq \max_i |\delta c_i^n| + (\Delta \tau) \mathcal{O} \left[(\Delta \tau) + (\Delta r_a)^2 \right]. \quad (\text{D.19})$$

The inequality (D.19) means that the maximum error of computation at a given discrete point for one step of computation increase by not more than $(\Delta \tau) \mathcal{O} \left[(\Delta \tau) + (\Delta r_a)^2 \right]$. Consequently, for N steps of computation, we obtain

$$\max_i |\delta c_i^N| \leq \max_i |\delta c_i^0| + O\left[(\Delta \tau) + (\Delta r_a)^2\right]. \quad (\text{D.20})$$

Now it is proved that, with vanishing $(\Delta \tau)$ and (Δr_a) , conditions (D.13), (D.14) and (D.16) are satisfied, the approximated solutions \mathbb{C}_i^n converge to the analytical solutions c_i^n at any grid points and the computation is stable.



สถาบันวิทยบริการ
จุฬาลงกรณ์มหาวิทยาลัย

APPENDIX E

Errors and Stability of the Computation for Simulations of the Capture of Ultra-Fine Particles in Two Dimensions

E.1 Errors of the Computation

We start with equation (4.44) of Chapter IV,

$$\begin{aligned} \frac{c_{i,j}^{n+1} - c_{i,j}^n}{\Delta\tau} = & \left(\frac{c_{i+1,j}^n - 2c_{i,j}^n + c_{i-1,j}^n}{(\Delta r_a)^2} \right) + \frac{1}{(r_a)_i} \left(\frac{c_{i+1,j}^n - c_{i-1,j}^n}{2(\Delta r_a)} \right) + \frac{1}{(r_a)_i^2} \left(\frac{c_{i,j+1}^n - 2c_{i,j}^n + c_{i,j-1}^n}{(\Delta\theta)^2} \right) \\ & - \frac{(G_r)_{i,j} c_{i,j}^n}{(r_a)_i} - (G_r)_{i,j} \left(\frac{c_{i+1,j}^n - c_{i-1,j}^n}{2(\Delta r_a)} \right) - \left(\frac{\partial G_r}{\partial r_a} \right)_{i,j} c_{i,j}^n \\ & - \frac{(G_\theta)_{i,j} \left(\frac{c_{i,j+1}^n - c_{i,j-1}^n}{2(\Delta\theta)} \right)}{(r_a)_i} - \frac{c_{i,j}^n}{(r_a)_i} \left(\frac{\partial G_\theta}{\partial \theta} \right)_{i,j} + \varepsilon_{i,j}^n, \end{aligned} \quad (E.1)$$

where $\varepsilon_{i,j}^n$ is a real number generally not equal to zero.

The value of $\varepsilon_{i,j}^n$ indicate the error of the computation occurred at a discrete radial position $((r_a)_i, \theta_j)$ at the n^{th} step of the computation. If the approximated solution $C_{i,j}^n$ approach to the analytical solution $c_{i,j}^n$ then $\varepsilon_{i,j}^n$ approach to zero.

From equation (E.1), by using Taylor's expansions, we can approximate the analytical solution at each grid points as

$$c_{i,j}^{n+1} \approx c_{i,j}^n + (\Delta\tau) \left(\frac{\partial c}{\partial \tau} \right)_{i,j}^n + \frac{(\Delta\tau)^2}{2} \left(\frac{\partial^2 c}{\partial \tau^2} \right)_{i,j}^n, \quad (E.2)$$

$$c_{i+1,j}^n \approx c_{i,j}^n + (\Delta r_a) \left(\frac{\partial c}{\partial r_a} \right)_{i,j}^n + \frac{(\Delta r_a)^2}{2} \left(\frac{\partial^2 c}{\partial r_a^2} \right)_{i,j}^n + \frac{(\Delta r_a)^3}{3!} \left(\frac{\partial^3 c}{\partial r_a^3} \right)_{i,j}^n + \frac{(\Delta r_a)^4}{4!} \left(\frac{\partial^4 c}{\partial r_a^4} \right)_{i,j}^n, \quad (E.3)$$

$$c_{i-1,j}^n \approx c_{i,j}^n - (\Delta r_a) \left(\frac{\partial c}{\partial r_a} \right)_{i,j}^n + \frac{(\Delta r_a)^2}{2} \left(\frac{\partial^2 c}{\partial r_a^2} \right)_{i,j}^n - \frac{(\Delta r_a)^3}{3!} \left(\frac{\partial^3 c}{\partial r_a^3} \right)_{i,j}^n + \frac{(\Delta r_a)^4}{4!} \left(\frac{\partial^4 c}{\partial r_a^4} \right)_{i,j}^n \quad (\text{E.4})$$

$$c_{i,j+1}^n \approx c_{i,j}^n + (\Delta \theta) \left(\frac{\partial c}{\partial \theta} \right)_{i,j}^n + \frac{(\Delta \theta)^2}{2} \left(\frac{\partial^2 c}{\partial \theta^2} \right)_{i,j}^n + \frac{(\Delta \theta)^3}{3!} \left(\frac{\partial^3 c}{\partial \theta^3} \right)_{i,j}^n + \frac{(\Delta \theta)^4}{4!} \left(\frac{\partial^4 c}{\partial \theta^4} \right)_{i,j}^n, \quad (\text{E.5})$$

$$c_{i,j-1}^n \approx c_{i,j}^n - (\Delta \theta) \left(\frac{\partial c}{\partial \theta} \right)_{i,j}^n + \frac{(\Delta \theta)^2}{2} \left(\frac{\partial^2 c}{\partial \theta^2} \right)_{i,j}^n - \frac{(\Delta \theta)^3}{3!} \left(\frac{\partial^3 c}{\partial \theta^3} \right)_{i,j}^n + \frac{(\Delta \theta)^4}{4!} \left(\frac{\partial^4 c}{\partial \theta^4} \right)_{i,j}^n. \quad (\text{E.6})$$

When these approximations are substituted in equation (E.1), we obtain

$$\begin{aligned} \varepsilon_{i,j}^n \approx & \left[\left(\frac{\partial c}{\partial \tau} \right)_{i,j}^n - \left(\frac{\partial^2 c}{\partial r_a^2} \right)_{i,j}^n - \frac{1}{(r_a)_i} \left(\frac{\partial c}{\partial r_a} \right)_{i,j}^n - \frac{1}{(r_a)_i} \left(\frac{\partial^2 c}{\partial \theta^2} \right)_{i,j}^n + \frac{(G_r)_{i,j}}{(r_a)_i} \right. \\ & \left. + (G_r)_{i,j} \left(\frac{\partial c}{\partial r_a} \right)_{i,j}^n + \left(\frac{\partial G_r}{\partial r_a} \right)_{i,j} c_{i,j}^n + \frac{(G_\theta)_{i,j}}{(r_a)_i} \left(\frac{\partial c}{\partial \theta} \right)_{i,j}^n + \frac{c_{i,j}^n}{(r_a)_i} \left(\frac{\partial G_\theta}{\partial \theta} \right)_{i,j} \right] \\ & + \left[\frac{(\Delta \tau)}{2} \left(\frac{\partial^2 c}{\partial \tau^2} \right)_{i,j}^n + \left\{ 2(G_r)_{i,j} \left(\frac{\partial^3 c}{\partial r_a^3} \right)_{i,j}^n - \frac{2}{(r_a)_i} \left(\frac{\partial^3 c}{\partial r_a^3} \right)_{i,j}^n - \left(\frac{\partial^4 c}{\partial r_a^4} \right)_{i,j}^n \right\} \frac{(\Delta r_a)^2}{12} \right. \\ & \left. + \left\{ \frac{2(G_\theta)_{i,j}}{(r_a)_i} \left(\frac{\partial^3 c}{\partial \theta^3} \right)_{i,j}^n - \frac{1}{(r_a)_i^2} \left(\frac{\partial^4 c}{\partial \theta^4} \right)_{i,j}^n \right\} \frac{(\Delta \theta)^2}{12} \right]. \quad (\text{E.7}) \end{aligned}$$

From this expression, we can see that the first part on the right hand side equal to zero and we have

$$\begin{aligned} \varepsilon_{i,j}^n \approx & \left(\frac{\partial^2 c}{\partial \tau^2} \right)_{i,j}^n \frac{(\Delta \tau)}{2} + \left\{ 2 \left((G_r)_{i,j} - \frac{1}{(r_a)_i} \right) \left(\frac{\partial^3 c}{\partial r_a^3} \right)_{i,j}^n - \left(\frac{\partial^4 c}{\partial r_a^4} \right)_{i,j}^n \right\} \frac{(\Delta r_a)^2}{12} \\ & + \left\{ \frac{2(G_\theta)_{i,j}}{(r_a)_i} \left(\frac{\partial^3 c}{\partial \theta^3} \right)_{i,j}^n - \frac{1}{(r_a)_i^2} \left(\frac{\partial^4 c}{\partial \theta^4} \right)_{i,j}^n \right\} \frac{(\Delta \theta)^2}{12} \quad (\text{E.8}) \end{aligned}$$

From equation (E.8), we can conclude that

$$\begin{aligned}
\max_{i,j} |\varepsilon_{i,j}^n| &\leq \max_{i,j} \left| \left(\frac{\partial^2 c}{\partial \tau^2} \right)_{i,j} \right| \frac{(\Delta \tau)^2}{2} \\
&+ \max_{i,j} \left| 2 \left((G_r)_{i,j} - \frac{1}{(r_a)_i} \right) \left(\frac{\partial^3 c}{\partial r_a^3} \right)_{i,j} - \left(\frac{\partial^4 c}{\partial r_a^4} \right)_{i,j} \right| \frac{(\Delta r_a)^2}{12} \\
&+ \max_{i,j} \left| \left(\frac{2(G_\theta)_{i,j}}{(r_a)_i} \right) \left(\frac{\partial^3 c}{\partial r_a^3} \right)_{i,j} - \frac{1}{(r_a)_i} \left(\frac{\partial^4 c}{\partial r_a^4} \right)_{i,j} \right| \frac{(\Delta \theta)^2}{12}
\end{aligned} \tag{E.9}$$

E.2 Stability of the Computation

From equation (4.42) of Chapter IV,

$$\begin{aligned}
\frac{\mathbb{C}_{i,j}^{n+1} - \mathbb{C}_{i,j}^n}{\Delta \tau} &= \left(\frac{\mathbb{C}_{i+1,j}^n - 2\mathbb{C}_{i,j}^n + \mathbb{C}_{i-1,j}^n}{(\Delta r_a)^2} \right) + \frac{1}{(r_a)_i} \left(\frac{\mathbb{C}_{i+1,j}^n - \mathbb{C}_{i-1,j}^n}{2(\Delta r_a)} \right) + \frac{1}{(r_a)_i^2} \left(\frac{\mathbb{C}_{i,j+1}^n - 2\mathbb{C}_{i,j}^n + \mathbb{C}_{i,j-1}^n}{(\Delta \theta)^2} \right) \\
&- \frac{(G_r)_{i,j} \mathbb{C}_{i,j}^n}{(r_a)_i} - (G_r)_{i,j} \left(\frac{\mathbb{C}_{i+1,j}^n - \mathbb{C}_{i-1,j}^n}{2(\Delta r_a)} \right) - \left(\frac{\partial G_r}{\partial r_a} \right)_{i,j} \mathbb{C}_{i,j}^n \\
&- \frac{(G_\theta)_{i,j}}{(r_a)_i} \left(\frac{\mathbb{C}_{i,j+1}^n - \mathbb{C}_{i,j-1}^n}{2(\Delta \theta)} \right) - \frac{\mathbb{C}_{i,j}^n}{(r_a)_i} \left(\frac{\partial G_\theta}{\partial \theta} \right)_{i,j} .
\end{aligned} \tag{E.10}$$

We write the approximated solutions at grid points as

$$\mathbb{C}_{i,j}^{n+1} = c_{i,j}^{n+1} + \delta c_{i,j}^{n+1} , \tag{E.11a}$$

$$\mathbb{C}_{i,j}^n = c_{i,j}^n + \delta c_{i,j}^n , \tag{E.11b}$$

$$\mathbb{C}_{i+1,j}^n = c_{i+1,j}^n + \delta c_{i+1,j}^n , \tag{E.11c}$$

$$\mathbb{C}_{i-1,j}^n = c_{i-1,j}^n + \delta c_{i-1,j}^n , \tag{E.11d}$$

$$\mathbb{C}_{i,j+1}^n = c_{i,j+1}^n + \delta c_{i,j+1}^n, \quad (\text{E.11e})$$

$$\mathbb{C}_{i,j-1}^n = c_{i,j-1}^n + \delta c_{i,j-1}^n. \quad (\text{E.11f})$$

When all expressions in equations (E.11a) to (E.11f) are substituted in equation (E.10) we obtain

$$\begin{aligned} \frac{\delta c_{i,j}^{n+1} - \delta c_{i,j}^n}{\Delta \tau} = & \left[\left(\frac{\delta c_{i+1,j}^n - 2\delta c_{i,j}^n + \delta c_{i-1,j}^n}{(\Delta r_a)^2} \right) + \frac{1}{(r_a)_i} \left(\frac{\delta c_{i+1}^n - \delta c_{i-1}^n}{2(\Delta r_a)} \right) + \frac{1}{(r_a)_i^2} \left(\frac{\delta c_{i,j+1}^n - 2\delta c_{i,j}^n + \delta c_{i,j-1}^n}{(\Delta \theta)^2} \right) \right. \\ & - \frac{(G_r)_{i,j}}{(r_a)_i} \delta c_{i,j}^n - (G_r)_{i,j} \left(\frac{\delta c_{i+1,j}^n - \delta c_{i-1,j}^n}{2(\Delta r_a)} \right) - \left(\frac{\partial G_r}{\partial r_a} \right)_{i,j} \delta c_{i,j}^n \\ & \left. - \frac{(G_\theta)_{i,j}}{(r_a)_i} \left(\frac{\delta c_{i,j+1}^n - \delta c_{i,j-1}^n}{2(\theta)} \right) - \frac{1}{(r_a)_i} \left(\frac{\partial G_\theta}{\partial \theta} \right)_{i,j} \delta c_{i,j}^n \right] \\ & + \left[- \left(\frac{c_{i,j}^{n+1} - c_{i,j}^n}{\Delta \tau} \right) + \left(\frac{c_{i+1,j}^n - 2c_{i,j}^n + c_{i-1,j}^n}{(\Delta r_a)^2} \right) + \frac{1}{(r_a)_i} \left(\frac{c_{i+1}^n - c_{i-1}^n}{2(\Delta r_a)} \right) \right. \\ & + \frac{1}{(r_a)_i^2} \left(\frac{c_{i,j+1}^n - 2c_{i,j}^n + c_{i,j-1}^n}{(\Delta \theta)^2} \right) - \frac{(G_r)_{i,j} c_{i,j}^n}{(r_a)_i} - (G_r)_{i,j} \left(\frac{c_{i+1,j}^n - c_{i-1,j}^n}{2(\Delta r_a)} \right) \\ & \left. - \left(\frac{\partial G_r}{\partial r_a} \right)_{i,j} c_{i,j}^n - \frac{(G_\theta)_{i,j}}{(r_a)_i} \left(\frac{c_{i,j+1}^n - c_{i,j-1}^n}{2(\Delta \theta)} \right) - \frac{1}{(r_a)_i} \left(\frac{\partial G_\theta}{\partial \theta} \right)_{i,j} c_{i,j}^n \right]. \quad (\text{E.12}) \end{aligned}$$

From section 4.2.3 of Chapter IV, the second part on the right hand side of equation (E.12) can be replaced by $O\left[(\Delta \tau) + (\Delta r_a)^2 + (\Delta \theta)^2\right]$ and we obtain

จุฬาลงกรณ์มหาวิทยาลัย

$$\begin{aligned}
\delta c_{i,j}^{n+1} = & \left[1 - \frac{2(\Delta\tau)}{(\Delta r_a)^2} - \frac{2}{\alpha^2 (r_a)_i^2} \frac{(\Delta\tau)}{(\Delta r_a)^2} - \left\{ \frac{(G_r)_{i,j}}{(r_a)_i} + \left(\frac{\partial G_r}{\partial r_a} \right)_{i,j} + \frac{1}{(r_a)_i} \left(\frac{\partial G_\theta}{\partial \theta} \right)_{i,j} \right\} (\Delta\tau) \right] \delta c_{i,j}^n \\
& + \left[\frac{(\Delta\tau)}{(\Delta r_a)^2} - \left(\frac{1}{2(r_a)_i} - \frac{(G_r)_{i,j}}{2} \right) \frac{(\Delta\tau)}{(\Delta r_a)} \right] \delta c_{i+1,j}^n \\
& + \left[\frac{(\Delta\tau)}{(\Delta r_a)^2} + \left(\frac{(G_r)_{i,j}}{2} - \frac{1}{2(r_a)_i} \right) \frac{(\Delta\tau)}{(\Delta r_a)} \right] \delta c_{i-1,j}^n \\
& + \left[\frac{1}{\alpha^2 (r_a)_i^2} \frac{(\Delta\tau)}{(\Delta r_a)^2} - \frac{(G_\theta)_{i,j}}{2\alpha (r_a)_i} \frac{(\Delta\tau)}{(\Delta r_a)} \right] \delta c_{i,j+1}^n \\
& + \left[\frac{1}{\alpha^2 (r_a)_i^2} \frac{(\Delta\tau)}{(\Delta r_a)^2} + \frac{(G_\theta)_{i,j}}{2\alpha (r_a)_i} \frac{(\Delta\tau)}{(\Delta r_a)} \right] \delta c_{i,j-1}^n \\
& + (\Delta\tau) \mathcal{O} \left[(\Delta\tau) + (\Delta r_a)^2 + (\Delta\theta)^2 \right] , \tag{E.13}
\end{aligned}$$

where the variable α is defined in the equation (4.52) of Chapter IV.

In the simulation, grid steps $\Delta\tau$, Δr_a and $\Delta\theta$ are set to make these following expressions become true

$$0 < \max_{i,j} \left| \left(\frac{1}{\alpha^2 (r_a)_i^2} \right) \frac{(\Delta\tau)}{(\Delta r_a)^2} - \frac{(G_\theta)_{i,j}}{2\alpha (r_a)_i} \frac{(\Delta\tau)}{(\Delta r_a)} \right| < 1 , \tag{E.14}$$

$$0 < \max_{i,j} \left| \left(\frac{1}{\alpha^2 (r_a)_i^2} \right) \frac{(\Delta\tau)}{(\Delta r_a)^2} + \frac{(G_\theta)_{i,j}}{2\alpha (r_a)_i} \frac{(\Delta\tau)}{(\Delta r_a)} \right| < 1 , \tag{E.15}$$

$$\max_i \left| \frac{1}{\alpha^2 (r_a)_i^2} \right| \ll 1 , \tag{E.16}$$

$$\max_{i,j} \left| \left\{ \frac{(G_r)_{i,j}}{(r_a)_i} + \left(\frac{\partial G_r}{\partial r_a} \right)_{i,j} + \frac{1}{(r_a)_i} \left(\frac{\partial G_\theta}{\partial \theta} \right)_{i,j} \right\} (\Delta\tau) \right| \ll 1 , \tag{E.17}$$

$$\max_{i,j} \left| \left(\frac{(G_r)_{i,j}}{2} - \frac{1}{2(r_a)_i} \right) \frac{(\Delta\tau)}{(\Delta r_a)} \right| \ll \frac{(\Delta\tau)}{(\Delta r_a)^2} . \quad (\text{E.18})$$

With all conditions in equations (E.14) to (E.18) are satisfied, we can approximate equation (E.13) as

$$\delta c_{i,j}^{n+1} \approx (1-2\xi)\delta c_{i,j}^n + \xi(\delta c_{i+1,j}^n + \delta c_{i-1,j}^n) + \beta(\delta c_{i,j+1}^n) + \gamma(\delta c_{i,j-1}^n) + (\Delta\tau)O\left[(\Delta\tau) + (\Delta r_a)^2\right] . \quad (\text{E.19})$$

where β and γ are defined as

$$\beta \equiv \max_{i,j} \left| \left(\frac{1}{\alpha^2 (r_a)_i^2} \right) \frac{(\Delta\tau)}{(\Delta r_a)^2} - \frac{(G_\theta)_{i,j} (\Delta\tau)}{2\alpha (r_a)_i (\Delta r_a)} \right| , \quad (\text{E.20})$$

and

$$\gamma \equiv \max_{i,j} \left| \left(\frac{1}{\alpha^2 (r_a)_i^2} \right) \frac{(\Delta\tau)}{(\Delta r_a)^2} + \frac{(G_\theta)_{i,j} (\Delta\tau)}{2\alpha (r_a)_i (\Delta r_a)} \right| . \quad (\text{E.21})$$

When the condition

$$0 \leq \xi \leq \frac{1}{2} \quad (\text{E.22})$$

is satisfied, all coefficients of δc_i^n , δc_{i+1}^n , $\delta c_{i-1,j}^n$, $\delta c_{i,j+1}^n$ and $\delta c_{i,j-1}^n$ are positive and we can obtain

$$\begin{aligned} |\delta c_{i,j}^{n+1}| \leq & (1-2\xi)|\delta c_{i,j}^n| + \xi(|\delta c_{i+1,j}^n| + |\delta c_{i-1,j}^n|) + \beta|\delta c_{i,j+1}^n| + \gamma|\delta c_{i,j-1}^n| \\ & + (\Delta\tau)O\left[(\Delta\tau) + (\Delta r_a)^2 + (\Delta\theta)^2\right] . \end{aligned} \quad (\text{E.23})$$

Equation (E.23) can be rewritten as

$$|\delta c_{i,j}^{n+1}| \leq \max(|\delta c_{i,j}^n|, |\delta c_{i+1,j}^n|, |\delta c_{i-1,j}^n|, |\delta c_{i,j+1}^n|, |\delta c_{i,j-1}^n|) + (\Delta\tau)O\left[(\Delta\tau) + (\Delta r_a)^2 + (\Delta\theta)^2\right] \quad (E.24)$$

Since the inequality (E.24) hold for all indices i then we can write

$$\max_{i,j} |\delta c_{i,j}^{n+1}| \leq \max_{i,j} |\delta c_{i,j}^n| + (\Delta\tau)O\left[(\Delta\tau) + (\Delta r_a)^2 + (\Delta\theta)^2\right]. \quad (E.25)$$

The inequality (E.25) means that the maximum error of computation at a given discrete point for one step of computation increase by not more than $(\Delta\tau)O\left[(\Delta\tau) + (\Delta r_a)^2 + (\Delta\theta)^2\right]$. Consequently, for N steps of computation, we obtain

$$\max_{i,j} |\delta c_{i,j}^N| \leq \max_{i,j} |\delta c_{i,j}^0| + O\left[(\Delta\tau) + (\Delta r_a)^2 + (\Delta\theta)^2\right]. \quad (E.26)$$

Now it is proved that, with vanishing $(\Delta\tau)$, (Δr_a) and $(\Delta\theta)$, conditions (E.14) to (E.18) and (E.22) are satisfied, the approximated solutions C_i^n converge to the analytical solutions c_i^n at any grid points and the computation is stable.

สถาบันวิทยบริการ
จุฬาลงกรณ์มหาวิทยาลัย

APPENDIX F

Approximating the Continuity Equation at the Point on the Impervious Surface

F.1 The Impervious Surface at the Outer Boundary of the Representative Cell

In two dimensional simulation of HGMS capture of ultra-fine particles by an assemblage of random cylindrical collectors, we use the effective medium treatment construct the model of the problem. The obtained model allows us to consider the capture process in only a representative cylindrical cell. In the simulation, the outer boundary of the representative cell is treated as an impervious surface. Consequently, the original continuity equation (2.5) of Chapter II will be approximated at all points on the outer boundary of the representative cell.

From the original continuity equation

$$\frac{\partial c}{\partial t} + \vec{\nabla} \cdot \vec{J} = 0 \quad . \quad (F.1)$$

In two dimensional circular cylindrical coordinates (r, θ) the term $\vec{\nabla} \cdot \vec{J}$ can be written as

$$\vec{\nabla} \cdot \vec{J} = \frac{\partial J_r}{\partial r} + \frac{J_r}{r} + \frac{1}{r} \frac{\partial J_\theta}{\partial \theta} \quad . \quad (F.2)$$

Consider the outer boundary of the representative cell as shown in Figure F.1. In the figure, the position of the outer boundary is specified by the symbol Q and radial coordinate at that point is r_Q . We assign a point specified by $Q-1$ at the radial coordinate r_{Q-1} which locate with a distance Δr from the outer boundary.

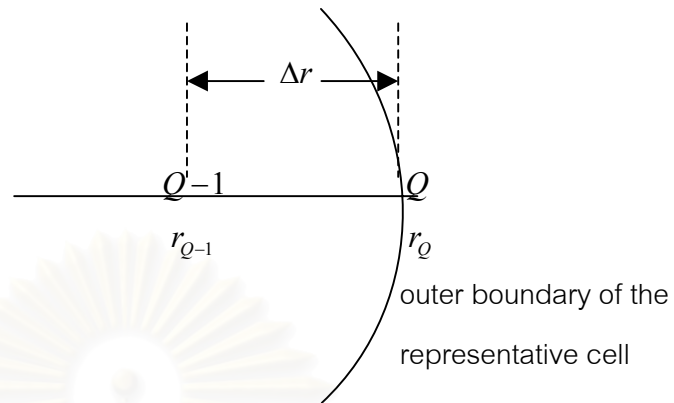


Figure F.1: Impervious surface at the outer boundary of the representative cell.

From equation (F.2), we can see that the term J_r at point Q equal to zero since point Q is on the impervious surface. By approximating the first term on the right hand side of equation (F.2), we can write $\vec{\nabla} \cdot \vec{J}$ at the point Q in approximated form as

$$(\vec{\nabla} \cdot \vec{J})_Q \approx \frac{1}{r} \frac{\partial J_\theta}{\partial \theta} + \left[\frac{(J_r)_Q - (J_r)_{Q-1}}{\Delta r} \right]. \quad (\text{F.3})$$

Equation (F.3) obtained by approximate the term $\partial J_r / \partial r$ at point Q by the first-order backward difference relation. From this equation we see that $(J_r)_Q = 0$.

By using these expressions in the equation (F.3),

$$J_r = -D \frac{\partial c}{\partial r} + v_r c, \quad (\text{F.4})$$

$$J_\theta = -\frac{D}{r} \frac{\partial c}{\partial \theta} + v_\theta c, \quad (\text{F.5})$$

where D is diffusion coefficient, v_r and v_θ are radial and angular components of particle drift velocity, respectively, we obtain

$$(\bar{\nabla} \cdot \bar{J})_Q \approx \frac{1}{r_Q} \frac{\partial}{\partial \theta} \left(-\frac{D}{r} \frac{\partial c}{\partial \theta} + v_\theta c \right)_Q - \frac{1}{(\Delta r)} \left(-D \frac{\partial c}{\partial r} + v_r c \right)_{Q-1}. \quad (\text{F.6})$$

By rearrange equation (F.6), we obtain

$$(\bar{\nabla} \cdot \bar{J})_Q \approx -\frac{D}{r_Q^2} \left(\frac{\partial^2 c}{\partial \theta^2} \right)_Q + \frac{1}{r_Q} \left(\frac{\partial (v_\theta c)}{\partial \theta} \right)_Q - \frac{1}{(\Delta r)} \left(v_r c - D \frac{\partial c}{\partial r} \right)_{Q-1}. \quad (\text{F.7})$$

Now the original continuity equation (F.1) can be approximated at the point Q on the outer boundary of the representative cell as

$$\left(\frac{\partial c}{\partial t} \right)_Q \approx \frac{D}{r_Q^2} \left(\frac{\partial^2 c}{\partial \theta^2} \right)_Q - \frac{1}{r_Q} \left(\frac{\partial (v_\theta c)}{\partial \theta} \right)_Q + \frac{1}{(\Delta r)} \left(v_r c - D \frac{\partial c}{\partial r} \right)_{Q-1}. \quad (\text{F.8})$$

When equation (F.8) is rewritten in terms of normalized radial distance (r_a) and normalized time (τ), defined in equations (2.15) and (2.24) of Chapter II, respectively, we obtain the approximated continuity equation used in the computation of concentration at any point on the boundary of the representative cell as

$$\left(\frac{\partial c}{\partial \tau} \right)_Q \approx \frac{1}{(r_a)^2} \left(\frac{\partial^2 c}{\partial \theta^2} \right)_Q - \frac{1}{(r_a)} \left(\frac{\partial (G_\theta c)}{\partial \theta} \right)_Q + \frac{1}{(\Delta r_a)} \left(G_r c - \frac{\partial c}{\partial r_a} \right)_{Q-1}. \quad (\text{F.9})$$

The function G_r and G_θ in equation (F.9) are defined in equations (2.26) and (2.31) of Chapter II, respectively.

F.2 The Impervious Surface at Surface of the Collector or the Surface of Saturation Regions

In this research, the surface of the collector and the surface of the saturation regions are considered as an impervious surface. The original continuity equation (2.5) will be approximated at all points on these surfaces.

Consider the surface of the collector or surface of the saturation region as shown in Figure F.2. In the figure, the position of impervious surface is specified by the symbol I and radial coordinate at that point is r_I . We assign a point specified by $I-1$ at the radial coordinate r_{I+1} which Δr forward the impervious surface.

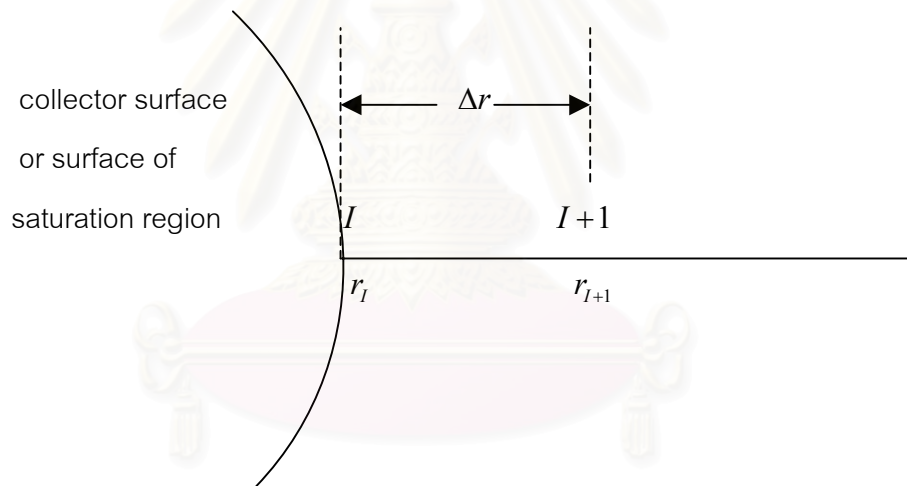


Figure F.2: Impervious surface at the surface of the collector or the surface of saturation regions.

From equation (F.2), the second term equal to zero at the impervious, By approximating the first term on the right hand side of equation (F.2), we can write $\vec{\nabla} \cdot \vec{J}$ at the point I in approximated form as

$$(\vec{\nabla} \cdot \vec{J})_I \approx \frac{1}{r} \frac{\partial J_\theta}{\partial \theta} + \left[\frac{(J_r)_{I+1} - (J_r)_I}{\Delta r} \right]. \quad (F.10)$$

Equation (F.10) obtained by approximate the term $\partial J_r / \partial r$ at point I by the first-order forward difference relation. From this equation we see that $(J_r)_I = 0$. By using expressions of J_r and J_θ in equations (F.4) and (F.5), we obtain

$$(\bar{\nabla} \cdot \bar{J})_I \approx \frac{1}{r_I} \frac{\partial}{\partial \theta} \left(-\frac{D}{r} \frac{\partial c}{\partial \theta} + v_\theta c \right)_I + \frac{1}{(\Delta r)} \left(-D \frac{\partial c}{\partial r} + v_r c \right)_{I+1}. \quad (\text{F.11})$$

By rearrange equation (F.11) we obtain

$$(\bar{\nabla} \cdot \bar{J})_I \approx -\frac{D}{r_I^2} \left(\frac{\partial^2 c}{\partial \theta^2} \right)_I + \frac{1}{r_I} \left(\frac{\partial (v_\theta c)}{\partial \theta} \right)_I + \frac{1}{(\Delta r)} \left(v_r c - D \frac{\partial c}{\partial r} \right)_{I+1}. \quad (\text{F.12})$$

Now the original continuity equation (F.1) can be approximated at the point I on the impervious of this case as

$$\left(\frac{\partial c}{\partial t} \right)_I \approx \frac{D}{r_I^2} \left(\frac{\partial^2 c}{\partial \theta^2} \right)_I - \frac{1}{r_I} \left(\frac{\partial (v_\theta c)}{\partial \theta} \right)_I + \frac{1}{(\Delta r)} \left(v_r c - D \frac{\partial c}{\partial r} \right)_{I+1}. \quad (\text{F.13})$$

When equation (F.13) is rewritten in terms of normalized radial distance (r_a) and normalized time, we obtain the approximated continuity equation used in the computation of concentration at any point on the surface of the collector or at the first point next to the surface of saturation region as

$$\left(\frac{\partial c}{\partial \tau} \right)_I \approx \frac{1}{(r_a)_I^2} \left(\frac{\partial^2 c}{\partial \theta^2} \right)_I - \frac{1}{(r_a)_I} \left(\frac{\partial (G_\theta c)}{\partial \theta} \right)_I + \frac{1}{(\Delta r_a)} \left(G_r c - \frac{\partial c}{\partial r_a} \right)_{I+1}. \quad (\text{F.14})$$

APPENDIX G

Steady-State Solutions of HGMS Continuity Equation

G.1 One Dimensional Case

From the equation (4.5) of Chapter IV, we obtain the steady-state solution of one dimensional HGMS continuity equation (2.25) of Chapter II as

$$c_s(r_a) = C_0 \exp \left[\int_{\infty}^{r_a} G_r(x) dx \right], \quad (\text{G.1})$$

where C_0 is the initial particle concentration.

In the case of single ferromagnetic cylindrical collector, the expression of function G_r is obtained as

$$G_r(r_a, \theta) = G_0^{ferro} \left[\frac{\cos(2\theta)}{r_a^3} + \frac{K_W}{r_a^5} \right], \quad (\text{G.2})$$

where the factor G_0^{ferro} is defined in the equation (2.28) of Chapter II.

When the expression of G_r in equation (G.2) is substituted in equation (G.1) we obtain the steady-state solution of HGMS continuity equation for the case of single ferromagnetic cylindrical collector as

$$c_s(r_a) = C_0 \exp \left[-\frac{G_0^{ferro}}{2} \left(\frac{\cos(2\theta)}{r_a^2} + \frac{K_W}{2r_a^4} \right) \right]. \quad (\text{G.3})$$

The equation (G.3) obtain by assign the outer boundary condition at infinity where the influence of the magnetic force is neglect and the value of concentration there equal to initial concentration C_0 .

G.2 Two Dimensional Case

From the original continuity equation

$$\frac{\partial c}{\partial t} + \vec{\nabla} \cdot \vec{J} = 0 \quad . \quad (G.4)$$

At steady-state, concentration at any points in fluid does not change with time hence $\partial c / \partial t = 0$ and we obtain

$$\vec{\nabla} \cdot \vec{J} = 0 \quad . \quad (G.5)$$

The equation (G.5) means that, at steady state, the diffusion flux (\vec{J}_D) at a given point must be balanced by the particle flux due to action of the external force (\vec{J}_F) at that point. By using expression of \vec{J}_D and \vec{J}_F in equations (2.7) and (2.8) of Chapter II, we obtain

$$-D\vec{\nabla}c + \vec{v}c = 0 \quad , \quad (G.6)$$

where \vec{v} is the drift velocity of the system of ultra-fine particles.

By substituting the expression of \vec{v} from equation (2.9) of Chapter II in equation (G.6), we obtain

$$\frac{\vec{\nabla}c}{c} = \frac{u\vec{F}}{D} \quad , \quad (G.7)$$

where u is the particle mobility in fluid and \vec{F} is the total external force acting on the system of ultra-fine particles.

By substituting the expression of D from equation (2.11) of Chapter II in equation (G.7), we obtain

$$\frac{\vec{\nabla}c}{c} = \frac{\vec{F}}{k_B T}, \quad (\text{G.8})$$

where T is the absolute temperature in Kelvin.

From equation (G.8), by using the mathematical property of gradient of a scalar function, we can write

$$\frac{\vec{\nabla}c}{c} \cdot d\vec{r} = \frac{dc}{c}, \quad (\text{G.9})$$

where $d\vec{r}$ is the infinitesimal displacement of position in space.

In this research, we study the capture of ultra-fine particles by consider that the magnetic force is the only dominate force that has influence to the capture process then $\vec{F} = \vec{F}_m$ in equation (G.8). Since the magnetic force can be expressed as the positive gradient of the magnetic potential energy U_m in the system that is considered then we can write

$$\frac{\vec{\nabla}c}{c} = \frac{\vec{\nabla}U_m}{k_B T}. \quad (\text{G.10})$$

When both sides in equation (G.10) are dotted with $d\vec{r}$ we obtain

$$\frac{dc}{c} = d\left(\frac{U_m}{k_B T}\right). \quad (\text{G.11})$$

Since dc/c can be written as $d(\ln c)$ then, from equation (G.11) we obtain

$$c(r_a, \theta) = \exp\left[\frac{U_m(r_a, \theta)}{k_B T}\right]. \quad (\text{G.12})$$

This equation is the steady-state solution of the continuity equation in

two dimensions.

The magnetic potential energy of the system of fluid (permeability μ_f) with an assembly of ultra-fine particles (permeability μ_p) as suspensions can be determined as

$$U_m(r_a, \theta) = \frac{1}{2} \mu_0 (\chi_p - \chi_f) H^2(r_a, \theta). \quad (\text{G.13})$$

With equations (G.12) and (G.13), we can calculate the steady-state concentration at any points around the collector in the computational domain.



สถาบันวิทยบริการ
จุฬาลงกรณ์มหาวิทยาลัย

BIOGRAPHY

Mr. Kanok Hournkumnuard was born on April 3, 1978 in Petchaburi, Thailand. He received Bachelor Degree in Control Engineering from the Faculty of Engineering, King Mongkut's Institute of Technology Ladkrabang in 1999. In year 2000, Mr. Kanok start his work as a staff of the Department of Physics at Silpakorn University, Nakorn-Pathom. Mr. Kanok is allowed to leave his work as a graduate student in Physics program at the Department of Physics, Chulalongkorn University since June 2001 until December 2004 with the scholarship supported by the UDC project.

Mr. Kanok had two oral presentations based on his research. The subject of the first oral presentation is "2-D Simulation of Ultra-fine Magnetic Particle Capture by HGMS" which was presented in the 12th Academic Congress of the Faculty of Science, Chulalongkorn University in March 2004. The subject of the second oral presentation is "Capture of Ultra-Fine Magnetic Particles in Static Fluid by High Gradient Magnetic Separation" which was presented in the 1th Academic Congress of the Faculty of Science and Technology, Phetchaburi Rajabhat University in March 2004.



สถาบันวิทยบริการ
จุฬาลงกรณ์มหาวิทยาลัย